Hyperspectral Remote Sensing of the Spatial and Temporal Heterogeneity of low Arctic Vegetation

The role of phenology, vegetation colour, and intrinsic ecosystem components

---

Alison Leslie Beamish

Univ.-Diss.

zur Erlangung des akademischen Grades
"doctor rerum naturalium"
(Dr. rer. nat.)
in der Wissenschaftsdisziplin Geoökologie

eingereicht an der
Mathematisch-Naturwissenschaftlichen Fakultät
Institut für Erd-und Umweltwissenschaften
der Universität Potsdam
und
Alfred Wegener Institut Helmholtz-Zentrum für Polar-und Meeresforschung

Potsdam, den 30.04.2018

For my parents, Jim and Gail

Table of Contents

Abstract

Arctic tundra ecosystems are experiencing warming twice the global average and Arctic vegetation is responding in complex and heterogeneous ways. Shifting productivity, growth, species composition, and phenology at local and regional scales have implications for ecosystem functioning as well as the global carbon and energy balance. Optical remote sensing is an effective tool for monitoring ecosystem functioning in this remote biome. However, limited field-based spectral characterization of the spatial and temporal heterogeneity limits the accuracy of quantitative optical remote sensing at landscape scales. To address this research gap and support current and future satellite missions, three central research questions were posed:

- Does canopy-level spectral variability differ between dominant low Arctic vegetation communities and does this variability change between major phenological phases?

- How does canopy-level vegetation colour images recorded with high and low spectral resolution devices relate to phenological changes in leaf-level photosynthetic pigment concentrations?

- How does spatial aggregation of high spectral resolution data from the ground to satellite scale influence low Arctic tundra vegetation signatures and thereby what is the potential of upcoming hyperspectral spaceborne systems for low Arctic vegetation characterization?

To answer these questions a unique and detailed database was assembled. Field-based canopy-level spectral reflectance measurements, nadir digital photographs, and photosynthetic pigment concentrations of dominant low Arctic vegetation communities were acquired at three major phenological phases representing early, peak and late season. Data were collected in 2015 and 2016 in the Toolik Lake Research Natural Area located in north central Alaska on the North Slope of the Brooks Range. In addition to field data an aerial AISA hyperspectral image was acquired in the late season of 2016. Simulations of broadband Sentinel-2 and hyperspectral Environmental and Mapping Analysis Program (EnMAP) satellite reflectance spectra from ground-based reflectance spectra as well as simulations of

EnMAP imagery from aerial hyperspectral imagery were also obtained.

Results showed that canopy-level spectral variability within and between vegetation communities differed by phenological phase. The late season was identified as the most discriminative for identifying many dominant vegetation communities using both ground-based and simulated hyperspectral reflectance spectra. This was due to an overall reduction in spectral variability and comparable or greater differences in spectral reflectance between vegetation communities in the visible near infrared spectrum.

Red, green, and blue (RGB) indices extracted from nadir digital photographs and pigment-driven vegetation indices extracted from ground-based spectral measurements showed strong significant relationships. RGB indices also showed moderate relationships with chlorophyll and carotenoid pigment concentrations. The observed relationships with the broadband RGB channels of the digital camera indicate that vegetation colour strongly influences the response of pigment-driven spectral indices and digital cameras can track the seasonal development and degradation of photosynthetic pigments.

Spatial aggregation of hyperspectral data from the ground to airborne, to simulated satellite scale was influenced by non-photosynthetic components as demonstrated by the distinct shift of the red edge to shorter wavelengths. Correspondence between spectral reflectance at the three scales was highest in the red spectrum and lowest in the near infrared. By artificially mixing litter spectra at different proportions to ground-based spectra, correspondence with aerial and satellite spectra increased. Greater proportions of litter were required to achieve correspondence at the satellite scale.

Overall this thesis found that integrating multiple temporal, spectral, and spatial data is necessary to monitor the complexity and heterogeneity of Arctic tundra ecosystems. The identification of spectrally similar vegetation communities can be optimized using non-peak season hyperspectral data leading to more detailed identification of vegetation communities. The results also highlight the power of vegetation colour to link ground-based and satellite data. Finally, a detailed characterization non-photosynthetic ecosystem components is crucial for accurate interpretation of vegetation signals at landscape scales.

Zusammenfassung

Das arktische Ökosystem erfährt gegenwärtig eine Erwärmung doppelt so stark wie der globale Durchschnitt, worauf die arktische Vegetation in komplexer und heterogener Weise reagiert. Die damit verbundenen Änderungen der Produktivität, des Wachstums, der Artenzusammensetzung, der Phänologie und des Reproduktionserfolges auf lokaler und landschaftlicher Ebene haben Auswirkungen auf die Funktionen des hiesigen Ökosystems sowie auf den globalen Kohlenstoff- und Energiehaushalt. Die Fernerkundung hat sich als überaus wirksam bei der Beobachtung von Veränderungen der Ökosystemfunktionen in diesem Biom erwiesen. Allerdings sind feldbasierte Messungen und spektrale Charakterisierungen der räumlichen und zeitlichen Heterogenität arktischer Vegetationsgemeinschaften limitiert und die Genauigkeit von Fernerkundungsdaten im Landschaftsmaßstab eingeschränkt. Um diese Forschungslücke zu schließen und aktuelle und zukünftige Satellitenmissionen zu unterstützen, wurden drei zentrale Forschungsfragen entwickelt:

- Wie unterscheidet sich die spektrale Variabilität des Kronendaches zwischen dominanten Vegetationsgemeinschaften der niederen Arktis und wie verändert sich diese Variabilität zwischen den wichtigsten phänologischen Phasen?

- Wie hängen Aufnahmen der Vegetationsfarbe des Kronendaches von hoch und niedrig auflösenden Geräten mit phänologischen Veränderungen des photosynthetischen Pigmentgehalts auf Blattebene zusammen?

- Wie beeinflusst die räumliche Aggregation von Daten mit hoher spektraler Auflösung von der Boden- bis zur Satelliten-Skala die arktischen Vegetationssignale der Tundra und welches Potenzial haben zukünftige hyperspektraler Satellitensysteme für die arktische Vegetationscharakterisierung?

Um diese Fragen zu beantworten, wurde eine detaillierte Datenbank aus sichtbaren Nahinfrarot-Spektralreflexionsmessungen, korrespondierenden Nadir-Digitalfotografien und Photosynthesepigment-Massenanteilen der Vegetationsoberfläche der dominanten nieder arktischen Pflanzengemeinschaften in drei phänologischen Phasen zusammengestellt. Die Daten wurden während der Vegetationsperioden 2015 und 2016 in der „Toolik Lake Research Natural Area" im nördlichen zentralen Alaska am nördlichen Ausläufer der „Brooks Range" gesammelt. Zusätzlich zu den Felddaten wurde in der Spätsaison 2016 ein hyperspektrales Luftbild aufgenommen. Neben Simulationen spektraler Signaturen von multispektralen Sentinel-2, sowie hyperspektralen EnMAP Satellitendaten aus bodenbasierten

Reflektanzen, wurden auch simulierte EnMAP Bilder aus den hyperspektralen AISA Luftbildern abgeleitet.

Die spektrale Variabilität innerhalb und zwischen den Vegetationsgemeinschaften war in verschiedenen phänologischen Phasen unterschiedlich. Die Spätsaison, wenn die Seneszenz der Pflanzen eintrat, war am geeignetsten, um viele der dominanten Vegetationsgemeinschaften zu identifizieren, wenn bodenbasierte sowie simulierte hyperspektrale Reflektanzen verwendet wurden. Dies wurde auf eine allgemeine Verringerung der spektralen Variabilität und vergleichbare oder größere Unterschiede in der spektralen Reflektion zwischen Vegetationsgemeinschaften im sichtbaren nahen Infrarotspektrum zurückgeführt.

Vegetationsfarbe, extrahiert aus den Rot-, Grün- und Blau- (RGB) Indizes digitaler Fotos, und pigmentgesteuerte Spektralindizes aus korrespondierenden bodenbasierten Spektralmessungen, zeigten starke signifikante Beziehungen. Ebenfalls zeigten die RGB-Indizes und der Chlorophyll- und Carotinoidpigmentgehalt einen mittleren linearen Zusammenhang, vergleichbar mit den Beziehungen zu den pigmentgesteuerten Spektralindizes. Die beobachteten Beziehungen zu den Breitband-RGB-Kanälen der Digitalkamera zeigen, dass die Vegetationsfarbe die Reaktion von pigmentgesteuerten Spektralindizes stark beeinflusst und die Entwicklung und den Abbau von photosynthetischen Pigmenten nachverfolgen kann.

Die räumliche Aggregation hyperspektraler Daten von der boden- über die luft- bis hin zur simulierten satellitengestützten Skala wurde durch nicht-photosynthetische Komponenten beeinflusst, wie die deutliche Verschiebung des Übergangs der roten spektralen Kante zu kürzeren Wellenlängen zeigte. Ferner war die Übereinstimmung zwischen dem spektralen Reflexionsvermögen der drei Skalen im roten Spektrum am höchsten und im nahen Infrarotbereich am niedrigsten. Durch künstliches Mischen von Streuspektren mit unterschiedlichen Anteilen erhöhte sich dieser Zusammenhang. Größere Streuanteile auf der Satellitenskala führten zu einer höheren Übereinstimmung als auf der luftgestützten Skala.

Die vorliegende Arbeit zeigt, dass die Integration mehrerer zeitlicher, spektraler und räumlicher Daten notwendig ist, um die Komplexität und Heterogenität der arktischen Vegetationsreaktionen in Reaktion auf klimatische Veränderugen zu überwachen. Die Identifizierung spektral ähnlicher Vegetationsgemeinschaften kann durch die Verwendung hyperspektraler Daten außerhalb der Hauptsaison optimiert werden und führt zu einer detaillierteren Ausgangsdatenlage. Die Ergebnisse zeigen auch die Vorteile der Vegetationsfarbe

für die Verknüpfung von Boden- und Satellitendaten auf. Schließlich ist die Charakterisierung nicht-photosynthetischer Ökosystemkomponenten für eine genaue quantitative Fernerkundung der Vegetation auf der Satellitenskala entscheidend.

Abbreviations

A: Absorbance

AMAP: Arctic Monitoring and Assessment Program

ARI1: Anthocyanin Reflectance Index 1

ARI2: Anthocyanin Reflectance Index 2

BD: Band Depth

Car: Carotenoids

CCI: Chlorophyll Carotenoid Index

Chl_a: Chlorophyll *a*

Chl_b: Chlorophyll *b*

Chl_{a+b}: Total chlorophyll

$Chl_{a:b}$: Chlorophyll *a* to chlorophyll *b* ratio

Chl:*Car*: Chlorophyll to carotenoid ratio

CCD/CMOS: Charge Couple Device/Complementary Metal Oxide Semiconductor

CO_2: Carbon dioxide

CRI1: Carotenoid Reflectance Index 1

CRI2: Carotenoid Reflectance Index 2

DLR: Deutsches Zentrum für Luft- und Raumfahrt

DMF: DiMethylFormamide

DOY: Day of Year

DT: Dry tundra

EnMAP: Environmental Mapping and Analysis Program

ENVI: Exelis Visual Information Solutions

GIFOV: Ground Instantaneous Field of View

GPP: Gross Primary Production

IDL: Interactive Data Language

IPCC: Inter Governmental Panel on Climate Change

IVG: Imnavait Vegetation Grid

ISI: InStability Index

L_{down}: Downwelling radiance

L_{up}: Upwelling radiance

LTER: Long-term Ecological Research

MAT: Moist acidic tussock tundra

MNT: Moist nonacidic tundra

MT: Mossy tussock tundra

NDVI: Normalized Difference Vegetation Index

nm: nanometers

NIR: Near Infrared

NSF: National Science Foundation

PRI: Photochemical Reflectance Index

PSSRa: Pigment Specific Simple Ratio a

PSSRb: Pigment Specific Simple Ratio b

PSRI: Plant Senescence Reflectance Index

R: Surface reflectance

R^2: Coefficient of Determination

RGB: Red, Green, Blue

RMSE: Root Mean Square Error

$RMSE_{prop}$: Root Mean Square Error Propogated

SZU: Stable zone unmixing

TLRNA: Toolik Lake Research Natural Area

TVG: Toolik Vegetation Grid

µg/mg: microgram per miligram

UTM: Universal Transverse Mercator

VI: Vegetation Index

VNIR: Visible-Near Infrared

1   Introduction

1.1   Scientific Background and Motivation

Arctic ecosystems have been the subject of intensive study in the last 50 years corresponding to a rise in the understanding and awareness of anthropogenic climate change and the phenomenon of Arctic amplification. Conclusive evidence of anthropogenic climate change and an accelerated warming at high latitudes have been demonstrated for decades and succinctly summarized by the Intergovernmental Panel on Climate Change (IPCC, 2014) and the Arctic Monitoring and Assessment Program (AMAP, 2017). The IPCC has published global assessments on the science, impacts, and mitigation of climate change since 1990 (IPCC, http://www.ipcc.ch/) and the AMAP has facilitated extensive study and aggregation of past, current, and future Arctic climate change impacts from a broad social and scientific perspective (AMAP, https://www.amap.no/).

The sensitivity of Arctic ecosystems to climate change is closely linked to properties of the modern cryosphere (i.e. snow, freshwater ice, sea ice, glaciers, ice caps, ice sheets, and permanently frozen ground (permafrost)), the stability of which depends on a consistently cold mean state. The vulnerability of the modern cryosphere to warming can have cascading effects in terrestrial Arctic tundra ecosystems at local and regional scales. This will have an influence on the global carbon budget and energy balance, biodiversity, as well as socially and culturally important subsistence activities for northern communities (Bliss and Matveyeva, 1992; Chapin et al., 2000; Hinzman et al., 2005; Oechel and Vourlitis, 1994).

Despite low ecosystem productivity and species diversity, the Arctic tundra biome sequesters significant amounts of atmospheric carbon dioxide (CO_2) into organic-rich soils due to low turnover rates. The resulting large soil organic carbon pool in permafrost soils is vulnerable to disturbance in a warming Arctic (Grosse et al., 2011; Hugelius et al., 2014; Schuur et al., 2015; Tarnocai et al., 2009). In addition, the largely prostrate and patchy nature of vegetation cover in combination with prolonged annual snow cover results in high surface albedo compared to boreal forests acting as a cooling mechanism to the atmosphere (Callaghan and Jonasson, 1995; Chapin et al., 2005). Current warming trends are disrupting these biome-scale mechanisms setting off important positive feedback loops that effect terrestrial ecosystem functioning. For example, warmer temperatures mobilize carbon and

nutrients increasing soil respiration, further warming air temperatures while also facilitating the expansion and growth of erect woody shrub species (Myers-Smith et al., 2011; Karhu et al. 2014). The expansion of taller shrubs in turn increases the accumulation of drifting winter snow, insulating the soil leading to winter decomposition and further release of carbon and nutrients (Sturm 2011). An increase in taller shrubs also reduces surface albedo by protruding through the snow, darkening the surface and enhancing absorption of incoming solar radiation causing further warming.

Additional changes to the growing season length, snow cover duration, frequency and severity of permafrost disturbance, depth of the perennially unfrozen active layer and the resulting changes to surface hydrology further impacts local functioning of terrestrial Arctic tundra ecosystems (Bhatt et al., 2010; Chapin et al., 2005; Elmendorf et al., 2012; Serreze et al., 2000).

1.1.1   Arctic Tundra Vegetation

The Arctic tundra biome spans approximately 7 million km^2 north from the transitional treelines of the Boreal/Taiga forests to the polar deserts and icecaps of the globe's northern most reaches (Bliss and Matveyeva, 1992) . This vast area has been broadly divided into low and high Arctic dictated by the resulting ecological effects of latitude and climate. Bliss (1992) describes the low Arctic as dominated by tundra, a generic term indicating 80–100% vegetation cover, while the high Arctic is dominated by polar desert and polar semi-desert with only 10–30% vegetation cover. More recently, (Walker et al., 2005) enhanced this broad classification of circumpolar Arctic tundra by defining five bioclimatic subzones ranging from the warmest and most vegetated to the coldest and least vegetated. The subzones include, from north to south, and most to least vegetated: (E) low shrub, (D) erect dwarf shrub, (C) hemi-prostrate dwarf-shrub, (B) prostrate dwarf shrub, and (A) cushion forb. Following a similar latitudinal gradient of temperature and vegetation cover, species diversity and richness also decreases with increasing latitude (Matveyeva and Chernov, 2000) . Although at the biome scale, species diversity is low, at the community scale, Arctic tundra ecosystems have diversity comparable to temperate grasslands and coniferous biomes (Bliss et al., 1981).

Tundra plants are morphologically adapted to harsh Arctic conditions having low stature and low biomass with high allocations to below-ground structures. These adaptations allow

plants to take advantage of an atmospheric surface boundary layer which can be up to 8°C warmer than air temperatures at 1 m above the ground and to maximize surface area for uptake of limited soil nutrients (Mølgaard, 1982). The low stature of vegetation also maximizes winter insulation by snow and minimizes desiccation by wind (Oberbauer and Dawson, 1992; Sturm et al., 2005). Further adaptations include photosynthetic capacity at low light levels and accelerated growth and reproduction as soon as areas are snow free due to overwinter storage of carbohydrates, shoots and flower buds (Billings and Mooney, 1968). Though hardy, many Arctic tundra species are also slow growing with relatively low fecundity, characteristics that could limit their adaptability to climate change.

Recent meta-analyses, field-based studies, and landscape scale studies have highlighted the concurrent non-linear landscape and plot-scale changes in Arctic vegetation productivity, species composition, species distribution, vegetative growth, reproductive success, and phenology in response to climatic changes (Bhatt et al., 2010; Bjorkman et al., 2017, 2015; Elmendorf et al., 2012; Parmentier and Christensen, 2013; Prevéy et al., 2017; Walker et al., 2006; Zhang et al., 2007). The overall research outcomes of the last decades reveal the dynamic complexity and heterogeneity of the response of tundra vegetation to climate change and associated feedbacks over space and time. For example, based on plot-scale data Prevéy et al. (2017) showed how the sensitivity of Arctic plant phenology to warming differs across climatic gradients implying a possible convergence of phenology with implications for gene flow across latitudes. From the landscape scale, the well documented phenomenon of tundra "greening" over the past 30 years extracted from satellite imagery (Bhatt et al. 2010) has shown an unprecedented decline in the most recent decade in some areas linked to large scale atmospheric circulation (Bhatt et al., 2013). These two studies serve as examples of the complexity of climate-driven vegetation changes across scales, mechanisms, and parameters of interest bringing into focus the need for consistent and reproducible data at multiple spatial and temporal scales.

1.1.2 Remote Sensing of Arctic Tundra Vegetation

Remote sensing data provide the potential to monitor the responses of Arctic tundra vegetation to climate change and associated feedbacks at multiple scales (Laidler et al., 2008; Laidler and Treitz, 2003; Stow et al., 2004). The spatial extent of aerial and satellite remote sensing provides the capability to undertake landscape and ecosystem scale studies for this

remote biome. Factors such as persistent cloud cover, low sun angle, and a very short growing season present challenges for acquisitions of consistent frequency and quality. Thus, integration of multiple temporal, spatial, radiometric, and spectral resolution data sources is necessary for detailed characterization of Arctic vegetation.

Currently, broadband spectral vegetation indices (VIs) are the most common application of remote sensing data in Arctic ecosystems due to the applicability, availability and temporal record of the data (Laidler et al., 2008; Olthof and Latifovic, 2007; Raynolds et al., 2011, 2006; Stow et al., 2004). Broadband VIs have become well-established proxies for many vegetation parameters including primary productivity, biomass, and vegetation type (Boelman et al., 2003; Laidler and Treitz, 2003; Muller et al., 1999; Raynolds et al., 2011). These indices are mostly based on a ratio between the red and near infrared (NIR) parts of the electromagnetic spectrum to maximize signal to noise ratio by reducing illumination differences and background soil signals. The red part of the electromagnetic spectrum is sensitive to the photosynthetic pigment chlorophyll and the NIR to plant cellular and canopy structure. Taken together, reflectance in the red and NIR can indicate the amount of green or photosynthetically active vegetation (Tucker, 1979). The normalized difference vegetation index (NDVI) is perhaps the most common of these broadband indices and has been widely used in quantitative remote sensing of Arctic vegetation (Boelman et al., 2003; Laidler and Treitz, 2003; Muller et al., 1999; Raynolds et al., 2011).

The availability and record length of established broadband satellite programs such as Landsat and MODIS represent highly valuable ecological records. However, the interpretation of broadband indices outside of peak growing season and for characterization of smaller Arctic vegetation communities as well as local spatial variations is limited (Laidler and Treitz, 2003). High heterogeneity in community-scale vegetation composition, soil moisture, and an abundance of litter and non-vascular components complicates interpretation of NDVI and other broadband VIs in sparsely vegetated areas and outside of the peak-growing season (Liu et al., 2017). Buchhorn et al (2013) found that surface moisture reduced reflectance in the NIR, in turn underestimating the biomass signal of low-Arctic tundra. Further, van Leeuwen and Huete, (1996) have demonstrated the importance of standing litter and soil in the interpretation of biophysical parameters. These results suggest that the small-scale heterogeneity of Arctic tundra vegetation and other internal ecosystem components are not well characterized at non-peak times, limiting our ability to gain a

complete and detailed picture of vegetation change in the Arctic.

Recent advances in optical remote sensing such as the European Space Agency's Sentinel-2 satellite (Drusch et al., 2012) and the German Aerospace Agency's Environmental Mapping and Analysis Program (EnMAP; Guanter et al., 2015) offer new platforms with improved spectral resolution facilitating the use of narrowband indices and the entire spectral feature space (Schaepman et al., 2009) of the electromagnetic spectrum. The technical developments of these platforms will provide new methods for improved characterization and monitoring of changes in heterogeneous low Arctic ecosystems in the context of climate change and Arctic amplification.

1.1.3 *Hyperspectral Remote Sensing of Arctic Vegetation*

Across the visible-near infrared electromagnetic spectrum (VNIR; 400–1400 nm) vegetated surfaces reflect incoming solar radiation in distinct patterns due to a combination of biochemical and biophysical properties. Three major photosynthetic pigment groups absorb incoming radiation strongly in the visible range (400–700 nm) of the electromagnetic spectrum, creating unique spectral reflectance signatures and influencing vegetation colour (Coops et al., 2003; Curran, 1989; Gitelson and Merzlyak, 1998; Gitelson et al., 2002). In the NIR (700–1400 nm), cellular and canopy structure of vegetation control reflectance. A phenomenon known as multiple scattering of radiation between air and plant cellular walls as well as canopy structure leads to high reflectance values, known as the NIR plateau (Gausman, 1974). The wavelength at which the transition between pigment absorption and the NIR plateau occurs is called the red-edge and is commonly used in vegetation remote sensing (Roberts et al., 2011; Thenkabail et al., 2000). The development, degradation, and relative contribution of each pigment as well as the changes in cellular and canopy structure can be tracked using hyperspectral resolution remote sensing (Sims and Gamon, 2002; Stylinski et al., 2002; Tieszen, 1972; Ustin and Curtiss, 1990).

By targeting specific wavelengths with the use of hyperspectral remote sensing data, opportunities for detailed monitoring for vegetation differentiation and more detailed biophysical information can be derived aiding characterization of the complexity and heterogeneity of Arctic ecosystems over space and time (Liu et al., 2017). Specific wavelengths and narrow band VIs are generally associated with chlorophyll, carotenoid, and anthocyanin content, which facilitate specific functions that control overall photosynthetic capacity

and thus can be used to extract biophysical information.

The increasing frequency and availability of hyperspectral remote sensing data will help to address some of the challenges associated with detailed observation of Arctic ecosystems. Ground-based and aerial hyperspectral data are crucial for a better characterization of Arctic biophysical properties and for informing the interpretation of optical satellite missions. High spectral resolution data can maximize signal to noise ratios through targeting specific wavelengths that show sensitivity to targeted parameters and insensitivity to background signals. Recent studies have demonstrated the superiority of narrowband hyperspectral remote sensing in estimating percent green cover and differentiating vegetation communities in Arctic ecosystems (Bratsch et al., 2016; Buchhorn et al., 2013; Liu et al., 2017). Overall, the application of hyperspectral remote sensing in Arctic ecosystems will improve our understanding of the spatio-temporal heterogeneity of this ecosystem and the environmental gradients dictating it, and in turn will improve the accuracy of environmental change monitoring.

1.2   Aims and Objectives

The main objectives of this research were to further our understanding of advanced optical remote sensing observations of Arctic vegetation using a bottom-up, in-situ approach, ultimately to inform the use of satellite-based observations for a more complete understanding of the spatial and temporal complexity of Arctic tundra ecosystems. The specific research questions that provide the basis for the three chapters of this thesis are outlined below:

1. Does canopy-level spectral variability differ between dominant low-Arctic vegetation communities and does this variability change between major phenological phases?
2. How does canopy-level vegetation colour images recorded with high and low spectral resolution devices relate to phenological changes in leaf-level photosynthetic pigment content?
3. How does spatial aggregation of high spectral resolution data from the ground to satellite scale influence low-Arctic tundra vegetation signals and thereby what is the potential of upcoming hyperspectral spaceborne systems for low Arctic vegetation characterisation?

A multi-spatial, seasonal, and spectral scale approach was used to address the three research

questions. A unique combination of ground-based, airborne, and simulated spaceborne data at fine to coarse spatial and spectral resolutions as well as leaf-level photosynthetic pigment data was acquired at three phenological phases representing early season/leaf-out, peak season/maximum canopy extent, and late season/senescence (Figure 1-1).
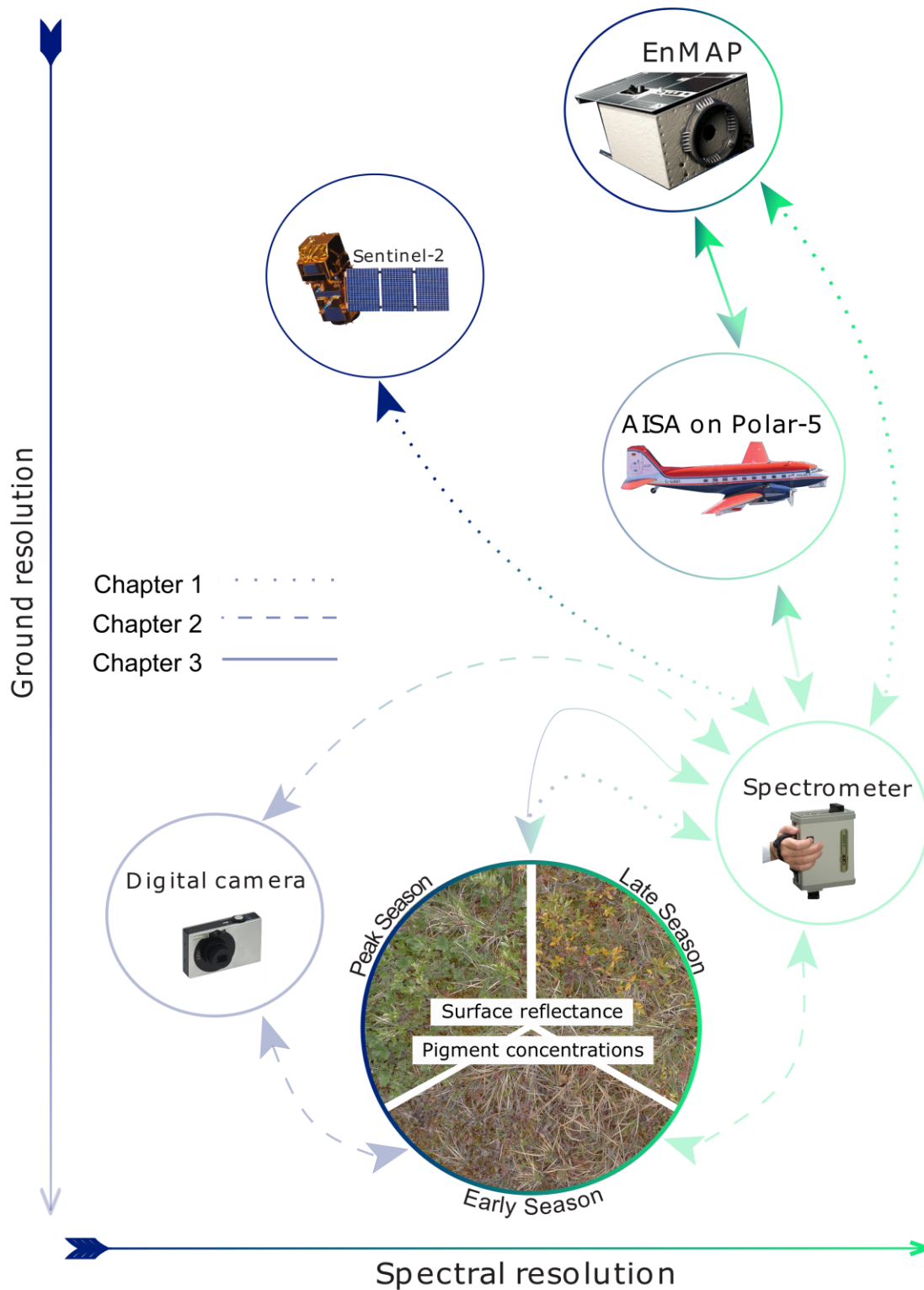
Figure 1-1 Schematic of the multi-scale approach of the thesis research and remote sensing devices used.

In the second chapter I explored the spectral variability of dominant vegetation communities at three major phenological phases using in-situ, canopy-level spectroscopy data and simulated broad and narrowband satellite reflectance spectra. I aimed to determine if by incorporating a phenological approach, the signal to noise ratio could be optimized thereby increasing the spectral separability of dominant vegetation communities. Following on this initial exploration of the importance of a phenological approach, in Chapter 3 I studied the potential of digital photography to act as a surrogate and gap-filling tool for in-situ, canopy-level spectroscopy and extracted biophysical indices. I related colour data extracted from digital photographs at three major phenological phases to both leaf-level photosynthetic pigment content and narrowband vegetation indices and discussed the implications for existing biophysical monitoring with broadband satellites. Finally, with the temporal and spatial complexity of this low-Arctic tundra ecosystem clearly demonstrated by the in-situ work of the previous two chapters, Chapter 4 studied how spatial aggregation influences vegetation hyperspectral signals from the ground to satellite scale. Using multi-spatial scale hyperspectral data from dominant vegetation communities as well as intrinsic ecosystem components of litter, moss, and water, we studied how these ubiquitous and complex components contribute to observed differences canopy-level reflectance from the ground to air- and space-borne scales.

1.3   Study Area and Data

1.3.1   Toolik Lake Research Natural Area

All fieldwork for this thesis was conducted between May and September of 2015 and 2016 based out of the Toolik Field Station (68°37'N, 149°35'W) in north central Alaska (Figure 1-2). The Toolik Field station and surrounding Toolik Lake Research Natural Area, which encompasses the two study sites of Toolik Lake and Imnavait Creek, is a National Science Foundation (NSF) Long-Term Ecological Research (LTER) station and has been an active research site since the 1970s. The study sites are situated within the Kuparuk River watershed on the North Slope of the Brooks Range, which includes the area from the summit of the Brooks Range north to the Arctic Ocean. The site is classified as Southern Arctic Foothills, a physiographic province of the North Slope (Walker et al., 1989) The Southern Arctic Foothills were subject to three major glaciation events (i.e. Sagavanirtok, Itkillik I, and Itkillik II) with the most recent deglaciation occurring 60,000–100,00 years before present

(Hamilton, 2003; Walker et al., 1989) . Distinct glacial terrain features and sandstone out-crops characterize the landscape with elevation changes as great as 750 m though the local relief is generally much lower. The Toolik Lake (68°37'N, 149°32'W) and Imnavait Creek (68°37'N, 148°18'W) sites differ primarily in their glacial histories with the Imnavait Creek site occurring on older Sagavanirtok substrates. The Toolik Lake landscape is more heter-ogeneous than Imnavait Creek with an abundance of small glacial lakes, kames, and mo-raines (Walker et al., 1994) The Southern Foothills are underlain by continuous permafrost and snow covered up to nine months a year. Predominant winds result in extensive redis-tribution of snow, particularly on north facing slopes and snow depths average around 50 cm prior to snowmelt. The climate of the Southern Foothills is highly variable as it is sub-ject to more continental influences than the more maritime northern physiographic prov-inces of the North Slope. The continental influence leads to warm summers and cold win-ters with mean annual temperature between -7 and -11°C and mean annual precipitation between 140 and 267 mm (Walker et al., 1989). There are minimal climatic differences between the Toolik Lake and Imnavait Creek study sites.

The dominant vegetation communities are dictated by surface moisture regimes and range from dry upland heaths, to moist tussock tundra, to wet sedge meadows. The most abundant vegetation type is the moist acidic tussock tundra community, which is representative of large swaths of the western North American and Siberian Arctic (Walker et al., 1994). The tussock-forming sedge *Eriophorum vaginatum* dominates this vegetation type and often occurs in complexes with *Sphagnum* species, ericaceous shrubs, and dwarf birch underlain by acidic substrates. The contribution of the secondary species is dictated by the size and age of the tussock; moss and shrubs are a common characteristic in larger, older tussocks (Shaver et al., 1986). There is a corresponding non-acidic moist sedge tundra community that is comparably dominant but is dominated by the non-tussock forming sedge *Carex bigelowii* with contributions from evergreen shrubs such as *Dryas integrifolia* (Walker et al., 1994). The most vegetated communities within the study site occur in upland water tracks and are dominated by the deciduous erect shrubs of diamond-leaf willow (*Salix pul-chra*) and dwarf birch (*Betula nana*). These communities have very defined margins with species taking advantage of surface depressions acting as pathways for overland water flow. The final group of communities is the dry to moist hemi-prostrate and prostrate dwarf shrub communities (Walker et al., 1994). The dry uplands are characterized by low-grow-

ing phenotypes (hemi-prostrate) of *Betula nana*, *Salix pulchra*, and Arctic blueberry (*Vaccinium uliginosum*) and occur on acidic substrates. The moister communities are dominated by the prostrate shrubs *Salix rotundifolia*, *Dryas integrifolia,* and *Cassiope tetragona* and occur on both acidic and nonacidic substrates. Wet sedge meadows were not included in this thesis due to the complex signal associated with standing water, a persistent feature of these communities.

All data collection was conducted in the Toolik Vegetation Grid (TVG), and Imnavait Vegetation Grid (IVG) (Figure 1-2). The TVG and IVG are 1 km^2 long-term monitoring sites established by NSF as part of the R4D (Response, Resistance, Resilience, and Recovery to Disturbance in Arctic Ecosystems) project. Elevation within the TVG ranges from 715–775 m above sea level with minimal changes in slope and aspect. In the IVG, elevation changes up to 100 m with a predominant west facing aspect in much of the grid. Both Vegetation Grids are systematically divided by equally spaced markers every 100 m corresponding to the intersection of Universal Transverse Mercator (UTM) coordinates. At each of the equally spaced markers excluding the outer bounds of the grid, are long-term 1 × 1 m monitoring plots representative of a single vegetation community that are described in detail by the Alaska Geobotany Center at the University of Alaska, Fairbanks (http://www.arcticatlas.org/) (Walker et al., 2002).
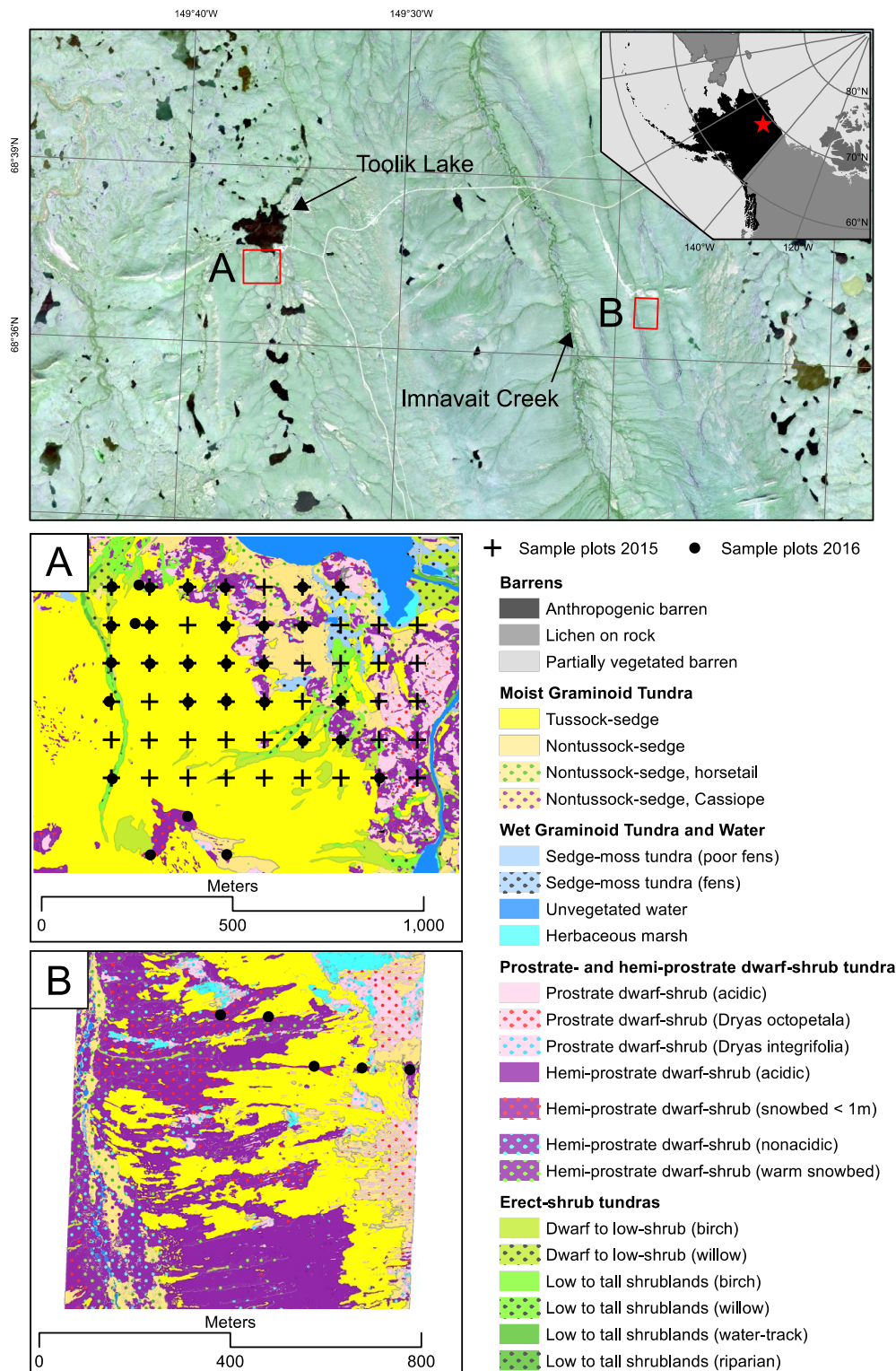
Figure 1-2 Location of the Toolik Lake and Imnavait Creek study sites in north central Alaska. Inset A is the Toolik Vegetation Grid and inset B is the Imnavait Vegetation Grid. Vegetation communities are defined by Walker et al., (2002). The crosses represent sites sampled in 2015; The closed circles represent sites visited in 2016. At each closed circle up to 4 additional sub plots in the immediate vicinity were sampled.

In 2015, data were collected systematically in a subset of the TVG encompassing the first 53 long-term monitoring plots from north to south (Figure 1-2A). This sampling design resulted in an uneven but spatially representative sample encompassing 12 distinct vegetation communities dominated by the moist acidic tussock tundra type. The IVG was not sampled in 2015. In 2016, data were collected with a more even sampling design in 37 long-term monitoring plots of the TVG encompassing eight distinct vegetation communities. In the IVG, a subset of six long-term monitoring plots located in the north-western part of the grid was sampled encompassing six distinct vegetation communities (Figure 1-2B). At each of the five long-term monitoring plots, four sub plots were established in the immediate vicinity, resulting in five plots per vegetation type and 20 plots total for the IVG.

Table 1-1 Overview of all data collected by year (2015 and 2016) and study site (Toolik Lake and Imnavait Creek). Plots is defined as the total number of long-term monitoring plots and sub plots visited. Obs is defined as the total number of individual measurements, photographs, or biomass samples collected for spectral reflectance, digital photographs, and pigment analysis.

| | | 2015 | | 2016 | | | |
| | | Toolik Lake | | Toolik Lake | | Imnavait Creek | |
Phenological phase	Parameter	Plots	Obs	Plots	Obs	Plots	Obs
Early season/ Leaf-out	Spectral reflectance	-	-	69	621	24	216
	Digital photographs	-	-	69	138	24	48
	Pigment analysis	-	-	26	105	-	-
Peak season/ Maximum canopy extent	Spectral reflectance	53	477	78	702	20	180
	Digital photographs	53	106	78	156	20	60
	Pigment analysis	27	173	30	115	-	-
Late season/ Senescence	Spectral reflectance	52	477	77	693	20	180
	Digital photographs	53	106	77	154	20	40
	Pigment analysis	26	98	27	99	-	-

1.3.2   In-situ Canopy-level Spectral Data

In-situ spectral radiance measurements were acquired in the TVG on July 5th, and August 24th in 2015 and June 4^{14th}, July 8th, and August 23rd in 2016. On June 17th, July 7th, and August 27th, 2016 spectral radiance measurements were collected in the IVG. The sequential data acquisition dates represent three seasons/major phenological phases of early season/leaf-out, peak season/maximum canopy extent, and late season/senescence. The spectroradiometer used was a GER 1500 with a spectral range of 350–1050 nm, 512 bands, a spectral resolution of 3 nm, a spectral sampling of 1.5 nm, and 8° field of view (Spectra Vista Co., Poughkeepsie, USA). Data were acquired under sunny conditions between 10:00 and 14:00 local time to ensure the highest solar zenith angle. Spectra were acquired with

the observer facing south at nadir approximately 1 m off the ground resulting in a Ground Instantaneous Field of View (GIFOV) of approximately 15 cm in diameter (Figure 1-3).

Figure 1-3 Example of field-based spectral reflectance measurement procedure in the Imnavait Creek study site,

Nine point measurements of upwelling radiance (L_{up}), collected systematically in a 3 × 3 grid from west to east and north to south in each 1 × 1 m plot were averaged and used to represent the spectral signature of each vegetation community. Downwelling radiance (L_{down}) was measured as the reflectance from a white Spectralon© plate. Surface reflectance (R) was processed as L_{up}/L_{down} × 100 (0–100%). Reflectance spectra were preprocessed with a Savitzky–Golay smoothing filter (n = 11) and subset to 400–900 nm to remove sensor noise at the edges of the radiometer detector.

1.3.3   True-colour Digital Photographs

In the same 1 × 1 m plots where in-situ spectral data were acquired, true-colour digital photographs were taken within days of the spectral acquisitions in both 2015 (TVG: July 8th, August 27th) and 2016 (TVG: June 14th, July 12th, August 18th; IVG: June 17th, July 10th, August 19th). Images were taken at nadir approximately 1 m off the ground with a

white 1 × 1 m frame for registration of off nadir images (Figure 1-4).

Figure 1-4 Example of the nadir digital photography in a single long-term monitoring plot at three major phenological phases. From left to right the photographs represent early, peak, and late season

Images were taken with a consumer-grade digital camera (Panasonic DM3 LMX, Japan) in raw format, between 10:00 and 14:00, under uniform cloud cover to reduce the influence of shadow and illumination differences. The digital camera collects colour values by means of the Bayer matrix (Bayer 1976) with individual pixels coded with a red (R), green (G), and blue (B) value between 0 and 256. RGB values of each pixel in each image were extracted using ENVI+IDL (Version 4.8; Harris Geospatial, Boulder, Colorado). To reduce the impact of non-nadir acquisitions, photo registration was done using the 1 × 1 m frame.

1.3.4 Leaf-level Photosynthetic Pigment Data

To measure leaf-level pigment content, leaves and stems (n = 213) of the dominant vascular species in a subset of the sample plots were collected at peak, and late season in 2015 and early, peak, and late season 2016 for chlorophyll and carotenoid analysis. Samples were placed in porous tea bags and preserved in a silica gel desiccant in an opaque container for up to three months until pigment extraction (Esteban et al. 2009). Each sample was homogenized by grinding with a mortar and pestle. Approximately 1.00 mg (+/- 0.05 mg) of homogenized sample was placed into a vial with 2 ml of dimethylformamide (DMF). Vials were then wrapped in aluminum foil to eliminate any degradation of pigments due to UV light and stored in a fridge (4°C) for 24 hrs. Samples were measured into a cuvette prior to spectrophotometric analysis (Milton Roy Spectronic 1201, ThermoFisher Scientific, Waltham, MA, USA) (Figure 1-5).

Figure 1-5 Left: Example of a silica gel-preserved biomass sample (*Salix pulchra*) prior to grinding and extraction. Right: Spectronix 1201 spectrophotometer used to measure absorbance (A) and pigment concentrations.

Bulk pigments concentrations were then estimated using a spectrophotometer measuring absorption at 646.8, 663.8 and 480 nm (Porra et al., 1989) . Absorbance (*A*) values at specific wavelengths were transformed into µg/mg concentrations of chlorophyll *a*, *Chl$_a$*, chlorophyll *b*, *Chl$_b$*, total chlorophyll, *Chl$_{a+b}$*, carotenoids, *Car*, using the following equations:

$$Chl_a = 12.00 * A^{663.8} - 3.11 * A^{646.8}$$ (1.1)

$$Chl_b = 20.78 * A^{646.8} - 4.88 * A^{663.8}$$ (1.2)

$$Chl_{a+b} = 17.67 * A^{646.8} + 7.12 * A^{663.8}$$ (1.3)

$$Car = (A^{480} - Chl_a) / 245$$ (1.4)

The chlorophyll *a* to chlorophyll *b* (*Chl$_{a:b}$*), as well as the chlorophyll to carotenoid ratios (*Chl*:*Car*) were calculated by dividing eq. (1.1) by eq. (1.2) and eq. (1.3) by eq. (1.4), respectively. Pigment concentration was calculated as the average concentration of the dominant species in each plot.

1.3.5 Airborne AISA Imagery

Hyperspectral imagery was acquired using an Airborne Imaging Spectrometer for Applications (AISA-Eagle sensor) mounted in a Basler BT-67 aircraft on August 27th 2016 under clear conditions between 12:20 and 12:50 pm local time. The acquisition was part of the AIRMETH campaign, a joint Alfred Wegener Institute and the German Research Centre for Geosciences (GFZ) mission in Alaska and the western Canadian Arctic. Five flight lines

were flown south to north in a west to east pattern at an altitude of approximately 1 km. Only the first three of the five flight lines flown were used in this thesis due to illumination issues in the last two acquired flight lines. The three flight lines encompassed an area approximately 700 ha in size, covering the entire TVG (Figure 4-2A). The AISA Eagle imager had 130 bands (404.9 – 1002.5 nm) with a bandwidth of 4 nm and a spatial resolution of 1.3 m nadir (Figure 4-2B). The data were atmospherically and radiometrically corrected. The radiometric correction was performed using instrument and sensor specific manufacturer's software CaligeoPro ©. The direct geometric correction was also performed using manufacturer's software by simultaneously using the measured IMU/GPS data stream. Subsequently, the geocorrected radiance data was atmospherically corrected based on ATCOR4 (Richer and Schläpfer, 2018). During this procedure a small spectral shift of the AISA sensor was detected and corrected. The resulting surface reflectance flight lines were subset to the first 110 bands (404.9 – 907.6 nm).

1.3.6   Simulated EnMAP and Sentinel-2 Reflectance Spectra

The upcoming EnMAP satellite will have a total of 242 bands (423–2450 nm) with a spectral resolution between 6.5 and 10 nm, and a ground sampling distance of approximately 30 m. A total of 95 EnMAP spectral bands were within the spectral range of the GER field spectroradiometer. To obtain EnMAP-like reflectance spectra, the GER ground-based surface reflectance spectra were interpolated to 1 nm and then spectrally resampled using the spectral response curves of the 95 visible near infrared (VNIR) EnMAP spectral bands to produce surface reflectance data commensurate with the EnMAP sensor. The Sentinel-2 satellite has 13 spectral bands (443–2190 nm) with a spectral resolution between 15 and 120 nm, from which the first 10 bands (band 1–8, 8a, 9) covered the spectral range of the GER radiometer. Data were simulated in the same way as the EnMAP procedure; interpolated to 1 nm and resampled using the spectral response curves of the 10 VNIR Sentinel-2 bands.

1.3.7   Simulated EnMAP Imagery

As part of the scientific preparatory program, an EnMAP End-to-End Simulation tool (EeteS) was developed by the GFZ to provide a complete and accurate simulation of image generation, calibration, and the processing chain (Segl et al., 2012, 2010). The individual AISA flight lines were used as input to the EeteS and Level 2A EnMAP-like flight lines of

the study area were generated (Figure 4-2C). The simulation begins by transforming the AISA reflectance data to EnMAP reflectance data by modelling atmospheric conditions, and accounting for the differences in spatial, spectral, and radiometric specifications of the two sensors. An EnMAP image is then simulated through the processing chain from onboard calibration, to atmospheric correction to orthorectification. The resulting EnMAP image had 78 bands (423 – 903 nm).

1.4 Thesis Structure and Author Contributions

The thesis contains an introduction (Chapter 1), three main chapters representing three manuscripts (Chapter 2, 3, and 4), and an overall synthesis and discussion (Chapter 5). Chapters 2 and 3 are original publications that have been published in peer-reviewed and ISI listed scientific journals and the third (Chapter 4) has been accepted for review in a peer-reviewed, ISI listed scientific journal. All work represents stand-alone independent research. There is some overlapping general information between the publications particularly in the description of the study area, methods, and introduction sections as all work was conducted in the same study area and data were used in multiple applications.

1.4.1 Chapter 2 - A Phenological Approach to Spectral Differentiation of Low-Arctic Tundra Vegetation Communities, North Slope Alaska

Authors: Alison L. Beamish, Nicholas C. Coops, Sabine Chabrillat and Birgit Heim

Remote Sensing, 2017, 9(11), 1200; doi:10.3390/rs9111200

This first published manuscript presents an exploration of the spectral variability of low-Arctic tundra in three major seasons representing early, peak, and late growing season. A. Beamish and B. Heim created the sampling design. A. Beamish conducted all fieldwork as well as statistical analyses, interpretation, generation of figures and tables, and wrote the manuscript. N. Coops contributed to the data analysis, data interpretation, manuscript organization and reviews. S. Chabrillat and B. Heim contributed to data interpretation and manuscript reviews.

1.4.2   Chapter 3 - Monitoring Pigment-driven Vegetation Changes in a Low Arctic Tundra Ecosystem Using Digital Cameras

Authors: Alison L. Beamish, Nicholas C. Coops, Txomin Hermosilla, Sabine Chabrillat, and Birgit Heim

Ecosphere, 2018, 9(2):e02123. 10.1002/ecs2.2123

This second published manuscript presents an assessment of the ability of digital photographs to act as a surrogate for in-situ spectral data to monitor pigment-driven changes in vegetation. A. Beamish and B. Heim created the sampling design. A. Beamish conducted all fieldwork and laboratory analyses as well as statistical analyses, interpretation, generation of figures and tables, and wrote the manuscript. T. Hermosilla wrote the code and performed data extraction from the digital photographs as well as contributed to reviews of the manuscript. N. Coops contributed to the data analysis methods, data interpretation, manuscript organization and reviews. S. Chabrillat and B. Heim contributed to data interpretation and manuscript reviews.

1.4.3   Implications of Litter and Non-vascular Components on Multiscale Hyperspectral Data in a low-Arctic Ecosystem

Authors: Alison L. Beamish, Nicholas C. Coops, Sabine Chabrillat, Maximilian Brell, and Birgit Heim

Remote Sensing of Environment, 2018, *in review* RSE-D-18-00542

The third manuscript, accepted for review in Remote Sensing of Environment, examines the spatial aggregation of spectral signatures of dominant vegetation communities and how non-photosynthetic and non-vascular ecosystem components contribute to signal. Artificial linear mixture analyses were used to examine the contribution of these components from the ground (15 cm) to the satellite scale (30 m). A. Beamish and N. Coops created the concept for the paper. A. Beamish conducted fieldwork, data analyses, interpretation, generation of figures and tables, and wrote the manuscript. Sabine Chabrillat supported with data analysis, data interpretation, and manuscript reviews. M. Brell conducted the atmospheric correction of the aerial remote sensing data. N. Coops contributed to the data analysis methods, data interpretation, manuscript organization and reviews. B. Heim supported with fieldwork during the aerial overflight and contributed to data interpretation and manuscript reviews.

2 A Phenological Approach to Spectral Differentiation of Low Arctic Tundra Vegetation Communities, North Slope Alaska

Alison L. Beamish [1], Nicholas C. Coops [2], Sabine Chabrillat [3] and Birgit Heim [1]

[1]   Alfred Wegener Institute, Helmholtz Centre for Polar and Marine Research, Research Unit Potsdam, Telegrafenberg, A45, 14473 Potsdam, Germany

[2]   Integrated Remote Sensing Studio (IRSS) Faculty of Forestry, University of British Columbia, 2424 Main Mall, Vancouver, BC V6T 1Z4, Canada

[3]   Helmholtz Centre Potsdam GFZ German Research Centre for Geosciences, Telegrafenberg, 14473 Potsdam, Germany

2.1 Abstract

Arctic tundra ecosystems exhibit small-scale variations in species composition, micro-topography as well as significant spatial and temporal variations in moisture. These attributes result in similar spectral characteristics between distinct vegetation communities. In this study we examine spectral variability at three phenological phases of leaf-out, maximum canopy, and senescence of ground-based spectroscopy, as well as a simulated Environmental Mapping and Analysis Program (EnMAP) and simulated Sentinel-2 reflectance spectra, from five dominant low Arctic tundra vegetation communities in the Toolik Lake Research Area, Alaska, in order to inform spectral differentiation and subsequent vegetation classification at both the ground and satellite scale. We used the InStability Index (ISI), a ratio of between endmember and within endmember variability, to determine the most discriminative phenological phase and wavelength regions for identification of each vegetation community. Our results show that the senescent phase was the most discriminative phenological phase for the identification of the majority of communities when using both ground-based and simulated EnMAP reflectance spectra. Maximum canopy was the most discriminative phenological phase for the majority of simulated Sentinel-2 reflectance data. As with previous ground-based spectral characterization of Alaskan low Arctic tundra, the blue, red, and red-edge parts of the spectrum were most discriminative for all three reflectance datasets. Differences in vegetation colour driven by pigment dynamics appear to be the optimal areas of the spectrum for differentiation using high spectral resolution field spectroscopy and simulated hyperspectral EnMAP and multispectral Sentinel-2 reflectance spectra. The phenological aspect of this study highlights the potential exploitation of more

extreme colour differences in vegetation observed during senescence when hyperspectral data is available. The results provide insight into both the community and seasonal dynamics of spectral variability to better understand and interpret currently used broadband vegetation indices and also for improved spectral unmixing of hyperspectral aerial and satellite data which is useful for a wide range of applications from fine-scale monitoring of shifting vegetation composition to the identification of vegetation vigour.

2.2   Introduction

Arctic tundra ecosystems exhibit small-scale variations in micro-topography as well as significant spatial and temporal variations in soil moisture. As a result, vegetation composition also exhibits small-scale heterogeneity leading to, at the community scale, Arctic tundra ecosystems having comparable species diversity to temperate grasslands and coniferous biomes (Bliss et al., 1981). Areas with common species complexes (i.e., multiple species occurring together) in combination with surface moisture conditions define tundra vegetation communities at the smallest scale, according to the Circumpolar Arctic Vegetation Map (Walker et al., 2005). Communities are often broadly divided into moisture regime such as xeric (dry), mesic (moist), or hydric (wet), and soil acidity (acidic, non-acidic) and then further divided depending on the species complexes present (Walker et al., 2005, 1994). Often the same species can be observed in multiple distinct complexes as different phenotypes. Large homogenous patches of one or two species rarely exist outside water tracks, disturbed areas, or dry uplands where erect and prostrate dwarf shrub species dominate. This combination of small-scale heterogeneity in vegetation composition and soil moisture as well as the prostrate nature of tundra species leads to highly mixed, variable, and often similar spectral signatures between distinct vegetation communities. The sometimes-dominant presence of non-vascular components (mosses and lichens) and barren areas also contribute to the unique spectral signatures of tundra landscapes (Hope et al., 1993). This high spectral similarity can be observed with ground-based Visible-Near Infrared (VNIR) remote sensing data making spectral separation challenging (Bratsch et al., 2016; Buchhorn et al., 2013; Riedel et al., 2005).

Currently, the broadband Normalized Difference Vegetation Index (NDVI) is the most commonly applied spectral index in Arctic vegetation remote sensing due to the simplicity, availability, and temporal scale of the data (Laidler et al., 2008; Olthof and Latifovic, 2007;

Stow et al., 2004). NDVI uses reflectance in the red and Near Infrared (NIR) wavelength regions and has been used as a proxy for many parameters of Arctic vegetation such as productivity, biomass, and community classification (Boelman et al., 2003; Laidler and Treitz, 2003; Muller et al., 1999). However, interpretation of NDVI is complex, especially outside of the peak growing season, given the aforementioned spatial and temporal heterogeneity of the biotic (vegetation composition) and abiotic (soil moisture) parameters of tundra ecosystems. Variable moisture conditions, similar canopy structure between some distinct tundra vegetation communities, and an abundance of standing litter all influence spectral reflectance in the NIR, which is sensitive to canopy and leaf cellular structures as well as moisture (Tucker, 1979). Previous research by Buchhorn et al. (2013) in low Arctic Alaska showed that surface moisture masked biomass reflectance in the NIR, indicating that NDVI values in phenological phases or vegetation communities with excessive surface moisture could be problematic. An additional consideration is that of standing litter, a ubiquitous characteristic of tundra vegetation communities, which has shown high reflectance in the NIR, especially in sparsely vegetated communities (Laidler and Treitz, 2003; van Leeuwen and Huete, 1996).

In the visible range of reflectance (400–700 nm), three major vegetation pigment groups absorb strongly in the visible spectrum creating unique spectral signatures and dictating plant colour (Curran, 1989). Carotenoid pigments that absorb in the blue and short wavelengths of the green spectral region are responsible for absorbing incident radiation and for providing energy to photosynthesis (Bartley and Scolnik, 1995; Young and Britton, 1990). Anthocyanins that absorb strongly in the green and in the short wavelengths of the red spectral region provide photoprotection as well as physical damage protection and influence recovery (Chalker-Scott, 1999; Close and Beadle, 2003; Gould et al., 2002; Steyn et al., 2002). Both carotenoids and anthocyanins have overlapping absorption regions with chlorophyll absorption, which occurs in the blue and red spectral region, respectively. Chlorophylls are the fundamental photosynthetic pigments that control light absorption by vegetation and in turn control photosynthetic capacity and primary productivity.

Given the seasonal dynamics of the biotic and abiotic parameters influencing spectral reflectance of tundra vegetation communities, it is important to consider how this influence changes over the growing season. Spectral differentiation of tundra vegetation communities at the ground-based scale and, potentially, with remote sensing imagery, could be improved

in different phenological phases through targeting specific wavelength regions where spectral differences are maximized and spectral variability is minimized. Previous research of ground-based spectral data has shown that narrow wavelengths (as opposed to broadband representations) in the blue, red, and, red-edge regions of the spectrum are important for differentiation of common Alaskan low Arctic vegetation communities at early and peak phenological stages, and that the location of the most important spectral regions for differentiation shifts with phenological phase (Bratsch et al., 2016). These spectral regions are strongly associated with pigment absorption and the observed shifts with phenological phase further support the role of pigment production and degradation in detailed assessment of tundra vegetation.

Hyperspectral ground-based remote sensing data are critical for supporting the development and interpretation of optical satellite missions. Accurate and detailed remote sensing of tundra communities will likely improve with the use of hyperspectral remote sensing data such as the upcoming Environmental Mapping and Analysis Program (EnMAP; Deutsches Zentrum für Luft- und Raumfahrt, (DLR)) (Guanter et al., 2015) and the operational, multispectral Sentinel-2 mission (Drusch et al., 2012). These two platforms represent new tools in Arctic vegetation remote sensing by combining improved spatial resolution and revisit rate (Sentinel-2: 10–20 m and five-day revisit rate with a constellation of two satellites) and spectral resolution to the freely available pool of remote sensing data. The operational Sentinel-2 satellites have 8 bands in the VNIR (490–865 nm) at a spatial resolution between 10 m and 20 m, and it is particularly promising for accurate tundra vegetation monitoring due to several narrow spectral bands within the red-edge wavelength region (~20–30 nm width at 705 nm, 740 nm, 783 nm, and 865 nm). EnMAP will have a total of 89 narrow continuous and contiguous bands (~6.5 nm width) in the VNIR at a spatial resolution of 30 m with a nominal revisit time of 27 days and an across track off-nadir pointing revisit time of 4 days. Detailed assessment of tundra vegetation that can be provided by these platforms will help to improve our understanding of the impacts of global change on tundra vegetation change from photosynthetic activity to shifting species composition.

In the following study we use ground-based VNIR spectral measurements collected at the canopy level in three major phenological phases to investigate the spectral variability within and between dominant Arctic tundra vegetation communities and how this changes

over the growing season. We also investigate the spectral variability of dominant communities with broader spectral resolution using simulated Sentinel-2 and simulated EnMAP spectral reflectance data. For this, the InStability Index (ISI) was calculated, a ratio of within and between endmember spectral variability at leaf-out, maximum canopy, and senescence, representing the start, middle, and end of the growing season, in a low Arctic tundra ecosystem. The ISI is a relatively new technique used as a first step in reducing spectral dimensionality of hyperspectral data before classification methods such as spectral angle mapper (Chance et al., 2016; Peterson et al., 2015; Somers and Asner, 2013; Somers et al., 2011, 2010) and has not yet been applied in Arctic tundra ecosystems. Based on the ISI calculations, this paper focuses on (1) the identification of the most discriminative (i.e., low within endmember variability and high between endmember variability) phenological phase for identifying dominant vegetation communities; (2) within the most discriminative phenological phase, identification of the most discriminative wavelength regions for identification of dominant vegetation communities; (3) determination of how the ISI results differ between ground-based and simulated recent and upcoming satellite (EnMAP, Sentinel-2) reflectance spectra.

2.3 Materials and Methods

2.3.1 Study Site and Low Arctic Vegetation Types

The study was conducted in the Toolik Lake Research Natural Area (TLRNA) (68°62.57′N, 149°61.43′W), which lies in the Kuparuk River watershed on the North Slope of the Brooks Range, Alaska. The TLRNA is representative of the Southern Arctic Foothills, a physiographic province of the North Slope with a combination of moist tussock tundra, wet sedge meadows and dry upland heaths (Walker et al., 1989). Data collection took place in a subset of the Toolik Vegetation Grid, a 1 km^2, long-term monitoring site established by the National Science Foundation (NSF) as part of the Department of Energy's R4D (Response, Resistance, Resilience, and Recovery to Disturbance in Arctic Ecosystems) project (Figure 2-1). The elevation of the Toolik Vegetation Grid ranges from 715–775 m a.s.l. with minimal changes in slope and aspect. Long-term 1 × 1 m monitoring plots are located beside equally spaced markers (100 m) delineating the intersection of the Universal Transverse Mercator (UTM) coordinates of the study area. The 1 × 1 m plots are representative of a single vegetation community at each site marker covering several square meters. The plots

24

are classified based on work by the Alaska Geobotany Center (http://www.arcticat-las.org/maps/themes/tl5c/tl5cvg) and the Circumpolar Arctic Vegetation Map (Walker et al., 2005). For the purpose of this study, we grouped the distinct communities as defined by the Alaska Geobotany Center into broader communities based on descriptions in Bratsch et al. (2016). These groups include moist acidic tussock tundra (MAT), moist non-acidic tundra (MNT), shrub tundra (ST), and mossy tussock tundra (MT). We added a fifth group of dry tundra (DT) to this analysis. Additionally, our definition of ST differed slightly as we restricted our measurements to communities with erect dwarf-shrubs *Salix pulchra* and *Betula nana,* while Bratsch et al. (2016) included measurements of the erect shrub *Salix alaxensis* and an erect phenotype of *Betula nana*. Descriptions of the broad communities based on Bratsch et al. (2016), descriptions of the distinct vegetation communities, and percentage cover within the Toolik Vegetation Grid, based on data provided by the Alaska Geobotany Center are presented in Table 2-1.Within the Toolik Vegetation Grid, the sampled vegetation communities make up 73% of the total vegetation cover and the abundances of each community within the grid are representative of larger areas in the Alaskan low Arctic (Bliss and Matveyeva, 1992; Muller et al., 1999; Tenhunen et al., 1992), and can be used for extrapolation to larger scale observations such as from satellite imagery at 10 m, 20 m or 30 m.
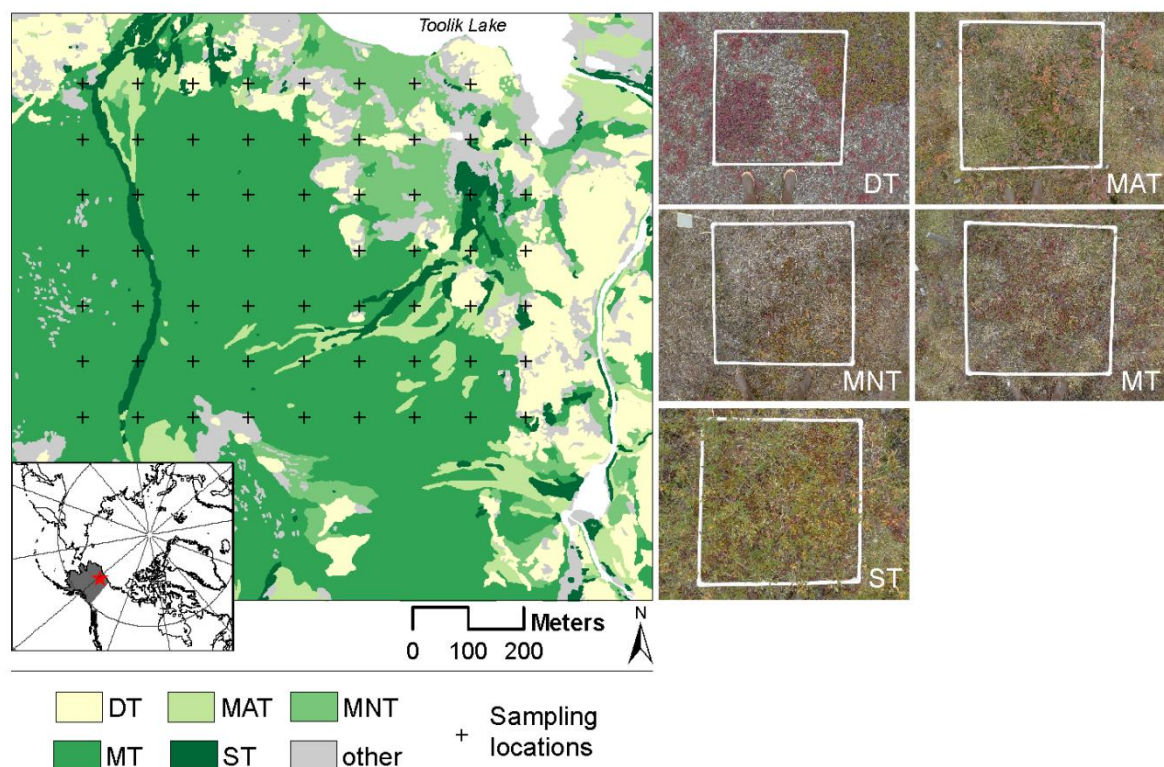
Figure 2-1 Sampling area within the Toolik Lake Research Natural Area (68°62.57′N, 149°61.43′W). Colours represent the aggregated vegetation communities as defined in Bratsch et al. (Bratsch et al., 2016) . Insets represent typical senescent stage photographs of the five vegetation communities, and the white frame represents a 1 × 1 m sampling area. DT: Dry tundra, MAT: Moist acidic tussock tundra, MNT: Moist nonacidic tundra, MT: Mossy tussock tundra, ST: Shrub tundra. Each black cross represents the location of the intersection of Universal Transverse Mercator (UTM) coordinates of the study area with a 1 × 1 m long-term monitoring plot near to where ground-based spectral data were collected.

Table 2-1 Detailed descriptions of the vegetation communities as defined by Bratsch et al. (2016) and the sub-communities included as defined by the Alaska Geobotany Center. % cover refers to the percentage cover of each community type within the 1 × 1 km Toolik Vegetation Grid.

Community	Description	Sub-community	Description	% Cover
Dry tundra	Upland sparsely vegetated areas with prostrate dwarf shrubs (Salix glauca) and abundant lichens	Dry tundra	Dryas octopetala-Selaginella sibirica, Dryas octopetala-Salix glauca: Prostrate dwarf-shrub, forb, fruticose-lichen tundra. Xeric, acidic, windblown or shallow winter snow cover, stony or with considerable bare soil. Ridge crests, dry river terraces. Dominated by Dryas octopetala, occasionally with Salix glauca.	4.2
Moist acidic tussock tundra	Occurs on soils with pH < 5.0–5.5 and is dominated by dwarf erect shrubs such as Betula nana and Salix pulchra, graminoids species (Eriophorum vaginatum) and acidophilous mosses	Shrubby tussock tundra dominated by Betula nana	Betula nana-Eriophorum vaginatum. Dwarf-shrub, sedge, moss tundra (shrubby tussock tundra dominated by dwarf birch, Betula nana). Mesic to subhygric, acidic, moderate snow. Lower slopes and water-track margins. Mostly on Itkillik I glacial surfaces.	3.1
		Shrubby tussock tundra dominated by Salix pulchra	Salix pulchra-Carex bigelowii. Dwarf-shrub, sedge, moss tundra (shrubby tussock tundra dominated by diamond-leaf willow, Salix pulchra). Subhygric, moderate snow, lower slopes with solifluction.	3.0
Moist non-acidic tundra	Dominated by mosses, graminoids (Carex bigilowii), and prostrate dwarf shrubs (Dryas integriolia)	Moist non-acidic tundra	Carex bigelowii-Dryas integrifolia, typical subtype; Tomentypnum nitens-Carex bigelowii, Salix glauca subtype: Nontussock sedge, dwarf-shrub, moss tundra (moist nonacidic tundra). Mesic to subhygric, nonacidic (pH > 5.5), shallow to moderate snow. Solifluction areas and somewhat unstable slopes. Some south-facing slopes have scattered glaucous willow (Salix glauca).	5.8

Table 2-1 continued

Com-munity	Description	Sub-commu-nity	Description	% Cover
Mossy tussock tundra	A moist acidic tussock tun-dra-type com-munity domi-nated by sedges (E. vaginatum) and abundant Sphagnum spp.	Moist acidic tussock tun-dra	Eriophorum vaginatum-Sphagnum; Carex bigelowii-Sphagnum: Tussock sedge, dwarf-shrub, moss tundra (tussock tundra, moist acidic tundra). Mesic to subhygric, acidic, shallow to moderate snow, stable. This unit is the zonal vegetation on fine-grained substrates with ice-rich permafrost. Some areas on steeper slopes with solifluc-tion are dominated by Bigelow sedge (Carex bigelowii).	54.2
Shrub tundra	Dominated by dwarf shrubs Betula nana and Salix pul-chra inter-spersed with graminoids, forbs, lichens and mosses	Dwarf shrub tundra domi-nated by Bet-ula nana	Betula nana-Rubus chamaemorus. Dwarf-shrub, moss tundra dominated by dwarf birch (Betula nana). Subhygric to hygric, acidic, moderate to moderately deep snow. Upland water tracks, margins of water tracks and lower slope areas. Somewhat drier areas have abundant lichens.	1.7
		Dwarf shrub tundra domi-nated by Sa-lix pulchra	Salix pulchra-Sphagnum warnstorfii. Dwarf-shrub or low-shrub tundra domi-nated by willows (Salix pulchra). Sub-hygric, acidic, moderate to moderately deep snow. Margins of upland water tracks, palsas and high-centered polygons.	1.1

2.3.2 Ground-Based Data and Sampling Protocol

To capture phenological variations in spectral reflectance, data were collected systemati-cally at three major phenological phases representing the start, middle, and end of the grow-ing season in 2015 and 2016 in 1 × 1 m plots within the Toolik Vegetation Grid. Spectral data were acquired to correspond to leaf-out (16 June 2016, Day of Year (DOY) 168), maximum canopy (7 July 2015, DOY 188 and 11 July 2016, DOY 193), and senescence (22 August 2015, DOY 234 and 17 August 2016, DOY 229). Ground-based phenological observations (n = 178) from the Toolik Field Station Environmental Data Center (https://toolik.alaska.edu/edc/, 2017), which monitors 15 dominant species in the dominant MAT vegetation type, confirm the dates as good approximations of these phenological phases. Leaf-out spectral data collection took place two weeks after average first date leaf-out (29 May 2016, DOY 150) accurately capturing the middle of the leaf-out. Maximum canopy data collection took place four days and one week after the average date of the last petal drop in 2015 (3 July, DOY 184) and 2016 (3 July, DOY 185), respectively. By col-lecting data after most species finished flowering, the maximum canopy signal was likely

less contaminated by non-green signals and fell within the time of peak productivity of the ecosystem. Senescence data were collected one month and three weeks after the average date of the first colour change, referring to the first visible signs of senescence in 2015 (18 July, DOY 199) and 2016 (27 July, DOY 209), respectively. The phenological phases used in this study are meant to represent the overall state of the vegetation, not specific phenological events such as the first day of the leaf-out, or first day senescence. Leaf-out is intended to capture the period when most of the vegetation has leafed-out but is not yet fully expanded; maximum canopy is intended to capture when most of the vegetation has fully expanded; senescence is intended to capture when most of the vegetation has experienced a colour change.

Spectral radiance measurements were collected using a GER 1500 field spectrometer (350–1050 nm; 512 bands, spectral resolution 3 nm, spectral sampling 1.5 nm, and 8° field of view). Spectra were collected under clear weather conditions at the highest solar zenith angle between 10:00 and 14:00 local time. Data were collected at nadir approximately 1 m off the ground resulting in a Ground Instantaneous Field of View (GIFOV) of approximately 15 cm in diameter. Nine point measurements of upwelling radiance (L_{up}) were collected in 1 × 1 m plots representative of the five vegetation communities and averaged to characterize the spectral variability and to reduce noise. Downwelling radiance (L_{down}) was measured as the reflectance from a white Spectralon© plate. Surface reflectance (R) was processed as $L_{up}/L_{down} \times 100$ (0–100%). Reflectance spectra were preprocessed with a Savitzky–Golay smoothing filter (n = 11) and subset to 400–985 nm to remove sensor noise at the edges of the radiometer detector. The total number of plots and spectral measurements collected over the two years by vegetation community is presented in Table 2-2.

Table 2-2 Number of spectral measurements and independent plots sampled by vegetation community.

Community	Spectral Measurements	Distinct Plots
Dry tundra	63	7
Moist acidic tussock tundra	126	17
Moist non-acidic tundra	144	14
Mossy tussock tundra	153	16
Shrub tundra	126	14

A continuum removal transformation of the ground-based reflectance spectra was conducted using the transform_speclib function in the hsdar package (Lehnert et al., 2016) in R Studio (R Core Team, 2015). This process normalizes reflectance spectra to a common baseline for comparison of absorption features. The removal of the continuum slope corrects the band minimum to the true band centre enhancing absorption features (Clark and Roush, 1984). A segmented hull continuum line was generated connecting local maxima of the reflectance spectra. The segmented hull continuum approach was applied in this analysis because it is superior in identifying small absorption features (Clark and King, 1987). Band depth (BD_λ) was calculated for each absorption feature using the following equation:

$$BD_\lambda = 1 - \frac{R_\lambda}{CV_\lambda} \tag{2.1}$$

where R is the continuum removed reflectance at wavelength λ; and CV is the continuum value at wavelength λ. The maximum band depth was calculated as the maximum band depth between a specified wavelength range.

2.3.3 EnMAP and Sentinel-2 Surface Reflectance Simulation

The upcoming EnMAP satellite will have a total of 242 bands (423–2450 nm) with a spectral resolution between 6.5 nm and 10 nm, from which 95 spectral bands are within the spectral range of the GER field spectroradiometer. The GER ground-based surface reflectance spectra were interpolated to 1 nm and then spectrally resampled using the spectral response curves of the 95 VNIR EnMAP spectral bands to produce surface reflectance data commensurate with the EnMAP sensor. The Sentinel-2 satellite has 13 spectral bands (443–2190 nm) with a spectral resolution between 15 nm and 120 nm, from which the first 10 bands (band 1–8, 8a, 9) covered the spectral range of the GER radiometer. Data were simulated in the same way as the EnMAP procedure; interpolated to 1 nm and resampled using the spectral response curves of the 10 VNIR Sentinel-2 bands.

2.4.3 Stable Wavelength Identification Using the InStability Index

The ground-based reflectance spectra as well as the spectrally simulated EnMAP and Sentinel-2 reflectance spectra were used to calculate the InStability Index (ISI) in order to identify discriminative wavelengths in differentiating dominant tundra vegetation communities (Somers et al., 2010, 2009). ISI comes from a classification method known as stable zone unmixing (SZU), a spectral mixture analysis used to determine fractional cover of endmembers in a pixel (Somers et al., 2010). ISI has been applied to hyperspectral imagery to create spectral subsets of data to map spectrally similar invasive species and detect oil spills (Chance et al., 2016; Peterson et al., 2015; Somers and Asner, 2013). The ISI is a ratio index calculated for each wavelength over the entire spectral range of the within-class variability and the between-class variability. We used ISI to explore which regions of the spectra are most discriminative for differentiation, i.e., maximizing between community variability while minimizing within community variability, and to examine how that changes over the growing season. ISI developed in Somers et al. (Somers et al., 2009) is calculated as follows for two endmembers at wavelength i:

$$ISI_i = \frac{\Delta_{within,i}}{\Delta_{between,i}} = \frac{1.96(\sigma_{1,i} + \sigma_{2,i})}{|R_{mean,1,i} - R_{mean,2,i}|} \tag{2.2}$$

where Rmean,1,i and Rmean,2,i are mean reflectance values for endmembers 1 and 2; and σ1,i and σ2,i are the standard deviations of the reflectance values. Somers et al., (2009) defined the sum of the standard deviation of endmembers 1 and 2 as an appropriate measure of within class variability and the average Euclidean distance between endmembers as an appropriate measure of between class variability. This equation was expanded to a multiple endmember scenario used in this study as follows:

$$ISI_i = \frac{\Delta_{within,i}}{\Delta_{between,i}} = \frac{m}{m(m-1)} \times \sum_{z=1}^{m-1} \sum_{j=z+1}^{m} \frac{1.96(\sigma_{z,i} + \sigma_{j,i})}{|R_{mean,z,i} - R_{mean,j,i}|} \tag{2.3}$$

where m is the total number of vegetation communities (n = 5); and z and j are the vegetation communities under consideration when comparing more than two communities. To calculate ISI values for each of the five communities, z was held constant as the target

vegetation community and j alternated between the four remaining communities as de-
scribed in Equation (1). These four sets of ISI values were then summed by wavelength
and multiplied by the multiple endmember correction factor $m/m(m-1)$ to get the final ISI
value of each community. Low ISI values indicate low within-community spectral varia-
bility compared to between-community spectral variability and discriminative wave-
lengths.

A second step was taken to identify the most discriminative wavelengths using a three-
wavelength moving window to identify local minima. The local minima were identified
using a three-wavelength moving window minimum approach. Previous research has
shown that ISI-selected wavelength subsets increase the accuracy of endmember detection
in spectrally similar surfaces (Somers and Asner, 2013; Somers et al., 2010). The ISI local
minimum technique allows for flexible adjustment based on the variability of specific parts
of the spectrum, i.e., the local minima technique does not penalize or omit more variable
parts of the spectrum just because they are highly variable. To simulate how wavelength
selection could differ with different spectral resolutions, the local minima technique was
performed on the simulated EnMAP and simulated Sentinel-2 reflectance spectra and com-
pared to ground-based data. While Sentinel-2 is not a hyperspectral instrument it has higher
spectral resolution in the red-edge spectral region than previous multispectral optical mis-
sions.

The selected wavelengths were then partitioned into five broad spectral regions to identify
the most influential ones based on known pigment absorption regions and canopy structure.
The five broad spectral regions considered were defined as: blue: 400–500 nm, absorption
of chlorophylls and carotenoids; green: 500–600 nm, anthocyanin absorption; red: 600–
680 nm, absorption of chlorophylls; red-edge transition: 680–800 nm; and NIR: 801–985
nm, leaf/canopy structure and water absorption.

2.4   Results

2.4.1   Spectral Characteristics by Phenological Phase

The smoothed and averaged reflectance spectra indicate that the five tundra vegetation
communities are relatively similar spectrally within each phenological phase and between

leaf-out and senescence. Leaf-out and senescence spectra both present flatter spectra compared to maximum canopy and less pronounced absorption in the red wavelength region (Figure 2-2). MNT had the most distinct reflectance spectra with notably lower reflectance in the NIR in all three phenological phases Table 2-3). DT had the greatest NIR reflectance at leaf-out and senescence while MAT and ST had the highest reflectance in the NIR at maximum canopy. At leaf-out all communities except the xeric DT site showed absorption around 750 nm and 980 nm, at two water-absorption wavelength regions. The chlorophyll and carotenoid absorption region between 400 nm and 500 nm and chlorophyll absorption region around 680 nm were deepest at maximum canopy in all communities. Reflectance in the NIR plateau from approximately 750 nm to 985 nm and absorption at the water-absorption region around 920 nm were also highest at maximum canopy in all communities except DT. The greatest difference in spectral reflectance in the visible spectrum appears around the 680 nm chlorophyll-absorption region in all three phenological phases. Characteristic changes in the slope of the red-edge transition between 681 nm and 800 nm known as the "blue shift" of stressed vegetation (Rock et al., 1988) were observed from leaf-out to maximum canopy and maximum canopy to senescence for all communities.
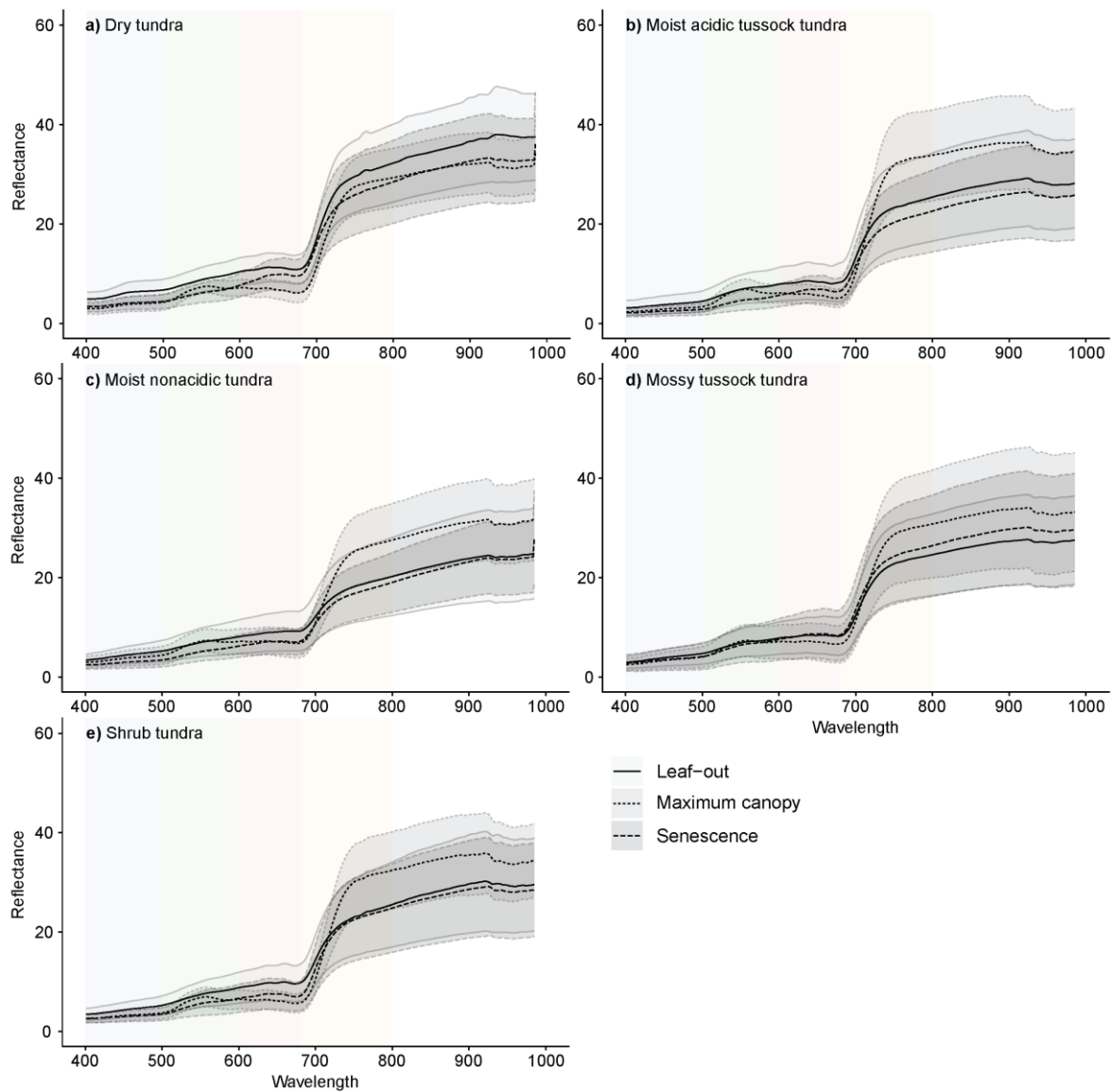
Figure 2-2 Mean (black line) and standard deviation (grey ribbon) of ground-based reflectance spectra of five dominant tundra vegetation communities in three major phenological phases of leaf-out, maximum canopy, and senescence. (a) Dry tundra; (b) moist acidic tussock tundra; (c) moist non-acidic tundra; (d) mossy tussock tundra; (e) shrub tundra.

Table 2-3 Metrics of ground-based reflectance spectra of five dominant tundra vegetation communities in three major phenological phases: leaf-out, maximum canopy, and senescence.

Vegetation Community	Date	Red Edge Inflection Point Wavelength (nm)	Max Reflectance			Max Continuum Removed Band Depth	
			550 nm (%)	750 nm (%)	920 nm (%)	Blue (400–550 nm)	Red (550–750 nm)
Dry tundra	Leaf-out	706	9.28	32.35	40.54	0.13	0.38
	Maximum canopy	710	9.01	31.54	37.10	0.26	0.64
	Senescence	704	7.33	36.28	44.19	0.21	0.37
Moist acidic tussock tundra	Leaf-out	706	10.08	32.19	37.70	0.20	0.41
	Maximum canopy	714	10.35	39.45	46.08	0.45	0.74
	Senescence	705	6.82	28.03	37.37	0.28	0.42
Moist non-acidic tundra	Leaf-out	706	7.59	21.38	26.79	0.14	0.23
	Maximum canopy	712	9.33	28.97	35.08	0.25	0.56
	Senescence	704	6.52	22.49	33.42	0.24	0.31
Mossy tussock tundra	Leaf-out	708	8.78	27.68	32.71	0.16	0.38
	Maximum canopy	713	8.94	32.20	39.76	0.29	0.62
	Senescence	707	8.86	29.31	34.59	0.24	0.40
Shrub tundra	Leaf-out	704	8.75	25.16	31.87	0.22	0.33
	Maximum canopy	714	8.10	30.96	37.61	0.38	0.70
	Senescence	705	6.09	26.24	33.65	0.26	0.46

2.4.2 InStability Index and Wavelength Selection of Ground-based Spectra

We used the ISI to examine the spectral variability by wavelength between vegetation communities at leaf-out, maximum canopy, and senescence (Table 2–4, Figure 2–3). Table 2–4 shows that when examining the entire VNIR reflectance spectrum, senescence appears to be the most discriminative phenological phase, related to relatively higher between-community variability versus within-community variability for differentiation of target vegetation communities according to cumulative ISI values. MAT, MT, and ST all had the lowest

cumulative ISI values during senescence while DT and MNT had lowest cumulative ISI values at leaf-out and maximum canopy, respectively.

Table 2-4 Cumulative ISI values of ground-based spectra of five dominant tundra vegetation communities: leaf-out, maximum canopy, and senescence. Bold values represent minimum cumulative values.

Vegetation Community	Leaf-Out ISI	Maximum Canopy ISI	Senescence ISI
Dry tundra	1532	148,112	8477
Moist acidic tussock tundra	69,256	15,867	7730
Moist non-acidic tundra	26,104	7393	9835
Mossy tussock tundra	38,139	150,136	13,047
Shrub tundra	71,140	17,715	6623

Figure 2-3 shows that at leaf-out, ISI values were consistently low at around 750 nm, but otherwise ISI values by wavelength showed large differences between communities. At maximum canopy, wavelengths > 450 nm in the blue reflectance spectrum had consistently low ISI values, and at senescence the entire blue spectrum had consistently low ISI values across all communities. At senescence, the water-absorption region at the end of the NIR between 920 nm and 985 nm had relatively low and stable ISI values in every community. Wavelengths around 700 nm, the beginning of the red edge, had low ISI values (discriminative) in all communities and all phenological phases. Leaf-out and maximum canopy had the most variable NIR ISI values, while at senescence values were consistently low except for single ISI peaks in the MT and MNT communities. Figure 2-3 also presents the results from the local minima technique applied to the ISI values per wavelength for the dominant tundra communities in all three phenological phases.

Figure 2-3 Ground-based Instability Index (ISI) analyses: ISI values per wavelength and 2. results of the ground-based ISI minima wavelength selection of five dominant tundra vegetation communities: (a) dry tundra; (b) moist acidic tussock tundra; (c) moist non-acidic tundra; (d) mossy tussock tundra; (e) shrub tundra; in the three major phenological phases of leaf-out, maximum canopy, and senescence. Background colors represent the five broad spectral regions considered for interpretation, associated with different pigments and chlorophyll absorptions. For visualization purposes, all ISI values greater than 100 were set to 100.

At leaf-out, in all communities except DT, the minima technique chose a discriminative wavelength within 6 nm of 440 nm, a region of strong chlorophyll and carotenoid absorption in the blue wavelength region (Figure 2-3). In the same communities a wavelength was selected between 660 nm and 680 nm, a region recognized as an absorption maximum of chlorophyll in the red spectrum, and one within 4 nm of 750 nm, the end of the red-edge transition where vegetation cellular structure drives the reflectance signal. In MT, MAT, and ST, a wavelength was selected within 6 nm of the 550 nm "green reflectance peak", a region with no chlorophyll absorption and anthocyanin absorption. In DT the majority of wavelength selection was in the NIR, not surprisingly given the sparse vascular plant cover and xeric moisture regime in this vegetation community. Wavelength selection was high in MAT, ST, and DT in the water-absorption NIR region between 920 nm and 985 nm.

At maximum canopy, in all communities including DT, the minima technique selected a wavelength within the 660–680 nm chlorophyll-absorption region in the red spectrum. In all communities, exactly 707 nm was selected by the minima technique a wavelength in the middle of the red edge and just after chlorophyll absorption stops and vegetation cellular structure takes over the reflectance signal. Additionally, a wavelength was selected within 4 nm of 950 nm in the water-sensitive NIR region in all communities. In MT, MAT, and ST, a wavelength was selected within 6 nm of the 550 nm "green peak".

At senescence in all communities, the minima technique selected 960 nm which lies within the water-absorption region between 920 nm and 985 nm, and in all communities except DT a wavelength was selected within 2 nm of 750 nm in the end of the red-edge transition. In MAT, MNT, and MT, a wavelength was selected within 4 nm of 440 nm, the chlorophyll and carotenoid absorption region and in MAT, MNT, and ST a wavelength was selected between 660 nm and 680 nm, the second chlorophyll-absorption region. The minima technique selected no wavelengths near the 550 nm "green peak".

2.4.3 *InStability Index and Wavelength Selection of Simulated Satellite Reflectance Spectra*

Simulated reflectance spectra of EnMAP and Sentinel-2 are shown in Figure 2-7. Cumulative ISI values from the simulated EnMAP reflectance spectra had similar phenological trends as ground-based spectra with minimums at senescence for MAT, MT, and ST and minimums at leaf-out and maximum canopy for DT and MNT, respectively (Table 2-5).

The simulated Sentinel-2 reflectance spectra had different phenological results with leaf-out identified as the most discriminative phase for MNT and maximum canopy the most discriminative for MAT, MT, and ST.

Table 2-5 Cumulative ISI values of simulated EnMAP and simulated Sentinel-2 reflectance spectra of five dominant tundra vegetation communities: leaf-out, maximum canopy, and senescence. Bold values represent minimum cumulative values.

Vegetation	Leaf-Out		Maximum Canopy		Senescence	
ISI	EnMAP	Sentinel-2	EnMAP	Sentinel-2	EnMAP	Sentinel-2
Dry tundra	401	38	7795	155	1125	53
Moist acidic tussock tundra	16,789	684	4570	225	2050	297
Moist non-acidic tundra	2834	129	1883	182	2687	339
Mossy tussock tundra	12,958	485	7933	218	2346	311
Shrub tundra	9694	807	4928	200	1724	351

ISI values of simulated EnMAP reflectance spectra (Figure 2-4) showed overall low variability in senescence with some ISI spikes in the green part of the reflectance spectrum and at longer NIR wavelengths. Leaf-out and maximum canopy ISI values were highly variable between vegetation communities. Longer wavelengths in the red-edge and green reflectance spectrum had consistently low values at leaf-out and maximum canopy in all communities, respectively. In Figure 2-5, it can be observed that the broader resolution Sentinel-2 showed less obvious phenological trends in ISI values by band. In general, the green and red bands had the highest ISI values while the red edge and NIR had the lowest in all communities and phenological phases.
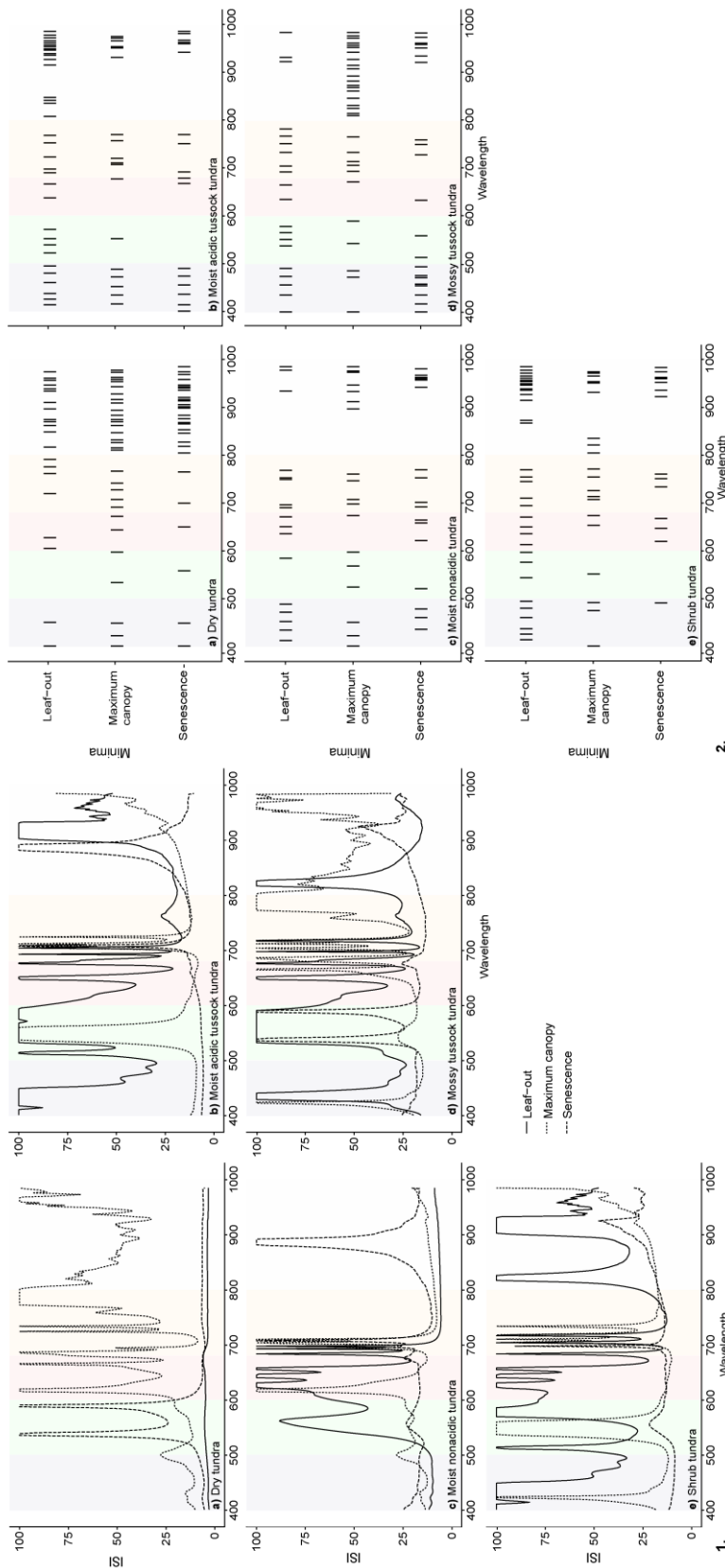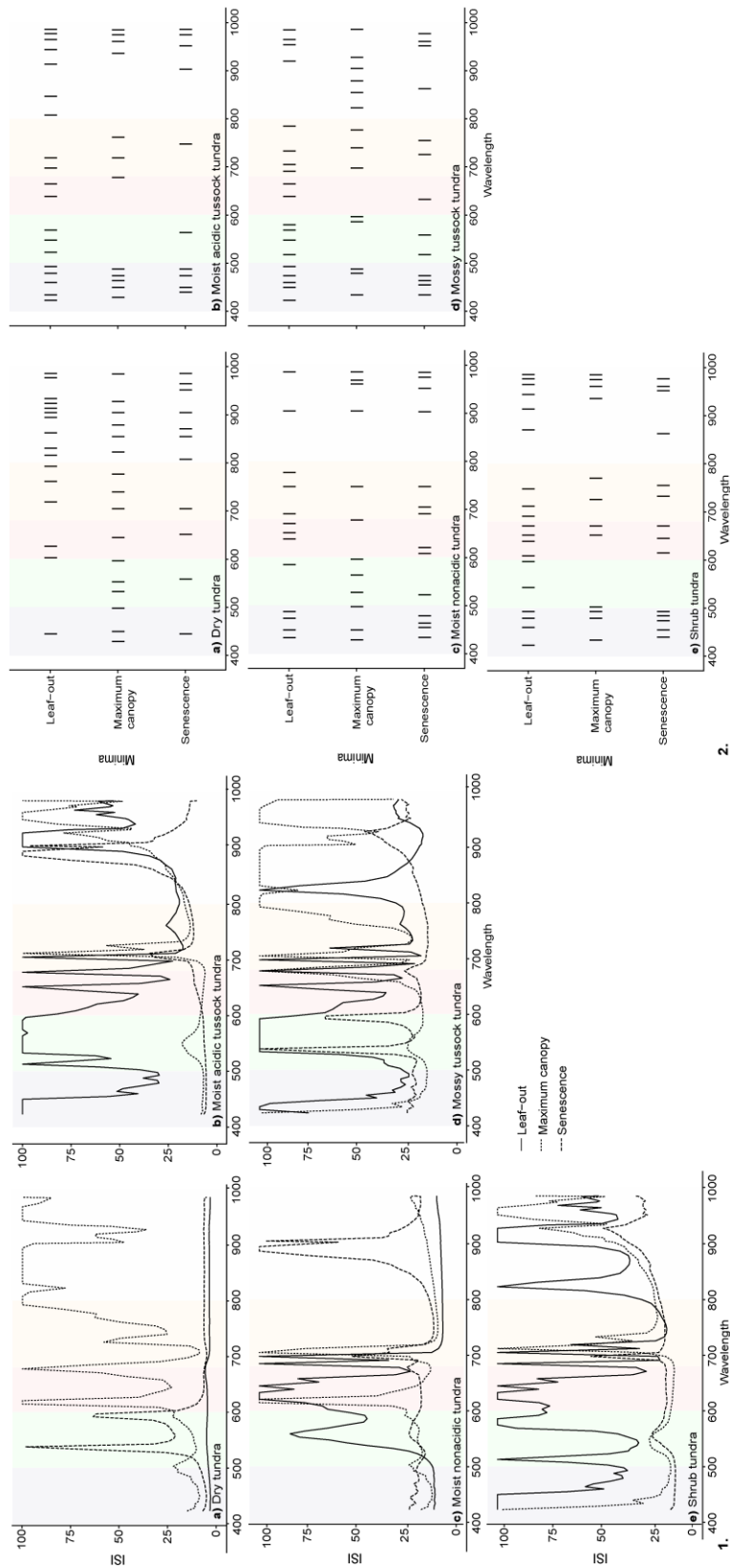
Figure 2-4 1. Simulated EnMAP Instability Index (ISI) analyses: ISI values per wavelength and 2. results of the ground-based ISI minima wavelength selection of five dominant tundra vegetation communities in the three major phenological phases of leaf-out, maximum canopy, and senescence. Background colors represent the five broad spectral regions considered for interpretation, associated with different pigments and chlorophyll absorptions. For visualization purposes all ISI values greater than 100 were set to 100. (a) dry tundra; (b) moist acidic tussock tundra; (c) moist non-acidic tundra; (d) mossy tussock tundra; (e) shrub tundra.
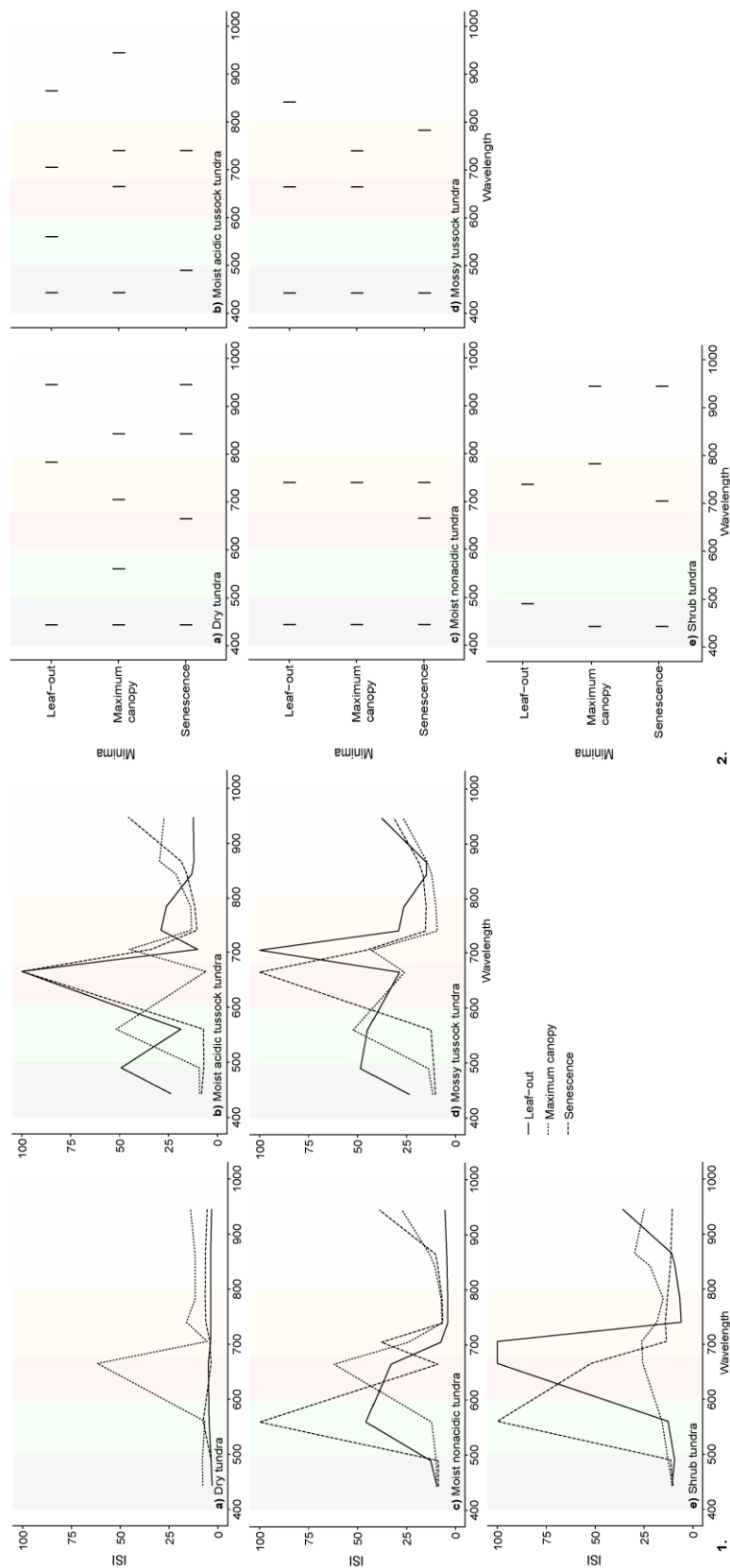
Figure 2-5 1. Simulated Sentinel-2 Instability Index (ISI) analyses: ISI values per wavelength and 2. results of the ground-based ISI minima wavelength selection of five dominant tundra vegetation communities in the three major phenological phases of leaf-out, maximum canopy, and senescence. Background colors represent the five broad spectral regions considered for interpretation, associated with different pigments and chlorophyll absorptions. For visualization purposes all ISI values greater than 100 were set to 100. (a) dry tundra; (b) moist acidic tussock tundra; (c) moist non-acidic tundra; (d) mossy tussock tundra; (e) shrub tundra.

The same minima technique was applied to ISI values of simulated satellite data. The results of the simulated EnMAP minima wavelength selection (Figure 2-4) were comparable to the ground-based data (Figure 2-3). At leaf-out, there was strong selection in the blue region in all communities except DT. In MAT, MNT, MT, and ST a wavelength was selected between 450 nm and 460 nm within the maximum chlorophyll-, carotenoid-absorption region. The minima technique also selected a wavelength between 670 nm and 680 nm in the chlorophyll-absorption maximum of the red spectrum region in all communities except DT. In both MNT and ST, wavelengths were selected around 750 nm where the reflectance signal becomes dominated by leaf cellular and canopy structure. In both MAT and MT, a wavelength was selected at 550 nm in the "green reflectance peak". As with ground-based data, the majority of wavelength selection in DT occurred in the NIR. The minima technique showed strong wavelength selection in all communities in the water absorption region between 920 nm and 985 nm, except in MNT which had only one.

At maximum canopy, the minima technique once again had strong selection in the blue spectrum with wavelengths selected at 450 nm within the maximum chlorophyll- and carotenoid-absorption region in DT, MAT, and MNT. In all communities except MT, a wavelength was selected between 670 nm and 680 nm in the red chlorophyll-absorption region. In DT and MT wavelengths around the 550 nm "green reflectance peak" were selected. As with leaf-out, minima wavelength selection was strong in the water sensitive NIR region between 920 nm and 985 nm in all communities.

At senescence in all communities except DT, a wavelength around 750 nm, the end of the red-edge transition, was selected. In all five communities, wavelength 952 nm was selected in the water sensitive NIR region as well as wavelengths between 440 nm and 455 nm within the chlorophyll- and carotenoid-absorption in the blue spectral region. Minima selection was overall high in the blue spectrum as with the other two phenological phases. In DT, MAT, and MT there was consistent wavelength selection around the 550 nm green-peak.

The simulated Sentinel-2 data had generally similar band selection (Figure 2-5) when compared in context to the broad defined spectral regions. At leaf-out, the narrow blue band was selected in all communities except ST, in which the broad blue aerosol band was selected. In all communities, a narrow band in the red edge was selected, except MT, which

had the broad NIR band selected. Only in MAT was the narrow NIR band selected, and only in DT was the water vapour NIR band centered at 945 nm selected.

Similar to leaf-out, the narrow blue band was selected by the minima technique in all communities at maximum canopy. Only in DT was there selection in the green band and in MAT and MT the red band. Narrow red-edge bands were selected in all communities. Only in DT was the broad NIR band selected, and in MAT and ST the water vapour band was selected.

At senescence, the narrow blue aerosol band was selected in all communities and the broad blue band was selected in MAT. There was no band selection in the green reflectance spectrum. In DT and MNT, the red band was selected and all in communities a narrow red-edge band was selected except in DT which had selection in the broad NIR band. In DT and ST, the NIR water-vapour band was selected.

2.5   Discussion

Investigation of the ground-based, as well as the simulated EnMAP and Sentinel-2 spectral variability of five dominant low Arctic tundra vegetation communities was undertaken using the InStability Index (ISI) at three major phenological phases of leaf-out, maximum canopy and senescence at Toolik Lake, Alaska. The ISI index was chosen as a tool to understand the seasonal dynamics of spectral variability and identify the phenological phase and regions of the spectrum that are best suited for a detailed assessment of representative tundra communities. In this study, we specifically focus on dominant tundra communities occurring on a circumarctic scale (tundra biomes C, D, E, Walker et al., (2005) excluding the spectrally distinguishable plant communities of wetlands and shrubs taller than half a meter that occur in disturbed areas or sheltered morphology. Previous studies utilize ISI and the minima wavelength technique with hyperspectral imagery as a pre-processing tool for spectral unmixing and classification (Chance et al., 2016; Peterson et al., 2015), but it is also an effective method to explore and understand the phenology of spectral variability by wavelength. We present a novel result of the influence of phenological phase on the variability of Arctic vegetation community reflectance spectra and how in turn this could improve the differentiation of these spectrally similar endmembers.

2.5.1   Phenological Phase and Wavelength Stability of Ground-based Spectra

The identification of senescence as the most discriminative phenological phase for the majority of vegetation communities is an important finding as mossy tussock tundra, moist acidic tussock tundra, and shrub tundra combined represent 63.1% of the Toolik Vegetation Grid and contribute greatly to Alaskan above-ground biomass at the ecosystem scale (Bliss and Matveyeva, 1992; Muller et al., 1999; Tenhunen et al., 1992). The observed discriminability of the senescence phenological phase could be explained by a combination of overall lower variability in reflectance and/or comparable or greater differences in mean reflectance boosting the differentiability of these three communities from the other communities in comparison to leaf-out and maximum canopy (Table 2–4, Figure 2–3). Previous characterizations of Arctic vegetation community reflectance spectra have suggested that distinct communities are spectrally more similar outside of the peak growing season but have not explicitly explored the influence or trade-off of accompanying spectral variability observed in the late season (Bratsch et al., 2016; Buchhorn et al., 2013). To date, the late season represents a relatively unexplored phenological phase spectrally, and this paper shows that it has potential given the relatively low ISI values in the visible and red-edge spectrum, providing independence from the litter and water-sensitive NIR plateau for characterization.

For the remaining two communities of MNT and DT, making up 10% of the study area, maximum canopy and leaf-out were the most discriminative phenological phases, respectively. For MNT, this is likely due to a maximum difference in chlorophyll absorption. Buchhorn et al., (2013) and Walker et al., (1995) have shown the "less green" nature of non-acidic communities compared to acidic ones as a result of species composition, including the dominating moss species and a lack of shrub species, leading to lower pigment absorption by chlorophyll (Buchhorn et al., 2013; Walker et al., 1994). The discriminability of the leaf-out phenological phase for identification of DT could be explained by a combination of sparse vegetation cover and large differences in spectral reflectance during leaf-out. These DT sites are subject to unique early-season conditions as they are generally located on upland, exposed areas and have shallow winter snow cover leading to earlier spring snowmelt and leaf-out of the vascular vegetation dominated by prostrate dwarf shrubs (Asner, 1998; Chuvieco et al., 2002; Curran, 1989; Walker et al., 2005). Higher reflectance in the visible and NIR spectrum could be the result of more advanced vegetation

phenology in combination with bright, dry surfaces dominated by small stones and lichens which have been shown to drive high reflectance in the NIR (Asner, 1998; Chuvieco et al., 2002). The advanced phenology and desiccation is supported by the average snow-free date of dry tundra phenology plots, as recorded by the Toolik Environmental Data Centre, which were snow-free 10 and 11 days earlier than moist acidic tussock tundra plots in 2015 and 2016, respectively.

The resulting wavelength selection from the ISI minima technique in the most discriminative phenological phase of each community predominantly identifies vegetation colour, driven by vegetation pigment concentration, as discriminative spectral regions for identification of specific communities. The identification of senescence as a discriminative phenological phase is particularly interesting, as the communities are visually most distinct at senescence when carotenoid (yellow to orange) and anthocyanin (red) pigments begin to dominate and chlorophyll (green) pigments are degrading. With the exception of DT, all communities had equal or greater wavelength selection in the combined visible and red-edge spectrum than the NIR. Slope and position of the red edge has been directly related to chlorophyll content in vascular plants (Filella and Penuelas, 1994) and this paper is in agreement with previous and well-established research linking absorption in the visible spectrum to vegetation colour and pigment concentration (Curran, 1989; Gitelson and Merzlyak, 1997; Gitelson et al., 2002; Stylinski et al., 2002; Ustin and Curtiss, 1990) but brings new insights to the potential of the senescent phase for optical discrimination of low-Artic vegetation. Current and upcoming missions will exploit visible wavelength regions by providing products such as the carotenoid reflectance index (CRI) from Sentinel-2, which uses the blue and shortwave red-edge wavelengths to measure the relative carotenoid-to-chlorophyll content.

2.5.2 *Phenological Phase and Wavelength Stability of Satellite Resampled Spectra*

The results from the simulated satellite reflectance spectra suggest that EnMAP has the spectral capabilities to capture the same general trends in wavelength selection as the ground-based spectra. The simulated EnMAP reflectance spectra had the same phenological trends in cumulative ISI values by vegetation community and comparable wavelength selection as GER spectra. This suggests that the spectral resolution is capable of capturing the same vegetation pigment dynamics as described for ground-based data. This result

highlights the benefit a hyperspectral imager will have for detailed characterization of tundra communities based on new spectral capabilities. This potential will have to be tested in further studies, with simulated images or with real EnMAP data taking into account the spatial mixing at the 30 m scale. Nevertheless, this study demonstrates that the EnMAP satellite has a high enough spectral resolution to be able to spectrally discriminate vegetation communities in low Arctic regions, with similar capabilities as much higher spectral resolution (3 nm) ground-based spectral data.

The simulated Sentinel-2 spectra differed from the ground-based spectral data, as maximum canopy as opposed to senescence was the most discriminative phenological phase for moist acidic tussock tundra, mossy tussock tundra, and shrub tundra communities; and leaf-out as opposed to maximum canopy was the most discriminative phenological phase for moist non-acidic tussock tundra selecting. The differences in ISI values from simulated Sentinel-2 by wavelength and the resulting phenological trends could be explained by the lower spectral resolution altering the ratio of spectral variability between and within communities in some spectral regions. Although the spectral variability was different by phenological phase and by wavelength, blue and red-edge bands of the simulated Sentinel-2 reflectance data were still selected as the most discriminative for the differentiation of communities. The high selection in the red-edge bands suggests that Sentinel-2 data will be superior to the broadband Landsat, which has lower spectral resolution in this part of the spectrum.

2.5.3 Influence of Spatial Scale

This study examines the spectral capabilities of simulated surface spectral data from the upcoming hyperspectral EnMAP mission and the currently operational multispectral Sentinel-2, without spatial simulation equivalent to the pixel resolution of the sensors. Such a spatial simulation including real hyperspectral imagery is out of the scope of this paper and will be a topic of further research. Nevertheless, as a first approximation, we can consider that such a spatial simulation would have resulted in a considerably lower within-community spectral variability for reflectance sampled at 100 m^2 (Sentinel-2 VIS and NIR bands) to 400 m^2 (Sentinel-2 red-edge and SWIR bands) and up to 900 m^2 (EnMAP). Indeed, the simulated sensor data show high ISI values caused by high within-community spectral variability due to sampling at a 0.15 m footprint spatial scale.

The aerial extent of mossy tussock tundra and moist acidic tussock tundra community patches in the Toolik Vegetation Grid are equivalent to the nominal scale of 400 m^2 to 900 m^2 pixels, providing pure pixels. Patches of dry tundra and moist non-acidic tundra in the Toolik Vegetation Grid occur in smaller patches but north-east of the grid these communities occur in large patches equivalent to pure pixels. Shrub tundra communities that generally occur along water tracks have lower spatial dimensions but sometimes occur in larger patches in tundra landscapes. As such, the studied communities will occur in both pure and mixed pixels of operational and future medium-resolution satellite sensors. Our study confirms a low between-community spectral variability resulting in challenging spectral classification of pure pixels as well as spectral unmixing of mixed pixels at 10 m to 30 m scales. Using ISI will support the selection of discriminative wavelength regions and indicate that a multi-phenological phase approach will benefit the differentiation of spectrally similar vegetation communities at the satellite scale; in particular, the use of senescent phase EnMAP reflectance spectra in the visible, particularly blue, and red-edge spectrums, and the use of leaf-out and maximum canopy phase simulated Sentinel-2 reflectance spectra.

2.6 Conclusions

To explore the spectral variability of dominant low Arctic tundra vegetation communities and the potential of ground-based and satellite new optical data for better discrimination and identification of different vegetation community types within tundra ecosystems, a relatively new ISI technique was used to identify the most spectrally discriminative phenological phase and regions within the VNIR spectral regions. Based on field data and ISI values, we support previous findings that heterogeneous tundra ecosystems are both spectrally similar and spectrally variable, making differentiation challenging. On the other hand, our results based on the ISI technique suggest that senescence is the most discriminative phenological phase for three tundra vegetation communities (moist acidic tussock tundra, mossy tussock tundra, and shrub tundra), which account for a majority of the study site and low Arctic biomass at the ecosystem scale. The use of the senescent phase optical satellite data to discriminate vegetation communities has not been previously explored and is one of the major results of this paper. As with previous ground-based spectral characterization of Alaskan low Arctic tundra on the Alaskan North Slope, the blue, red and red-edge parts

of the spectrum are observed as important for vegetation community identification. Furthermore, differences in vegetation colour driven by pigment concentration appear to be the most discriminative areas of the spectrum to differentiate specific vegetation communities. In this paper, the phenological aspect provides an added perspective, highlighting the potential exploitation of more extreme colour differences in vegetation observed during senescence.

Our study also highlights the potential of upcoming EnMAP and operational Sentinel-2 satellites to characterize the spectral variability of tundra vegetation communities based on their spectral capabilities. The VIS and red-edge wavelength regions were the most discriminative for both sensors and, as with the ground-based data, this result suggests a multi-phenological phase approach could improve differentiation at the satellite scale. Senescence was also the most discriminative phenological phase for the identification of the majority of communities when using EnMAP reflectance spectra, while simulated Sentinel-2 data identified the maximum canopy as the most discriminative phenological phase. The results provide insight into both the community and seasonal dynamics of spectral variability, in order to better understand and interpret currently used broadband vegetation indices and also for improved spectral unmixing of hyperspectral aerial and satellite data. This is useful for a wide range of applications, from fine-scale monitoring of shifting vegetation composition to the identification of vegetation vigour.

2.7 Acknowledgements

2.8 Supplementary Material

Figure 2-6 Mean (black line) and standard deviation (grey ribbon) of simulated EnMAP reflectance spectra of five dominant tundra vegetation communities in three major phenological phases of leaf-out, maximum canopy, and senescence. a) dry tundra, b) moist acidic tussock tundra, c) moist non-acidic tundra, d) mossy tussock tundra, e) shrub tundra.
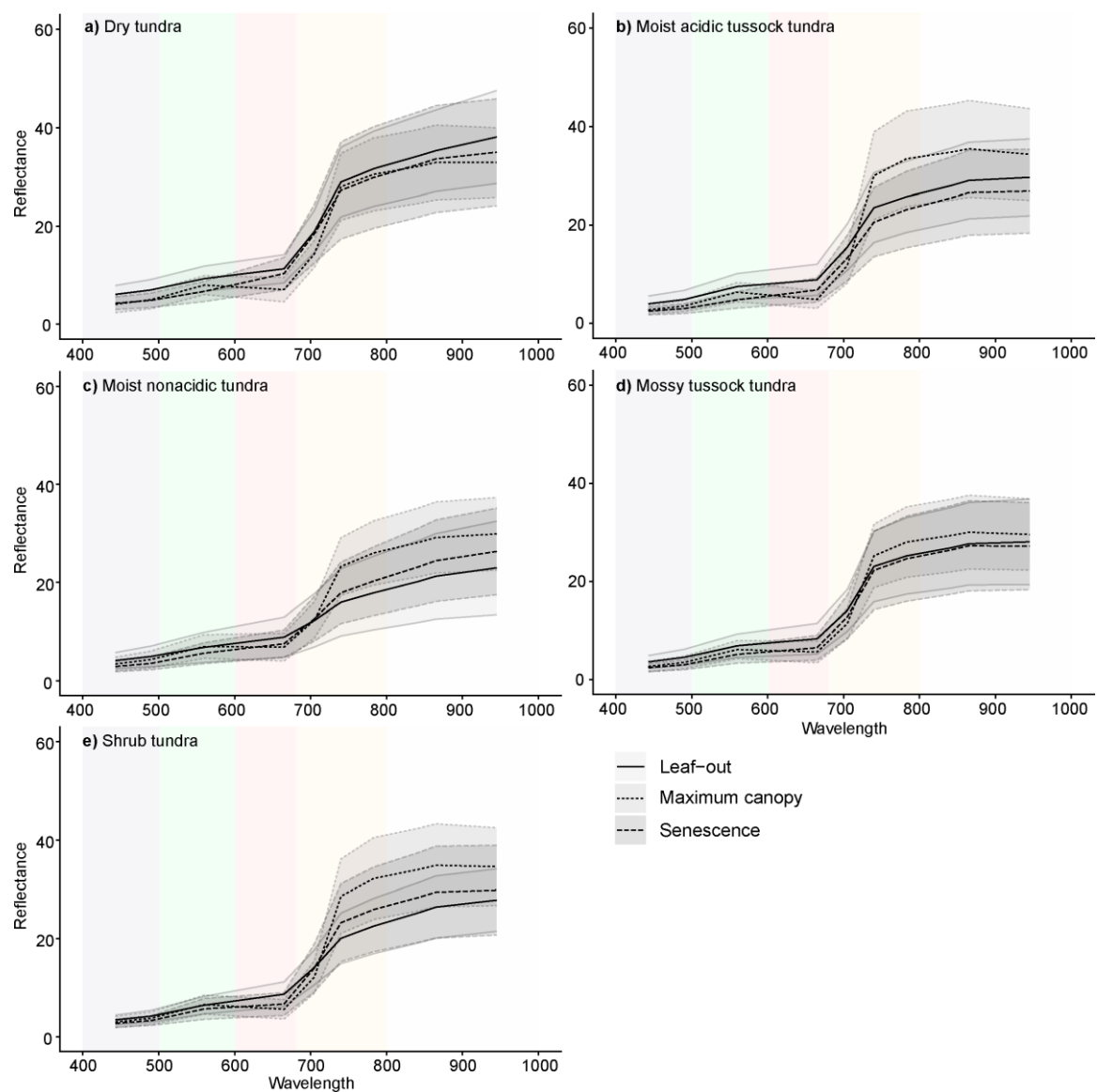
Figure 2-7 Mean (black line) and standard deviation (grey ribbon) of simulated Sentinel-2 reflectance spectra of five dominant tundra vegetation communities in three major phenological phases of leaf-out, maximum canopy, and senescence. a) dry tundra, b) moist acidic tussock tundra, c) moist nonacidic tundra, d) mossy tussock tundra, e) shrub tundra.

2.8.1 Data Publication

All data are publically available on the Open Access library Pangaea (www.pangaea.de)

https://doi.org/10.1594/PANGAEA.885801

https://doi.org/10.1594/PANGAEA.885784

https://doi.org/10.1594/PANGAEA.885808

3 Monitoring Pigment-driven Vegetation Changes in a Low Arctic Tundra Ecosystem Using Digital Cameras

Alison L. Beamish[1], Nicholas C. Coops[2], Txomin Hermosilla[2] Sabine Chabrillat[3], and Birgit Heim[1]

[1] Alfred Wegener Institute, Periglacial Research, Telegrafenberg A45, 14473 Potsdam, Germany

[2] Integrated Remote Sensing Studio (IRSS), Faculty of Forestry, University of British Columbia, 2424 Main Mall, Vancouver, British Columbia V6T1Z4 Canada

[3] Helmholtz Centre Potsdam (GFZ), German Research Centre for Geosciences, Telegrafenberg A17, 14473 Potsdam, Germany

3.1 Abstract

Arctic vegetation phenology is a sensitive indicator of a changing climate and rapid assessment of vegetation status is necessary to more comprehensively understand the impacts on foliar condition and photosynthetic activity. Airborne and spaceborne optical remote sensing have been successfully used to monitor vegetation phenology in Arctic ecosystems by exploiting the biophysical and biochemical changes associated with vegetation growth and senescence. However, persistent cloud cover and low sun angles in the region make the acquisition of high quality temporal optical data within one growing season challenging. In the following study, we examine the capability of "near-field" remote sensing technologies, in this case digital, true colour cameras to produce surrogate in-situ spectral data to characterize changes in vegetation driven by seasonal pigment dynamics. Simple linear regression was used to investigate relationships between common pigment-driven spectral indices calculated from field-based spectrometry and red, green, and blue (RGB) indices from corresponding digital photographs in three dominant vegetation communities across three major seasons at Toolik Lake, North Slope, Alaska. We chose the strongest and most consistent RGB index across all communities to represent each spectral index. Next, linear regressions were used to relate RGB indices and extracted leaf-level pigment concentration with a simple additive error propagation of the root mean square error (RMSE). Results indicate that the green-based RGB indices had the strongest relationship with chlorophyll a and total chlorophyll, while a red-based RGB index showed moderate relationships with the chlorophyll to carotenoid ratio. The results suggest that vegetation colour contributes

strongly to the response of pigment-driven spectral indices and RGB data can act as a surrogate to track seasonal vegetation change associated with pigment development and degradation. Overall, we find that low-cost easy-to-use digital cameras can monitor vegetation status and changes related to seasonal foliar condition and photosynthetic activity in three dominant, low Arctic vegetation communities.

3.2   Introduction

Changes to the functioning of Arctic ecosystems, such as shifts in photosynthetic activity, net primary productivity, and species composition influence global climate change and the resulting feedbacks (Bhatt et al., 2010; Parmentier and Christensen, 2013; Zhang et al., 2007). Climatic changes have been accompanied by broad-scale shifts in Arctic vegetation community composition and species distribution, as well as fine-scale shifts in individual plant reproduction and phenology (Bhatt et al., 2010; Bjorkman et al., 2015; Elmendorf et al., 2012; Prevéy et al., 2017; Walker et al., 2006). Changes in vegetation phenology can impact overall ecosystem functioning as a result of mismatched species-climate interactions. This in turn can impact species photosynthetic activity and growth through increased vulnerability to events such as frost, soil saturation, or disruption to species chilling requirements (Cook and Wolkovich, 2012; Høye et al., 2013; Inouye and McGuire, 1991; Wheeler et al., 2015; Yu et al., 2010).

In Arctic ecosystems snow pack conditions and timing of snowmelt, rather than temperature, are primary drivers of the onset of vegetation phenology (Billings and Bliss, 1959; Bjorkman et al., 2015). Changing snowmelt dynamics due to changes in winter precipitation and spring temperatures have been shown to directly influence tundra vegetation phenology throughout the growing season (Bjorkman et al., 2015). Thus, the onset of the growing season, the leaf-out stage, acts as a benchmark of phenology and identification and characterization of this stage are key to understanding the overall and subsequent phenology and fitness of tundra vegetation (Iler et al., 2013; Wheeler et al., 2015). The timing of maximum expansion and elongation of leaves and stems and when vegetation is at, or near, peak photosynthetic activity, peak greenness, are also important benchmarks of phenological phases. Peak greenness marks the climax of the growing season, the timing and magnitude of which can indicate ecosystem functioning, and acts as a benchmark for long-term

monitoring of tundra productivity (Bhatt et al., 2010, 2013) A final benchmark of phenological phase is the end of the growing season, senescence. In combination with leaf-out, senescence dictates growing season length and has implications for overall seasonal productivity and carbon assimilation (Park et al., 2016). Characterizing key biophysical properties of Arctic vegetation associated with these three benchmark phenological phases is important for accurate monitoring and quantification of local and regional changes in Arctic vegetation and in turn Arctic and global changes to energy and carbon cycling, as well as associated feedbacks. The presence and seasonal changes in vegetation pigment concentration can be used to infer biophysical properties including photosynthetic activity and foliar condition at key phenological phases of Arctic vegetation.

The major photosynthetic pigment groups of chlorophyll and carotenoids absorb strongly in the visible spectrum creating unique spectral signatures (Coops et al., 2003; Curran, 1989; Gitelson and Merzlyak, 1998; Gitelson et al., 2002). Chlorophyll pigments are the dominant factor controlling the amount of light absorbed by a plant and therefore photosynthetic potential, which ultimately dictates primary productivity. Carotenoids (carotenes and xanthophylls) are responsible for absorbing incident radiation and providing energy to the photosynthetic process and are often used to provide information on the physiological status of vegetation (Bartley and Scolnik, 1995; Young and Britton, 1990). The third major pigment group of anthocyanins (water-soluble flavonoids) have a less concise function in vegetation providing photoprotection (Close and Beadle, 2003; Steyn et al., 2002), drought and freezing protection (Chalker-Scott, 1999) and they have been shown to play a role in recovery from foliar damage (Gould et al., 2002). Photosynthetic pigments influence a wide range of plant functioning from photosynthetic efficiency to protective functions (Demmig-Adams and Adams, 1996) and can be measured destructively through laboratory analysis or non-destructively using high spectral resolution remote sensing (Gitelson et al., 2006, 2002, 2001, 1996).

The development and degradation of chlorophyll pigments as a result of vegetation emergence, stress, or senescence causes a distinct shift in spectral signatures in the visible spectrum to shorter wavelengths due to a narrowing of the major chlorophyll absorption feature (550 – 750 nm) and an overall reduction in spectral absorption (Ustin and Curtiss, 1990). Carotenoids (yellow to orange) and anthocyanins (blue to red) have less straightforward seasonal, and therefore spectral, shifts. The spectral absorption by carotenoid pigments can

result in mixed or masked spectral absorption with chlorophyll signals due to overlapping absorption features in the visible spectrum (400 – 700 nm). Carotenoids and anthocyanins often have relatively higher concentrations in senesced and young leaves when chlorophyll concentrations are relatively low (Sims and Gamon, 2002; Stylinski et al., 2002; Tieszen, 1972). However in general, the predictable and distinct spectral features created by changes in vegetation pigment concentration allow inferences of ecological parameters such as photosynthetic activity, nutrient concentration, and biomass (Asner and Martin, 2008; Mutanga and Skidmore, 2004; Mutanga et al., 2004; Ustin et al., 2009)

Of particular interest for in-situ and laboratory spectroscopy of vegetation and phenology are the spectral characterization of the xanthophyll cycle (carotenoids) and the ratio between photosynthetic pigments of carotenoids and chlorophyll as they relate to radiation use efficiency and in turn radiative transfer models (Blackburn, 2007; Gamon et al., 2016; Garbulsky et al., 2011). Radiative transfer models are used to simulate leaf and canopy spectral reflectance and transmittance, and have been the basis for the inverse determination of biophysical and biochemical parameters of vegetation based on spectral reflectance (Féret et al., 2011). Even at lower spectral resolution, the importance of pigments and pigment dynamics related to the xanthophyll cycle can be seen in available products for recent satellite missions, for example the European Space Agency's (ESA) Sentinel-2 provides many pigment-driven vegetation indices (see https://www.sentinel-hub.com/develop/documentation/eo_products/Sentinel2EOproducts).

While highly valuable, in-situ reflectance spectroscopy, like optical remote sensing, is challenging for remote Arctic field sites. Remote locations, challenges associated with field-based monitoring, and atmospheric and illumination conditions of optical satellite imagery of these areas limit available optical data, hindering phenological studies. To complement the use of airborne and satellite imagery to measure vegetation pigments and classify biophysical properties in Arctic ecosystems, the use of true-colour digital photography and Red Green Blue (RGB) indices to infer photosynthetic activity and foliar condition is a promising area of study and should be examined (Anderson et al., 2016; Beamish et al., 2016). Research has shown that Arctic vegetation changes are complex with strong site and species-specific responses through space and time (Bjorkman et al., 2015; Elmendorf et al., 2012; Walker et al., 2006). True-colour digital photography represents both a simple and cost-effective way to increase data volume both spatially and temporally to capture site and

species specific responses. Data from consumer-grade digital cameras has extremely high spatial resolution and high data collection capabilities and is less weather dependent than airborne and optical satellite remote sensing as varying illumination can be easily corrected (Nijland et al., 2014; Richardson et al., 2007). Large-scale, true-colour, repeatable digital photography networks in temperate ecosystems such as the PhenoCam network (http://phenocam.sr.unh.edu/webcam/) highlight the existing ecological applications of this method. Additional work by Richardson et al. (2007) and (Coops et al., 2012) demonstrates the link between ground-based true-colour camera systems and satellite scale (Landsat and MODIS) observations. In addition to phenological parameters, well-established RGB indices derived from consumer-grade digital cameras have been shown to accurately identify vegetation cover in Arctic tundra and temperate forests (Beamish et al., 2016; Ide and Oguma, 2010; Nijland et al., 2014; Richardson et al., 2007), and can be closely related to Gross Primary Production (GPP) in grasslands, temperate forests, Arctic tundra, and wetlands (Ahrends et al., 2009; Anderson et al., 2016; Migliavacca et al., 2011; Westergaard-Nielsen et al., 2013) , as well as containing a sensitivity to changes in plant photosynthetic pigments (Ide and Oguma, 2013).

In this study we examine the capability of in-situ, true-colour digital photography to act as a surrogate for in-situ spectral data in assessing pigment-driven vegetation changes associated with three key seasons representing early, peak, and late season, in three dominant, low Arctic tundra vegetation communities. To do this we asked the following research questions: (1) what are the relationships between RGB indices and in-situ, pigment-driven spectral indices? (2) How do these relationships change with community type and season? (3) To what extent do the indices represent actual chlorophyll and carotenoid content? We conclude with proposing the RGB indices best suited as proxies for in-situ spectral data for monitoring seasonal vegetation change and the related pigment dynamics in a low Arctic tundra.

3.3   Methods

3.3.1   Study Site

Data was collected at the Toolik Field Station (68°62.57 N, 149°61.43 W) on the North Slope of the Brooks Range, in north central Alaska in the growing season of 2016. The Toolik area is representative of the Southern Arctic Foothills, a physiographic province of the North Slope (Walker et al., 1989). Vegetation is a combination of moist tussock tundra, wet sedge meadows and dry upland heaths. Data was acquired in the Toolik Vegetation Grid, a 1 × 1 km long-term monitoring site established by the National Science Foundation (NSF) as part of the Department of Energy's R4D (Response, Resistsnce, Resilience, and Recovery to Disturbance in Arctic Ecosystems) project (Figure 3-1). Vegetation monitoring plots (1 × 1 m) are positioned in close proximity to equally spaced site markers delineating the intersection of the Universal Transverse Mercator (UTM) coordinates and each point within the grid. A subset of the grid was sampled for the purpose of this study representing three distinct and dominant vegetation communities as defined by (Bratsch et al., 2016) (Figure 3-1). The communities include moist acidic tundra (MAT), moist non acidic tundra (MNT), and moss tundra (MT). A detailed description and representativeness (% cover of the Toolik Vegetation Grid) of the three vegetation communities sampled within the Long-term Toolik Vegetation Grid are shown in Table 3–1.
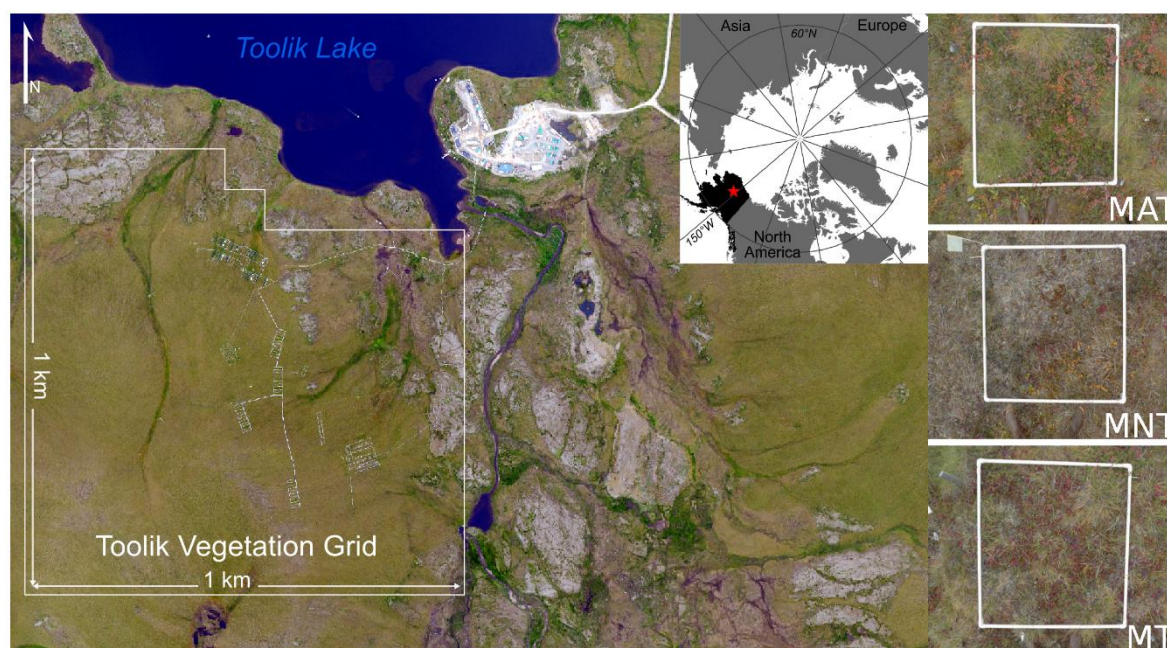
Figure 3-1 Toolik Vegetation Grid located in the Toolik Research Area on the North Slope of the Brooks Range in northern Alaska and a late season example plots of the three vegetation communities monitored in the study. MAT: Moist acidic tussock tundra, MNT: moist non-acidic tundra, MT: moss tundra.

3.3.2 Digital Photographs

In order to capture the three major seasons of early, peak, and late, we acquired true-colour digital photographs on three days in the 2016 growing season (June 16th (Day of Year (DOY) 165), July 11th (DOY 192), August 17th (DOY 229)). Images were taken at nadir approximately 1 m off the ground with a white 1 × 1 m frame for registration of off nadir images (Figure 3-1). According to the Toolik Lake Environmental Data Centre (https://toolik.alaska.edu/edc/, 2017) phenology record that monitors 15 dominant species at the Toolik Field Station, the first image acquisition date occurred two weeks after the average date of first leaf-out (May 29th, DOY 149) accurately capturing the peak of the early leaf-out phase. The second acquisition took place one week after average date of last flower petal drop (July 3rd, DOY 185) and within one week of recorded full green-up (end of June). The final acquisition took place three weeks after average first day of fall colour change (July 27th, DOY 209) and within the range of recorded peak fall colours (mid-August).

Table 3-1 Description of the three vegetation communities monitored in this study.

Com-mu-nity	Description	Detailed Description	% Cover
Moist acidic tus-sock tundra	Occurs on soils with pH < 5.0–5.5 and is dominated by dwarf erect shrubs such as Betula nana and Salix pulchra, graminoids species (Eriophorum vaginatum) and aci-dophilous mosses	Betula nana-Eriophorum vaginatum. Dwarf-shrub, sedge, moss tundra (shrubby tussock tun-dra dominated by dwarf birch, Betula nana). Mesic to subhygric, acidic, moderate snow. Lower slopes and water-track margins. Mostly on Itkillik I glacial surfaces. Salix pulchra-Carex bigelowii. Dwarf-shrub, sedge, moss tundra (shrubby tussock tundra dominated by diamond-leaf willow, Salix pul-chra). Subhygric, moderate snow, lower slopes with solifluction.	6.1
Moist non-acidic tundra	Dominated by mosses, graminoids (Carex big-ilowii), and prostrate dwarf shrubs (Dryas in-tegriolia)	Carex bigelowii-Dryas integrifolia, typical sub-type; Tomentypnum nitens-Carex bigelowii, Sa-lix glauca subtype: Nontussock sedge, dwarf-shrub, moss tundra (moist nonacidic tundra). Mesic to subhygric, nonacidic (pH > 5.5), shal-low to moderate snow. Solifluction areas and somewhat unstable slopes. Some south-facing slopes have scattered glaucous willow (Salix glauca).	5.8
Mossy tus-sock tundra	A moist acidic tussock tundra-type community dominated by sedges (E. vaginatum) and abundant Sphagnum spp.	Eriophorum vaginatum-Sphagnum; Carex bige-lowii-Sphagnum: Tussock sedge, dwarf-shrub, moss tundra (tussock tundra, moist acidic tun-dra). Mesic to subhygric, acidic, shallow to moderate snow, stable. This unit is the zonal vegetation on fine-grained substrates with ice-rich permafrost. Some areas on steeper slopes with solifluction are dominated by Bigelow sedge (Carex bigelowii).	54.2

Images were acquired with a consumer-grade digital camera (Panasonic DM3 LMX, Osaka, Japan) in raw format, between 10:00 h and 14:00 h, under uniform cloud cover to reduce the influence of shadow and illumination differences. The digital camera collects colour values by means of the Bayer matrix (Bayer 1976) with individual pixels coded with a red, green, and blue value between 0 and 256. RGB values of each pixel in each image were extracted using ENVI+IDL (Version 4.8; Harris Geospatial, Boulder, Colorado). To reduce the impact of non-nadir acquisitions, photo registration was undertaken using the 1 × 1 m frame. Table 3-2 shows the normalized RGB channels and RGB indices calculated based on the normalized red, green, and blue values of the digital photographs, hereafter referred to as RGB indices.

Table 3-2 Calculated red, green blue (RGB) indices from RGB channels of digital photographs.

Index	Formula	Source
nG	G/(R+B+G)	
nR	R/(R+B+G)	
nB	B/(R+B+G)	
GR	nG/nR	
GB	nG/nB	
2G-RB	2*nG–(nR+nB)	Richardson et al. (2007)

Digital camera indices 2G-RB and nG have been used to monitor vegetation phenology and biomass extensively (Beamish et al., 2016; Ide and Oguma, 2013; Richardson et al., 2007). Additionally, we defined new RGB indices to examine their representativeness to selected pigment-driven spectral indices (Table 3-3). We chose these RGB indices as they represented as closely as possible the mathematical formulas of selected pigment-driven indices presented in the field-based spectral data section below.

Table 3-3 Pseudo pigment-driven red, green, blue (RGB) indices calculated from RGB channels of digital photographs.

Indices	Formula
nBG	(nB-nG)/(nB+nG)
nRG	(nR-nG)/(nR+nG)
RGr	((nR-nG)/nR)
nG^{-1}	(1/nG)
2R-GB	2*nR–(nG+nB)

3.3.3   Field-based Spectral Data

Within one week of the digital photographs, field-based spectral measurements of each vegetation plot were acquired using a GER 1500 field spectroradiometer (Spectra Vista Corporation New York, USA). Spectral data were acquired on June 14th (DOY 165), July 8th (DOY 189), and August 23rd (DOY 235) in 2016 with a spectral range of 350 – 1050 nm, 512 bands, a spectral resolution of 3 nm, a spectral sampling of 1.5 nm, and an 8° field of view. Data were acquired under clear weather conditions between 10:00 and 14:00 local time corresponding to the highest solar zenith angle. In each plot, radiance data were acquired at nadir approximately 1 m off the ground resulting in an approximately 15 cm diameter ground instantaneous field of view (GIFOV). To reduce noise and characterize the spectral variability in each plot, an average of nine point measurements of upwelling radiance (Lup) in each of the 1 × 1 m plots was used. Downwelling radiance (Ldown) was measured as the reflection from a white Spectralon© plate. Surface reflectance (R) was processed as:

$$R = \frac{L_{up}}{L_{down}} \times 100 \tag{3.1}$$

Reflectance spectra (0–100%) were preprocessed with a Savitzky-Golay smoothing filter (n=11) and to remove sensor noise at the spectral limits of the radiometer data was subset to 400 – 985 nm.

Using the spectral reflectance data, we calculated common pigment-driven vegetation indices, focusing on vegetation colour, and those produced as remote sensing products by the European Space Agency (ESA) and the North American Space Agency (NASA), a brief description of each is provided below (Table 3-4). The indices that were calculated from the field-based GER data are hereafter referred to as pigment-driven spectral indices.

The Photochemical Reflectance Index (PRI) is an indicator of photosynthetic radiation use efficiency and was first proposed by (Gamon et al., 1992). The Plant Senescence Reflectance Index (PSRI) is sensitive to senescence induced reflectance changes from changes in chlorophyll and carotenoid content and was proposed by (Merzlyak et al., 1999). The Pigment Specific Simple Ratios (PSSRa and b) aim to model chlorophyll a and b, respectively (Blackburn, 1999, 1998) and (Sims and Gamon, 2002). Chlorophyll Carotenoid Index (CCI) was developed to track the phenology of photosynthetic activity of evergreen species by (Gamon et al., 2016) . The Carotenoid Reflectance Indices (CRI1 and CRI2) use the reciprocal reflectance at 508 and 548 nm and 508 and 698 nm respectively in order to remove the effect of chlorophyll (Gitelson et al., 2002). The Anthocyanin Reflectance Indices (ARI1 and ARI2) developed by (Gitelson et al., 2006, 2001) are designed to reduce the influence of chlorophyll absorption to isolate the anthocyanin absorption by taking the difference between the reciprocal of green (550 nm) and the red-edge (700 nm). ARI2 includes a multiplication by the near infrared (NIR) to reduce the influence of leaf thickness and density.

Table 3-4 Pigment-driven spectral indices.

Indices	Short	Formula	Source
Photochemical Reflectance Index	PRI	$(\rho_{533} - \rho_{569}) / (\rho_{533} + \rho_{569})$	Gamon and Field (1992)
Plant Senescence Reflectance Index	PSRI	$(\rho_{678} - \rho_{498}) / \rho_{748}$	Merzlyak et al. (1999)
Pigment Specific Simple Ratio	PSSR	PSSRa = ρ_{800} / ρ_{671} PSSRb = ρ_{800} / ρ_{652}	Blackburn (1998, 1999); Sims and Gamon (2002)
Chlorophyll carotenoid index	CCI	$(\rho_{531} - \rho_{645}) / (\rho_{531} + \rho_{645})$	Gamon et al. (2016)
Carotenoid Reflectance Index 1	CRI1	$(1/\rho_{508}) - (1/\rho_{548})$	Gitelson et al. (2002)
Carotenoid Reflectance Index 2	CRI2	$(1/\rho_{508}) - (1/\rho_{698})$	Gitelson et al. (2002)
Anthocyanin Reflectance Index 1	ARI1	$(1/\rho_{550}) - (1/\rho_{700})$	Gitelson et al. (2001)
Anthocyanin Reflectance Index 2	ARI2	$\rho_{800} * [(1/\rho_{550}) - (1/\rho_{700})]$	Gitelson et al. (2001)

3.3.4 *Vegetation Pigment Concentration*

To estimate how accurately plot-level indices represent actual leaf-level pigment concentrations, leaves and stems (n = 213) of the dominant vascular species in a subset of the sampled plots were collected at early, peak, and late season for chlorophyll and carotenoid analysis. Samples were placed in porous tea bags and preserved in a silica gel desiccant in an opaque container for up to 3 months until pigment extraction (Esteban et al. 2009). Each sample was homogenized by grinding with a mortar and pestle. Approximately 1.00 mg (+/- 0.05 mg) of homogenized sample was placed into a vial with 2 ml of dimethylformamide (DMF). Vials were then wrapped in aluminum foil to eliminate any degradation of pigments due to UV light and stored in a fridge (4°C) for 24 hrs. Samples were measured into a cuvette prior to spectrophotometric analysis. Bulk pigments concentrations were then estimated using a spectrophotometer measuring absorption at 646.8, 663.8 and 480 nm (Porra et al., 1989). Absorbance (A) values at specific wavelengths were transformed into µg/mg concentrations of chlorophyll a, Chl_a, chlorophyll b, Chl_b, total chlorophyll, Chl_{a+b}, carotenoids, Car, using the following equations:

$$Chl_a = 12.00 * A^{663.8} - 3.11 * A^{646.8}$$

(3.2)

$$Chl_b = 20.78 * A^{646.8} - 4.88 * A^{663.8}$$

(3.3)

$$Chl_{a+b} = 17.67 * A^{646.8} + 7.12 * A^{663.8}$$

(3.4)

$$Car = (A^{480} - Chl_a) / 245$$

(3.5)

The chlorophyll a to chlorophyll b ($Chl_{a:b}$), as well as the chlorophyll to carotenoid ratios
(*Chl:Car*) were calculated by dividing eq. (3.2) by eq. (3.3) and eq. (3.4) by eq. (3.5), re-
spectively. Pigment concentration was calculated as the average concentration of the dom-
inant species in each plot.

3.3.5 Data Analyses

We examined the potential of digital camera RGB data as a proxy for identified pigment-
driven vegetation indices using existing and new RGB indices. Simple linear regression
was performed between RGB indices defined in Table 3-2 and Table 3-3 and hyperspectral
PRI, PSRI, PSSR, CCI, CRI, and ARI indices defined in Table 3-4 (Table 3-6). The RGB
and spectral indices from significant RGB/spectral linear regressions were then chosen for
linear regression with Chl_a, Chl_b, $Chl_{a:b}$, and *Car:Chl* for each vegetation community to
explore how well the chosen indices represent actual leaf-level pigment concentration.

As we assume RGB indices can be used in place of pigment-driven spectral indices, we
wanted to include the error associated with spectral indices as a proxy for leaf-level pig-
ments to more accurately estimate uncertainties. To do this, we used a simple additive error
propagation of root mean square error of the selected RGB/pigment and spectral/pigment
regressions using the following equations:

$$RMSE = \sqrt{\frac{\sum_{t=1}^{n}(X_{obs,t} - X_{model,t})^2}{n}} \tag{3.6}$$

$$RMSE_{prop} = \sqrt{(RMSE_{z \sim y})^2 + (RMSE_{x \sim y})^2} \tag{3.7}$$

Where $RMSE$ is the root mean square error, $X_{obs,t}$ and $X_{model,t}$ are the actual and predicted
values of the linear regression t, respectively and where $RMSE_{prop}$ is the propagated
RMSE of RGB~pigment regressions using the RMSE of the RGB~pigment regressions
($RMSE_{z \sim y}$) and the RMSE of the spectral~pigment regressions ($RMSE_{x \sim y}$) (Table 3–8).
All analyses were performed in R (R Core Team, 2017) and an alpha of 0.05 was used.

3.4   Results

3.4.1   RGB Indices as a Surrogate for Pigment-driven Spectral Indices

The strength of the relationships between the RGB indices and the pigment-driven spectral indices was variable between vegetation communities (Table 3-5). The most consistent and strongest regressions across the three vegetation communities were selected and are presented in Table 3-5 and Figure 3-2. The strongest three regressions were observed between RGr and ARI2 in MT ($R^2 = 0.77$, $p < 0.01$, RMSE = 0.04), followed by RG and PSRI in MAT ($R^2 = 0.75$, $p < 0.01$, RMSE = 0.05) and MNT ($R^2 = 0.75$, $p < 0.01$, RMSE = 0.04) (Figure 3-2).
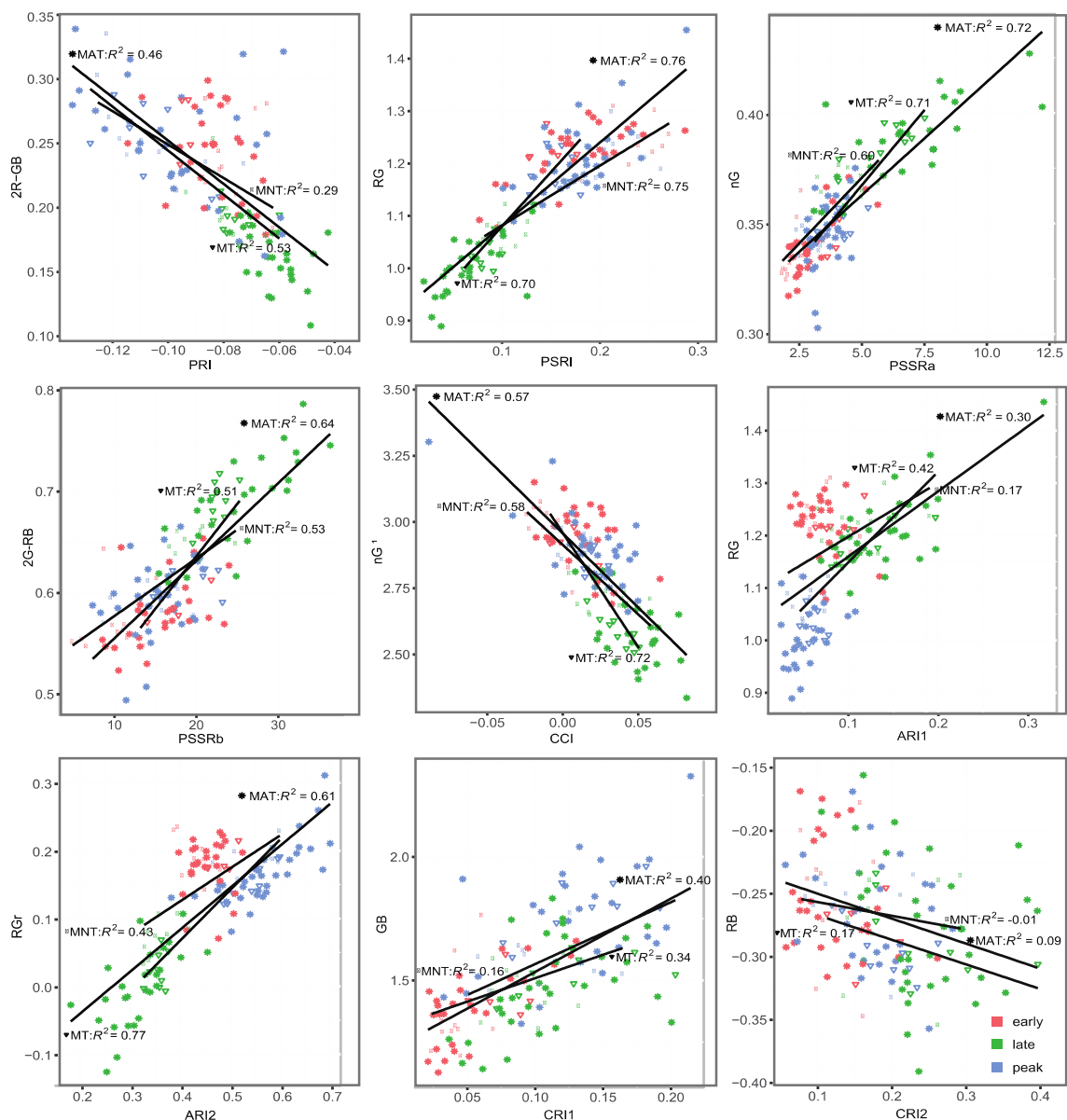
Figure 3-2 Simple linear regression between the six best RGB indices and pigment-driven spectral indices across three seasons in each community type. MAT: Moist acidic tussock tundra, MNT: moist non-acidic tundra, MT: moss tundra, RMSE: root mean square error.

PSRI had the strongest relationships across the three communities while the carotenoid reflectance indices of CRI1 and CRI2 and the anthocyanin index of ARI1 had the weakest relationships. In general, MT had the strongest and most consistent regressions across all indices followed by MAT and finally MNT. We chose the following six RGB indices, 2G-RB, 2R-GB, nG, nG-1, RG, and RGr, representing the pigment-driven indices of PSSRb, PRI, PSSRa, CCI, PSRI, and ARI2, respectively, for linear regression with leaf-level pigment concentration.

Table 3-5 The most consistent, significant linear regressions between Red, Green, Blue (RGB) indices and pigment-driven spectral indices in the three communities. Bold values represent moderate to strong (R2 > 0.40) significant linear regressions. MAT: Moist acidic tussock tundra, MNT: moist non-acidic tundra, MT: moss tundra, RMSE: root mean square error. See Table 2-1 – 3-3 for definitions of both spectral and RGB indices.

Spectral	RGB	MAT			MNT			MT		
		R^2	p-value	RMSE	R^2	p-value	RMSE	R^2	p-value	RMSE
PRI	2R-GB	**0.46**	**<0.01**	**0.04**	0.29	<0.01	0.04	**0.53**	**<0.01**	**0.03**
PSRI	RG	**0.78**	**<0.01**	**0.05**	**0.75**	**<0.01**	**0.04**	**0.70**	**<0.01**	**0.05**
PSSRa	nG	**0.72**	**<0.01**	**0.01**	**0.60**	**<0.01**	**0.01**	**0.71**	**<0.01**	**0.01**
PSSRb	2G-RB	**0.64**	**<0.01**	**0.04**	**0.53**	**<0.01**	**0.03**	**0.51**	**<0.01**	**0.03**
CCI	nG^{-1}	**0.56**	**<0.01**	**0.04**	**0.58**	**<0.01**	**0.02**	**0.73**	**<0.01**	**0.02**
CRI1	GB	**0.40**	**<0.01**	**0.18**	0.16	0.02	0.14	0.34	<0.01	0.14
CRI2	RB	0.09	<0.01	0.05	-0.01	0.43	0.04	0.17	0.03	0.02
ARI1	RG	0.30	<0.01	0.10	0.17	0.01	0.07	**0.42**	**<0.01**	**0.07**
ARI2	RGr	**0.63**	**<0.01**	**0.06**	**0.43**	**<0.01**	**0.04**	**0.77**	**<0.01**	**0.04**

3.4.2   RGB Indices as a Surrogate for Leaf-level Pigment concentration

The relationships between selected RGB indices and pigment concentration suggest high variability in both fit and uncertainty across the three vegetation communities (**Error! Reference source not found.**). In general, the indices performed best across all communities when predicting Chl_a with the strongest observed in MNT. nG, representing PSSRa, had the single strongest regression with Chl_a in MNT (R2 = 0.61, p < 0.01, RMSE-P = 0.89) and this relationship was also moderate in MAT and MT. Chl_{a+b} and $Chl_{a:b}$ also showed weak to moderate correlations but performance across communities was more variable than Chl_a. Both Chl_{a+b} and $Chl_{a:b}$ showed moderate correlations with all indices except 2R-GB in MNT and MAT, respectively. 2R-GB, representing PRI, also had a moderate relationship with $Chl:Car$ in MT (R2 = 0.53, p < 0.01, RMSE = 0.21) but poor performance in the other two communities. The indices performed worst when predicting Chl_b with R2 ≤ 0.27 in all cases.

Table 3-6 Simple linear regression between the selected Red, Green, Blue (RGB) indices, and the spectral index they are representing in parentheses, and pigment concentration with the propagated root mean square error (RMSE–P). Veg: vegetation community, Pig: Pigment concentration. Bold values represent moderate (R2 > 0.40) significant linear regressions. MAT: Moist acidic tussock tundra, MNT: moist non-acidic tundra, MT: moss tundra, RMSE: root mean square error. See Table 3-1 – 3-3 for definitions of both spectral and RGB indices.

Pigment μg/mg a)	Veg	RGB (spectral)											
		2G-RB (PSSRb)				2R-GB (PRI)				nG (PSSRa)			
		R^2	p-value	RMSE	RMSE-P	R^2	p-value	RMSE	RMSE-P	R^2	p-value	RMSE	RMSE-P
Chl_a	MAT	**0.38**	**0.00**	0.31	0.48	0.17	0.02	0.35	0.52	0.39	0.00	0.30	0.42
	MNT	**0.59**	**0.01**	0.12	0.22	0.06	0.26	0.18	0.25	**0.61**	**0.01**	**0.12**	**0.22**
	MT	**0.41**	**0.01**	0.30	0.48	0.23	0.06	0.34	0.50	**0.40**	**0.01**	**0.30**	**0.47**
Chl_b	MAT	-0.02	0.45	0.12	0.18	-0.01	0.44	0.12	0.19	-0.01	0.43	0.12	0.18
	MNT	0.27	0.09	0.07	0.11	-0.14	0.84	0.09	0.11	0.26	0.09	0.07	0.11
	MT	0.08	0.18	0.20	0.29	0.06	0.20	0.20	0.28	0.08	0.18	0.20	0.28
Chl_{a+b}	MAT	0.30	0.00	0.20	0.31	0.15	0.03	0.22	0.33	0.31	0.00	0.20	0.28
	MNT	**0.53**	**0.02**	0.08	0.15	-0.02	0.39	0.12	0.16	0.54	0.01	0.08	0.15
	MT	0.24	0.05	0.20	0.29	0.16	0.10	0.20	0.30	0.24	0.05	0.20	0.28
$Chl_{a:b}$	MAT	**0.50**	**0.00**	0.32	0.53	0.15	0.03	0.41	0.61	**0.50**	**0.00**	**0.32**	**0.51**
	MNT	-0.02	0.38	0.28	0.41	0.33	0.06	0.23	0.37	0.01	0.34	0.28	0.39
	MT	0.12	0.13	0.32	0.36	0.04	0.25	0.33	0.41	0.12	0.13	0.32	0.39
$Chl:Car$	MAT	0.19	0.01	0.18	0.25	0.12	0.04	0.19	0.26	0.20	0.01	0.18	0.26
	MNT	0.01	0.34	0.21	0.30	-0.14	0.93	0.22	0.31	0.01	0.34	0.21	0.31
	MT	0.23	0.06	0.19	0.27	**0.53**	**0.00**	**0.15**	**0.21**	0.24	0.05	0.19	0.29

Table 3-6 continued

b)		nG-1 (CCI)				RG (PSRI)				RGr (ARI2)			
		R²	p-value	RMSE	RMSE-P	R²	p-value	RMSE	RMSE-P	R²	p-value	RMSE	RMSE-P
Chl_a	MAT	0.37	0.00	0.31	0.49	0.35	0.00	0.31	0.46	0.38	0.00	0.31	0.45
	MNT	**0.60**	**0.01**	**0.12**	**0.22**	**0.56**	**0.01**	**0.13**	**0.21**	**0.55**	**0.01**	**0.13**	**0.15**
	MT	0.39	0.01	0.31	0.47	0.35	0.02	0.32	0.47	0.36	0.02	0.31	0.47
Chl_b	MAT	-0.02	0.49	0.12	0.19	-0.02	0.44	0.12	0.19	0.00	0.36	0.12	0.19
	MNT	0.26	0.09	0.07	0.11	0.04	0.29	0.08	0.11	0.03	0.30	0.08	0.11
	MT	0.08	0.19	0.20	0.27	0.08	0.18	0.20	0.28	0.08	0.18	0.20	0.47
Chl_{a+b}	MAT	0.30	0.00	0.20	0.32	0.28	0.00	0.21	0.31	0.31	0.00	0.20	0.30
	MNT	**0.53**	**0.02**	**0.08**	**0.15**	**0.43**	**0.03**	**0.09**	**0.14**	**0.43**	**0.03**	**0.09**	**0.11**
	MT	0.24	0.05	0.20	0.27	0.23	0.06	0.28	0.42	0.23	0.06	0.28	0.41
Chl_{a:b}	MAT	**0.51**	**0.00**	**0.31**	**0.54**	**0.43**	**0.00**	**0.34**	**0.52**	**0.43**	**0.00**	**0.34**	**0.51**
	MNT	0.00	0.35	0.28	0.39	0.22	0.12	0.25	0.37	0.21	0.12	0.25	0.35
	MT	0.12	0.13	0.32	0.39	0.10	0.16	0.32	0.39	0.11	0.15	0.32	0.40
Chl:Car	MAT	0.19	0.01	0.18	0.27	0.20	0.01	0.18	0.26	0.23	0.01	0.18	0.24
	MNT	0.01	0.34	0.21	0.30	-0.05	0.46	0.21	0.31	-0.06	0.47	0.22	0.28
	MT	0.24	0.05	0.19	0.29	0.36	0.02	0.17	0.27	0.35	0.02	0.17	0.23

3.5 Discussion

The relationships between selected RGB indices and pigment-driven spectral indices support the capability of digital cameras to act as a surrogate for in-situ spectral data and for the study of seasonal vegetation changes associated with pigment dynamics in dominant low Arctic vegetation communities. Evidence for the capability of digital cameras as an ecological monitoring tool of vegetation phenology, biomass, and productivity and the relationships of these parameters to spectrally-derived vegetation indices exists in a variety of ecosystems (Ahrends et al., 2009; Anderson et al., 2016; Beamish et al., 2016; Coops et al., 2010; Ide and Oguma, 2010; Migliavacca et al., 2011; Nijland et al., 2014; Westergaard-Nielsen et al., 2013). Our study adds to this knowledge base by expanding to pigment-driven vegetation indices chosen for their indication of photosynthetic efficiency, a parameter of high interest in vegetation remote sensing. In addition, we showcase the utility of a ground-based camera system in an ecosystem characterized by challenging acquisition conditions for spectral data.

There are some technical considerations when using these types of digital cameras that need to be considered such as consumer-grade digital cameras typically have limited range charge couple device/complementary metal oxide semiconductor (CCD/CMOS) sensors and employ automatic exposure adjustments with changing environmental brightness and local illumination. This in turn affects the comparability of images collected under different conditions however this can be overcome through the use of band ratios which are insensitive to brightness. Local illumination differences caused by direct sunlight can still introduce error, however, the Arctic is subject to unique illumination conditions because of the low solar zenith angle, long periods of daylight, and frequent cloud cover leading to frequent diffuse illumination conditions. Previous research has suggested collection of data under uniform cloud cover (diffuse conditions) is ideal (Ide and Oguma, 2010). All images in this study were collected under uniform cloud cover by choice however when considering a framework of high frequency (daily or hourly) data collection these phenomena should be taken into consideration. Additionally, this study does not take into account the impact of atmospheric scattering common in shorter wavelengths (blue) of air- and space-borne platforms. This phenomenon would presumably reduce the correlation in the blue channel and thus its use should be minimized when inferring relationships between air- and

spaceborne platforms. However, the use of the blue channel in ground-based remote sensing as in this study is less of a concern as atmospheric scattering is minimal at this near-sensing scale. Another consideration is that digital cameras contain what is known as a Bayer colour filter array that combines one blue, one red, and two green sensors into an image pixel making green the most sensitive channel in the camera to mirror the sensitivity of the human eye (Bayer, 1976).

From the standpoint of the human eye and digital cameras, all of the best performing RGB indices except one provide a measure of vegetation greenness and the weaker relationships seen with the carotenoid and anthocyanin (non-green pigments) indices are indicative of the cameras overall green-bias or green sensitivity. The best performing RGB green band-based indices of 2G-RB, nG, nG-1, RG, and rGR had the strongest relationships ($R2 >$ 0.43) with the pigment-driven spectral indices of PSSRb, PSSRa, CCI, PSRI, and ARI2, respectively, across all three vegetation communities. The moderate to strong relationships observed in all three communities suggest these RGB indices can be used to monitor seasonal vegetation changes associated with pigment-driven colour changes, mostly related to the amount of green or chlorophyll pigments, in dominant low Arctic vegetation communities (Figure 3-2). Though we found an overall weakness in RGB indices to accurately predict leaf-level pigment concentration, a number of significant weak to moderate relationships between Chl_a and Chl_{a+b} with the green RGB indices suggests they do capture seasonal changes in chlorophyll content. Moderate to weak relationships between pigment concentration and pigment-driven spectral indices have also been reported, even with data collected concurrently at the leaf-level, due to variations in species-specific plant structure and developmental stage (Sims and Gamon, 2002). The pigment concentration presented in this study is an approximation using the mean of dominant vascular species and does not take into account the influence of moss or standing litter, both of which influence greenness, especially at early and late season when vascular vegetation is not fully expanded. This combination of roughly estimated pigment concentration, a greenness signal that is not only composed of vascular species, especially at early and late season, and species-specific characteristics could explain the weak correlations and the differences between communities. However, it should be noted that all indices demonstrated a significant moderate correlation in at least one community with pigment concentration. The five pigment-driven spectral indices used in this study target different pigment groups however all are

relevant for the monitoring of foliar condition and photosynthetic activity suggesting the cameras can also indirectly infer changes to non-green pigment groups through an absence or changes in the greenness or chlorophyll pigments. Though the green RGB indices were generally the most consistent and had the strongest relationships, we also found that PRI is well represented by 2R-GB and nR in MT and MAT (Table 3–5, Table 3–7, Table 3–8). Since the pigment-driven spectral index of PRI is a prominently used index for estimating photosynthetic light use efficiency (Gamon et al., 1997, 1992; Peñuelas et al., 1995), the use of digital camera nR to monitor this parameter is a particularly interesting result.

Current operational satellite missions provide an excellent opportunity for global monitoring of foliar condition with relatively high spatial resolution. Here we focused on exploring the spectral information in the visible wavelength region related to tundra vegetation colour, driven by pigment dynamics. The broadband spectral settings of major operational satellite missions are at first consideration not optimal for capturing the detailed spectral reflectance of vegetation as represented by narrowband spectral vegetation indices. However, we show that RGB colour values from consumer-grade digital cameras measuring even broader-band spectral information show correlations with reputed pigment-driven spectral indices such as CCI, PSSRa and ARI2 indices. Our results suggest vegetation colour contributes strongly to the response of these hyperspectral indices. The use of narrowband spectral indices related to vegetation colour and pigment dynamics in order to monitor vegetation status and condition is already occurring with the Earth Observation System (EOS) products from the Sentinel-2 multispectral satellite and will become more common in the future with upcoming hyperspectral satellite missions such as the Environmental Mapping and Analysis Program (EnMAP) planned for 2020.

3.6 Conclusions

Results of this study support the utility of digital cameras to act as a surrogate for in-situ spectral data to monitor pigment dynamics as a result of seasonal changes in a low Arctic ecosystem. The RGB indices using the green band perform best as proxies for pigment-driven spectral indices. We highlight nG as a proxy for PSSRa in particular because of moderate to strong relationships with both spectral and pigment data suggesting this RGB index can track changes in chlorophyll a content. We also suggest 2G-RB as a proxy for PSSRb, nG-1 for CCI, RG for PSRI and RGr as a proxy for ARI1. Though the accuracy of

pigment prediction for these indices is not as strong, there is evidence that RGB indices do track seasonal changes. This method represents a promising gap-filling tool and complimentary data source for optical remote sensing of vegetation in logistically and climatically challenging Arctic ecosystems. The implementation of low-cost time-lapse systems or nadir point measurements by an observer with consumer-grade digital cameras is highly feasible and proven in Arctic tundra ecosystems and this study increases the possible applications of this method.

3.7   Supplementary Material

Table 3-6 Complete table of simple linear regressions between all pigment-driven spectral indices and Red, Green, and Blue (RGB) indices. Bold values represent moderate ($R^2 > 0.40$) significant linear regressions. MAT: Moist acidic tussock tundra, MNT: moist non-acidic tundra, MT: moss tundra, RMSE: root mean square error. RMSE: root mean square error. See Table 3-1 – 3-3 for definitions of both spectral and RGB indices.

RGB	Veg	Spectral								
a)		PRI			PSRI			PSSRa		
		R^2	p-value	RMSE	R^2	p-value	RMSE	R^2	p-value	RMSE
nG	MAT	0.08	0.01	0.03	**0.70**	**0.00**	**0.01**	**0.72**	**0.00**	**0.01**
	MNT	-0.03	0.73	0.02	**0.71**	**0.00**	**0.01**	**0.60**	**0.00**	**0.01**
	MT	0.33	0.00	0.02	**0.71**	**0.00**	**0.01**	**0.71**	**0.00**	**0.01**
nR	MAT	**0.46**	**0.00**	**0.01**	**0.49**	**0.00**	**0.01**	0.28	0.00	0.02
	MNT	0.29	0.00	0.01	0.32	0.00	0.01	0.17	0.01	0.01
	MT	0.53	0.00	0.01	0.51	0.00	0.01	0.21	0.02	0.01
nB	MAT	0.03	0.07	0.02	0.18	0.00	0.02	0.34	0.00	0.02
	MNT	0.14	0.02	0.02	0.08	0.07	0.02	0.13	0.03	0.02
	MT	0.00	0.33	0.01	0.34	0.00	0.01	**0.69**	**0.00**	**0.01**
GR	MAT	0.25	0.00	0.08	**0.78**	**0.00**	**0.05**	**0.70**	**0.00**	**0.05**
	MNT	0.06	0.10	0.06	**0.80**	**0.00**	**0.03**	**0.63**	**0.00**	**0.04**
	MT	**0.45**	**0.00**	**0.06**	**0.73**	**0.00**	**0.04**	**0.60**	**0.00**	**0.05**
GB	MAT	-0.01	0.57	0.24	**0.43**	**0.00**	**0.18**	**0.60**	**0.00**	**0.15**
	MNT	0.02	0.23	0.15	0.32	0.00	0.13	0.33	0.00	0.12
	MT	0.17	0.03	0.16	**0.59**	**0.00**	**0.11**	**0.80**	**0.00**	**0.08**
nBG	MAT	-0.01	0.93	0.07	**0.42**	**0.00**	**0.06**	**0.55**	**0.00**	**0.05**
	MNT	0.03	0.19	0.05	0.33	0.00	0.04	0.34	0.00	0.04
	MT	0.14	0.05	0.05	**0.57**	**0.00**	**0.03**	**0.78**	**0.00**	**0.02**
RGr	MAT	0.24	0.00	0.08	**0.77**	**0.00**	**0.04**	**0.68**	**0.00**	**0.05**
	MNT	0.07	0.08	0.06	**0.76**	**0.00**	**0.03**	**0.57**	**0.00**	**0.04**

	MT	**0.45**	**0.00**	**0.05**	**0.72**	**0.00**	**0.04**	**0.58**	**0.00**	**0.05**
nG^{-1}	MAT	0.05	0.02	0.19	**0.70**	**0.00**	**0.11**	**0.68**	**0.00**	**0.11**
	MNT	-0.03	0.83	0.13	**0.70**	**0.00**	**0.07**	**0.60**	**0.00**	**0.08**
	MT	0.31	0.00	0.12	**0.70**	**0.00**	**0.08**	**0.70**	**0.00**	**0.08**
2R-GB	MAT	**0.46**	**0.00**	**0.04**	**0.49**	**0.00**	**0.04**	0.28	0.00	0.04
	MNT	0.29	0.00	0.04	0.32	0.00	0.03	0.17	0.01	0.04
	MT	**0.53**	**0.00**	**0.03**	**0.51**	**0.00**	**0.03**	0.21	0.02	0.03

Table 3-7 continued

b)		PSSRb			CCI			CRI1		
		R^2	p-value	RMSE	R^2	p-value	RMSE	R^2	p-value	RMSE
nG	MAT	**0.64**	**0.00**	**0.02**	**0.53**	**0.00**	**0.02**	0.38	0.00	0.02
	MNT	**0.52**	**0.00**	**0.01**	**0.57**	**0.00**	**0.01**	0.24	0.00	0.01
	MT	**0.49**	**0.00**	**0.01**	**0.72**	**0.00**	**0.01**	0.19	0.02	0.02
nR	MAT	0.17	0.00	0.02	0.25	0.00	0.02	0.03	0.05	0.02
	MNT	0.06	0.11	0.01	0.08	0.07	0.01	0.00	0.30	0.01
	MT	0.09	0.10	0.01	0.29	0.01	0.01	-0.05	0.78	0.01
nB	MAT	0.38	0.00	0.02	0.20	0.00	0.02	0.33	0.00	0.02
	MNT	0.20	0.01	0.01	0.20	0.01	0.01	0.09	0.06	0.02
	MT	**0.56**	**0.00**	**0.01**	**0.58**	**0.00**	**0.01**	**0.43**	**0.00**	**0.01**
GR	MAT	**0.57**	**0.00**	**0.06**	**0.50**	**0.00**	**0.08**	0.29	0.00	0.08
	MNT	**0.45**	**0.00**	**0.04**	**0.51**	**0.00**	**0.04**	0.21	0.01	0.05
	MT	0.38	0.00	0.06	**0.63**	**0.00**	**0.05**	0.09	0.09	0.07
GB	MAT	**0.58**	**0.00**	**0.15**	0.38	0.00	0.18	**0.40**	**0.00**	**0.18**
	MNT	0.35	0.00	0.12	0.38	0.00	0.12	0.16	0.02	0.14
	MT	**0.57**	**0.00**	**0.11**	**0.74**	**0.00**	**0.09**	0.34	0.00	0.14
nBG	MAT	**0.55**	**0.00**	**0.05**	**0.42**	**0.00**	**0.16**	**0.41**	**0.00**	**0.06**
	MNT	0.38	0.00	0.04	**0.40**	**0.00**	**0.04**	0.18	0.01	0.05
	MT	**0.59**	**0.00**	**0.03**	**0.73**	**0.00**	**0.03**	0.34	0.00	0.04
RGr	MAT	**0.55**	**0.00**	**0.06**	**0.51**	**0.00**	**0.07**	0.27	0.00	0.08
	MNT	**0.41**	**0.00**	**0.04**	**0.46**	**0.00**	**0.04**	0.18	0.01	0.05
	MT	0.36	0.00	0.06	**0.62**	**0.00**	**0.04**	0.08	0.10	0.07
nG^{-1}	MAT	**0.61**	**0.00**	**0.12**	**0.56**	**0.00**	**0.13**	0.39	0.00	0.15
	MNT	**0.53**	**0.00**	**0.09**	**0.58**	**0.00**	**0.09**	0.25	0.00	0.11
	MT	**0.50**	**0.00**	**0.11**	**0.72**	**0.00**	**0.08**	0.19	0.03	0.13
2R-GB	MAT	0.17	0.00	0.05	0.25	0.00	0.05	0.03	0.05	0.05
	MNT	0.06	0.11	0.04	0.08	0.07	0.04	0.00	0.30	0.04
	MT	0.09	0.10	0.04	0.29	0.01	0.03	-0.05	0.78	0.04

Table 3-7 continued

c)		CRI2			ARI1			ARI2		
		R^2	p-value	RMSE	R^2	p-value	RMSE	R^2	p-value	RMSE
nG	MAT	-0.01	0.50	0.03	0.21	0.00	0.02	**0.46**	**0.00**	**0.02**
	MNT	-0.03	0.80	0.02	0.14	0.03	0.02	0.23	0.00	0.01
	MT	-0.05	0.85	0.02	0.33	0.00	0.02	**0.69**	**0.00**	**0.01**
nR	MAT	0.04	0.04	0.02	0.26	0.00	0.02	**0.57**	**0.00**	**0.01**
	MNT	-0.02	0.56	0.01	0.09	0.06	0.01	**0.41**	**0.00**	**0.01**
	MT	0.08	0.10	0.01	**0.43**	**0.00**	**0.01**	0.69	0.00	0.01
nB	MAT	0.06	0.01	0.02	0.01	0.19	0.02	0.03	0.06	0.02
	MNT	-0.02	0.46	0.02	-0.02	0.56	0.02	-0.03	0.77	0.02
	MT	0.03	0.21	0.01	0.03	0.21	0.01	0.20	0.02	0.01
GR	MAT	-0.01	0.88	0.10	0.26	0.00	0.08	**0.62**	**0.00**	**0.06**
	MNT	-0.04	0.97	0.06	0.17	0.01	0.05	**0.42**	**0.00**	**0.05**
	MT	-0.03	0.53	0.08	0.39	0.00	0.06	**0.77**	**0.00**	**0.04**
GB	MAT	0.02	0.09	0.23	0.09	0.00	0.23	0.21	0.00	0.21
	MNT	-0.02	0.56	0.15	0.02	0.20	0.15	0.00	0.33	0.15
	MT	-0.04	0.60	0.18	0.18	0.03	0.16	**0.48**	**0.00**	**0.13**
nBG	MAT	0.03	0.07	0.07	0.08	0.00	0.07	0.19	0.00	0.07
	MNT	-0.02	0.53	0.05	0.03	0.19	0.05	0.00	0.35	0.05
	MT	-0.03	0.58	0.05	0.17	0.03	0.05	**0.46**	**0.00**	**0.04**
RGr	MAT	-0.01	0.75	0.09	0.28	0.00	0.08	**0.63**	**0.00**	**0.06**
	MNT	-0.04	0.92	0.06	0.18	0.01	0.05	**0.43**	**0.00**	**0.04**
	MT	-0.02	0.49	0.07	**0.41**	**0.00**	**0.06**	**0.77**	**0.00**	**0.04**
nG^{-1}	MAT	-0.01	0.50	0.20	0.21	0.00	0.18	**0.44**	**0.00**	**0.15**
	MNT	-0.03	0.76	0.13	0.13	0.03	0.12	0.21	0.01	0.12
	MT	-0.05	0.84	0.15	0.33	0.00	0.12	**0.68**	**0.00**	**0.08**
2R-GB	MAT	0.04	0.04	0.05	0.26	0.00	0.05	0.57	0.00	0.03
	MNT	-0.02	0.56	0.04	0.09	0.06	0.04	0.41	0.00	0.03
	MT	0.08	0.10	0.04	**0.43**	**0.00**	**0.03**	**0.69**	**0.00**	**0.02**

Table 3-7 Complete table of simple linear regressions between all pigment-driven spectral indices and pigment concentration. Pigment: Chl_a: chlorophyll a, Chl_b: chlorophyll b, Chl_{a+b}: total chlorophyll, $Chl_{a:b}$: chlorophyll a to b ratio. Veg: vegetation communities. MAT: Bold values represent moderate ($R^2 > 0.40$) significant linear regressions. Moist acidic tussock tundra, MNT: moist non-acidic tundra, MT: moss tundra, RMSE: root mean square error. See Table 3-1 – 3-3 for definitions of both spectral and RGB indices.

Pigment	Veg									
a)		PRI			PSRI			PSSRa		
		R^2	p-value	RMSE	R^2	p-value	RMSE	R^2	p-value	RMSE
Chl_a	MAT	0.27	0.00	0.02	**0.42**	**0.00**	**0.05**	**0.56**	**0.00**	**1.37**
	MNT	0.24	0.10	0.01	0.25	0.10	0.05	0.07	0.25	0.89
	MT	0.24	0.06	0.01	0.28	0.05	0.03	0.24	0.06	1.00
Chl_b	MAT	0.07	0.07	0.02	0.06	0.10	0.06	**0.51**	**0.00**	**1.44**
	MNT	0.17	0.15	0.01	-0.01	0.38	0.05	0.01	0.33	0.92
	MT	0.15	0.12	0.01	0.11	0.16	0.04	0.10	0.17	1.09
Chl_{a+b}	MAT	0.25	0.00	0.02	0.35	0.00	0.05	**0.51**	**0.00**	**1.44**
	MNT	0.33	0.06	0.01	0.19	0.14	0.05	0.01	0.33	0.92
	MT	0.10	0.17	0.01	0.11	0.16	0.04	0.10	0.17	1.09
$Chl_{a:b}$	MAT	0.13	0.03	0.02	0.00	0.05	45.22	0.29	0.00	1.74
	MNT	-0.11	0.67	0.01	0.37	0.05	29.81	0.03	0.30	0.91
	MT	-0.04	0.45	0.01	0.11	0.04	28.62	0.09	0.18	1.10
$Chl:Car$	MAT	0.17	0.01	0.02	0.01	0.05	54.42	0.10	0.04	1.95
	MNT	-0.03	0.42	0.01	**0.62**	**0.06**	**33.19**	-0.14	0.91	0.99
	MT	0.50	0.01	0.01	0.21	0.04	28.54	-0.09	0.77	1.20
b)		PSSRb			CCI			CRI1		
		R^2	p-value	RMSE	R^2	p-value	RMSE	R^2	p	RMSE
Chl_a	MAT	0.31	0.00	5.23	0.23	0.01	0.40	0.12	0.03	0.06
	MNT	0.02	0.32	3.77	0.06	0.26	0.18	-0.14	0.89	0.04
	MT	0.16	0.11	2.60	0.29	0.03	0.34	-0.06	0.55	0.05
Chl_b	MAT	0.14	0.02	5.85	0.02	0.48	0.20	0.02	0.23	0.06
	MNT	-0.07	0.51	3.94	-0.11	0.68	0.09	-0.10	0.60	0.04
	MT	-0.05	0.51	2.91	0.22	0.06	0.181	-0.09	0.77	0.05
Chl_{a+b}	MAT	0.31	0.00	5.25	0.09	0.08	0.26	0.10	0.04	0.06
	MNT	-0.03	0.42	3.87	-0.02	0.39	0.12	-0.14	1.00	0.04
	MT	0.01	0.31	2.82	0.21	0.07	0.29	-0.08	0.71	0.05
$Chl_{a:b}$	MAT	0.19	0.01	5.69	0.24	0.01	0.44	0.03	0.18	0.06
	MNT	-0.14	0.97	4.07	0.04	0.29	0.27	0.06	0.26	0.04

Table 3-8 continued

	MT	0.44	0.01	2.12	0.05	0.22	0.22	0.00	0.35	0.04
Chl:Car	MAT	0.26	0.00	5.43	0.01	0.12	0.57	-0.01	0.42	0.06
	MNT	-0.07	0.52	3.95	-0.11	0.64	0.22	-0.02	0.39	0.04
	MT	0.21	0.07	2.52	-0.08	0.81	0.22	0.26	0.05	0.04

c)		CRI2			ARI1			ARI2		
		R^2	p	RMSE	R^2	p	RMSE	R^2	p	RMSE
Chl$_a$	MAT	-0.03	0.79	0.10	0.18	0.01	0.05	**0.42**	**0.00**	**0.09**
	MNT	0.07	0.25	0.07	**0.40**	**0.04**	**0.03**	**0.83**	**0.00**	**0.03**
	MT	-0.08	0.67	0.08	0.10	0.17	0.04	0.31	0.04	0.07
Chl$_b$	MAT	-0.03	0.98	0.10	0.02	0.23	0.05	0.06	0.10	0.12
	MNT	0.01	0.33	0.07	0.04	0.29	0.04	0.22	0.11	0.07
	MT	-0.07	0.60	0.08	0.06	0.22	0.04	0.16	0.11	0.08
Chl$_{a+b}$	MAT	-0.03	0.79	0.10	0.16	0.01	0.05	0.36	0.00	0.10
	MNT	0.05	0.27	0.07	0.29	0.08	0.04	**0.74**	**0.00**	**0.04**
	MT	-0.07	0.60	0.08	0.09	0.19	0.04	0.20	0.08	0.08
Chl$_{a:b}$	MAT	-0.01	0.45	0.09	0.20	0.01	0.05	0.35	0.00	0.10
	MNT	-0.14	0.92	0.07	-0.07	0.50	0.05	0.16	0.15	0.07
	MT	-0.05	0.50	0.08	-0.09	0.78	0.04	-0.08	0.69	0.09
Chl:Car	MAT	0.22	0.00	0.08	**0.44**	**0.00**	**0.04**	0.37	0.00	0.10
	MNT	0.30	0.08	0.06	**0.40**	**0.04**	**0.03**	0.21	0.12	0.07
	MT	**0.70**	**0.00**	**0.04**	**0.85**	**0.00**	**0.02**	**0.53**	**0.00**	**0.06**

3.7.1 Data Publication

All data are publically available on the Open Access library Pangaea (www.pangaea.de)

https://doi.org/10.1594/PANGAEA.886340

https://doi.org/10.1594/PANGAEA.886337

https://doi.org/10.1594/PANGAEA.886335

4 Implications of Litter and Non-vascular Components on Multiscale Hyperspectral Data in a Low Arctic Ecosystem

Beamish A.L.1, Brell M.2, Chabrillat S.2, Coops N.C.3, Heim B.1

[1]   Alfred Wegener Institute, Helmholtz Centre for Polar and Marine Research, Research Unit Potsdam, Telegrafenberg A45, 14473, Potsdam, Germany

[2]   Helmholtz Centre Potsdam (GFZ), German Research Centre for Geosciences, Telegrafenberg A17, 14473, Potsdam, Germany

[3]   Integrated Remote Sensing Studio (IRSS) Faculty of Forestry, University of British Columbia, 2424 Main Mall, Vancouver, V6T1Z4 Canada

4.1 Abstract

The spatio-temporal heterogeneity of terrestrial Arctic ecosystems including an abundance of litter and non-vascular components and moisture conditions, presents unique challenges for accurate and detailed monitoring of vegetation change. At the plot scale, narrowband spectral data has been shown to be superior to broadband data in monitoring and characterizing terrestrial Arctic vegetation but how these signals scale spatially is still relatively unknown. In the following study we use senescent stage ground-based, airborne and simulated satellite spectral data to examine how spatial aggregation influences spectral signatures of six dominant low Arctic vegetation communities. A linear mixing analysis was applied using litter, moss, and water (dark) spectra to explore the influence of different combinations on these cover types on broader spatial resolutions typical of air and spaceborne sensors. The mixture analysis was conducted across ten biophysically important wavelengths. Results suggest that litter was the most influential ecosystem components when data were spatially aggregated from the ground to airborne scale and that influence increased further from the ground to spaceborne scale. Mixtures of up to 70% litter and moss resulted in the greatest convergence of ground-based and airborne spectral reflectance. At the spaceborne scale only mixtures of litter resulted in a convergence of spectral reflectance with percent mixtures up to 75% in the majority of sampled communities. As expected convergence varied by vegetation community but in general was greatest in the tussock sedge-shrub communities. The influence of litter has important implications for monitoring vegetation at the satellite scale as these ecosystem components influence the interpretation of biophysical variables. This is of particular importance in the tussock

sedge-shrub communities, which are dominant across the western North American and Siberian Arctic. This study represents a snap shot of the heterogeneity of Arctic tundra ecosystems. With continuing accessibility and coverage of high-resolution spectral data, better spatio-temporal characterization of non-vascular/non-photosynthetic components will greatly improve our understanding of Arctic heterogeneity and the environmental gradients driving it.

Keywords: hyperspectral remote sensing, low Arctic, vegetation, linear mixing

4.2   Introduction

Terrestrial Arctic vegetation is inherently heterogeneous, defined locally by surface moisture and micro-topographic gradients as well as broadly by climatic, geological, and geographical gradients. These local and regional factors influence vegetation over both time and space. For example, the timing of snowmelt, which is broadly dictated by climate and geographic position and locally influenced by micro-topography, is the main driver of the onset of vegetation phenology and also influences surface moisture regimes (Billings and Bliss, 1959). As such, changes within one season such as delayed or advanced snowmelt can influence vegetation phenology, which in turn can influence overall productivity and reproductive success of species (Bjorkman et al., 2015; Iler et al., 2013; Wheeler et al., 2015). At broader scales, persistent changes in the depth of the snowpack and timing of snowmelt driven by climate change could alter surface hydrological regimes changing the habitat suitability with implications for the composition and biodiversity of some slow-growing and low-fecundity Arctic species (Wrona et al., 2016). In Arctic ecosystems, local and regional changes in terrestrial vegetation from phenology to species composition are particularly important to characterize and monitor, as Arctic vegetation is a sensitive indicator of climate change (Elmendorf et al., 2012; Prevéy et al., 2017). The spatio-temporal gradients of Arctic ecosystems have direct implications for monitoring vegetation, and perhaps more importantly, monitoring ecosystem transitions in a changing Arctic.

Accurately characterizing the spatio-temporal heterogeneity of Arctic vegetation is a challenge, as it requires consistent and reproducible data at many scales and frequencies. The multitude of currently available remote sensing data offers significant potential despite the often challenging acquisition conditions. Persistent cloud cover, low sun angle, and polar night combined with the prostrate nature of Arctic plants and ubiquity of standing litter and

non-vascular species create unique challenges for remote sensing of Arctic vegetation at high temporal frequencies.

Tussock tundra vegetation communities cover much of the Arctic tundra in western North America and Siberia (Walker et al., 1994). These communities are dominated by the tussock-forming sedge *Eriophorum vaginatum* with an abundant Sphagnum species and are underlain by acidic substrates. A non-tussock sedge community also dominates the correspondingly abundant nonacidic substrates dominated by *Carex bigelowii* (Walker et al., 1994) with an abundance of the evergreen dwarf shrub *Dryas integrifolia*. Due to low decomposition rates and sequential seasonal growth, both sedges maintain persistent and high fractions of standing litter throughout the growing season. As previously mentioned, these sedge-dominated tussock communities occur in complexes with dwarf-shrubs and moss species (Shaver et al., 1986). Deciduous dwarf shrub species that dominate on acidic substrates follow a more seasonal pattern with peaks in litter fraction following snowmelt and late senescence. Evergreen and seasonal green species, which dominate in the nonacidic substrates, have sequential growth or re-greening (of over-wintering leaves) growth patterns resulting in greater and persistent litter fractions (Mayo et al., 1973). Many moss species exists within tussock and other Arctic tundra vegetation communities across a wide gradient of moisture conditions, often as an "understory" species. Sphagnum species create a dominant vegetation complex with *E. vaginatum* in acidic tussock tundra types. Some of these bryophyte species can adjust their productivity with moisture availability, greening up when water is abundant and browning when water is limited (Gaalen et al., 2007; Oechel et al., 1978). Spatio-temporal patterns of surface moisture also influence the optical properties of Arctic tundra beyond the broad-scale moisture gradients (Stow et al., 2004). When the perennially unfrozen top layer of soil, known as the active layer, is at a minimum, limiting infiltration and resulting in some communities high fractions of standing water. At senescence, when the green cover fraction is minimized water may also become a dominant fraction in the wetter water track and sedge marsh communities. The spatio-temporal influence of persistent standing litter, moss abundance, and surface moisture are likely not limited to seasons when the green cover fraction is at a minimum. The contributing proportions may change within a season and between years highlighting the importance of accurate characterization of these ecosystem components.

The role of high spectral resolution remote sensing data including imaging spectroscopy

(IS) at multiple spatial scales is of particular interest in Arctic ecosystems to attempt to address and overcome some of the unique conditions presented by these ecosystems. Ground-based and airborne spectral measurements have been used extensively in many ecosystems to characterize vegetation from functional groups to individual species as well as retrieval of a range of biophysical parameters such as biomass, photosynthetic activity, and phenological stage. The application of these high-spectral resolution data in Arctic ecosystems remains largely limited to ground-based characterization of vegetation functional types or communities and airborne characterization of geological units (Beamish et al., 2017; Bratsch et al., 2016; Buchhorn et al., 2013; Huemmrich et al., 2013; Rogge et al., 2014). Though recent studies have highlighted the superiority of high spectral resolution plot-based data in monitoring and characterizing vegetation (Liu et al., 2017). Recent projects, such as the North American Space Agency's (NASA) Arctic-Boreal Vulnerability Experiment (ABoVE) airborne campaign as well as the German Aerospace Agency's (DLR) upcoming hyperspectral Environmental Mapping and Analysis Program (EnMAP) satellite are increasing the coverage and availability of detailed IS data in Arctic ecosystems (Guanter et al., 2015). The EnMAP mission in particular will provide landscape scale IS data at a spatial, spectral, and temporal scale previously not available likely providing new insights into changing Arctic vegetation. EnMAP simulation studies have shown that the sensor will be capable of monitoring gradual ecosystem change even in sparsely vegetated systems (Leitão et al., 2015; Schwieder et al., 2014). Though the temporal frequency of acquisitions will remain a challenge due to the frequency of inclement weather, the detailed data provided by successful acquisitions will complement existing and concurrent data acquisitions.

Given the limited availability of IS data in Arctic ecosystems, we have a limited understanding of how the spatio-temporal heterogeneity of Arctic ecosystems and resulting spectral characteristics are represented at multiple spatial scales. To successfully and effectively apply IS data to questions of Arctic vegetation change, the non-photosynthetic and non-vascular aspects of Arctic ecosystem heterogeneity and the resulting complexity of linking vegetation signals from the ground to air and spaceborne scales should be examined.

Accurate interpretation of high resolution imagery requires knowledge of the ecosystem components influencing spectral reflectance both internal and external to the studied area (Guyot et al. 1992). Internal factors include biotic components such as fractional species

coverage and geometry, understory and soil properties, and phenological stage while external factors can range from weather conditions to viewing angle of the sensor to the ground in relation to the sun (Guyot et al. 1992, Schaaf et al., 1994). Chen, (1999) defines and measures the heterogeneity caused by intrinsic and extrinsic components using either texture or contexture. Contexture is defined by the size, shape, area, and distribution of the components and is generally considered as the fractional cover within a pixel. Indices calculated within a specified viewing window calculate the average variability of both continuous and discreet ecosystem components which has been shown to greatly misrepresent the biophysical variables of the targeted vegetation (Chen, 1999). Contexture-based approaches, that is, scaling by sub-pixel cover fractions, have shown to greatly improve estimations of biophysical parameters such as leaf-area-index (LAI) (Chen, 1999).

To better understand the impact of this spatially heterogeneous landscape we in this research examine the spectral characteristics of six low Arctic vegetation communities at the ground-based, airborne and simulated satellite scale during the senescent season. We compared ground-based spectral signatures of six dominant vegetation communities to corresponding spectral signals from a hyperspectral Airborne Imaging Spectrometer for Applications (AISA-Eagle, 1.3 m) and simulated Environmental Mapping and Analysis Program (EnMAP, 30 m). Ground-based spectra from non-photosynthetic and non-vascular ecosystem components including water, litter, and moss were then individually and iteratively mixed with ground-based spectra of each vegetation community and convergence to hyperspectral AISA and simulated EnMAP data was evaluated at specific wavelength regions corresponding to photosynthetic pigment absorption as well as vegetation canopy and cellular structure. Mixed spectra were then used to calculate relevant narrow band vegetation indices (VIs) and compared to ground-based values and leaf-level pigment concentration. From these results we hope to highlight the influence of these dynamic non-vascular and non-photosynthetic ecosystem components have on the biophysical interpretation of green vegetation signals in low Arctic ecosystems.

4.3   Materials and Methods

4.3.1   Study Site

The Toolik Lake Research Natural Area (68°62.57 N, 149°61.43 W) is located in north

central Alaska on the North Slope of the Brooks Range, representative of the North Slope physiographic province of the Southern Arctic Foothills (Walker et al., 1989). Dominant vegetation types are dictated by soil moisture and include moist tussock tundra, wet sedge meadows, and dry upland heaths. The Toolik Vegetation Grid within the Toolik Lake Research Natural Area is a long-term monitoring site established by the National Science Foundation as part of the R4D Project (Response, Resistsnce, Resilience, and Recovery to Disturbance in Arctic Ecosystems). We sampled six dominant vegetation communities within the Toolik Vegetation Grid. The sampled vegetation communities are representative of the Alaskan low Arctic and can be used for comparison with larger scale airborne (1.3 m) and satellite (30 m) observations. Detailed descriptions of the six vegetation communities, as defined by the hierarchal physiognomic classification of the Alaska Geobotany Center, and representative photographs taken during the senescent season can be found in Table 4-1 and Figure 4-1, respectively.
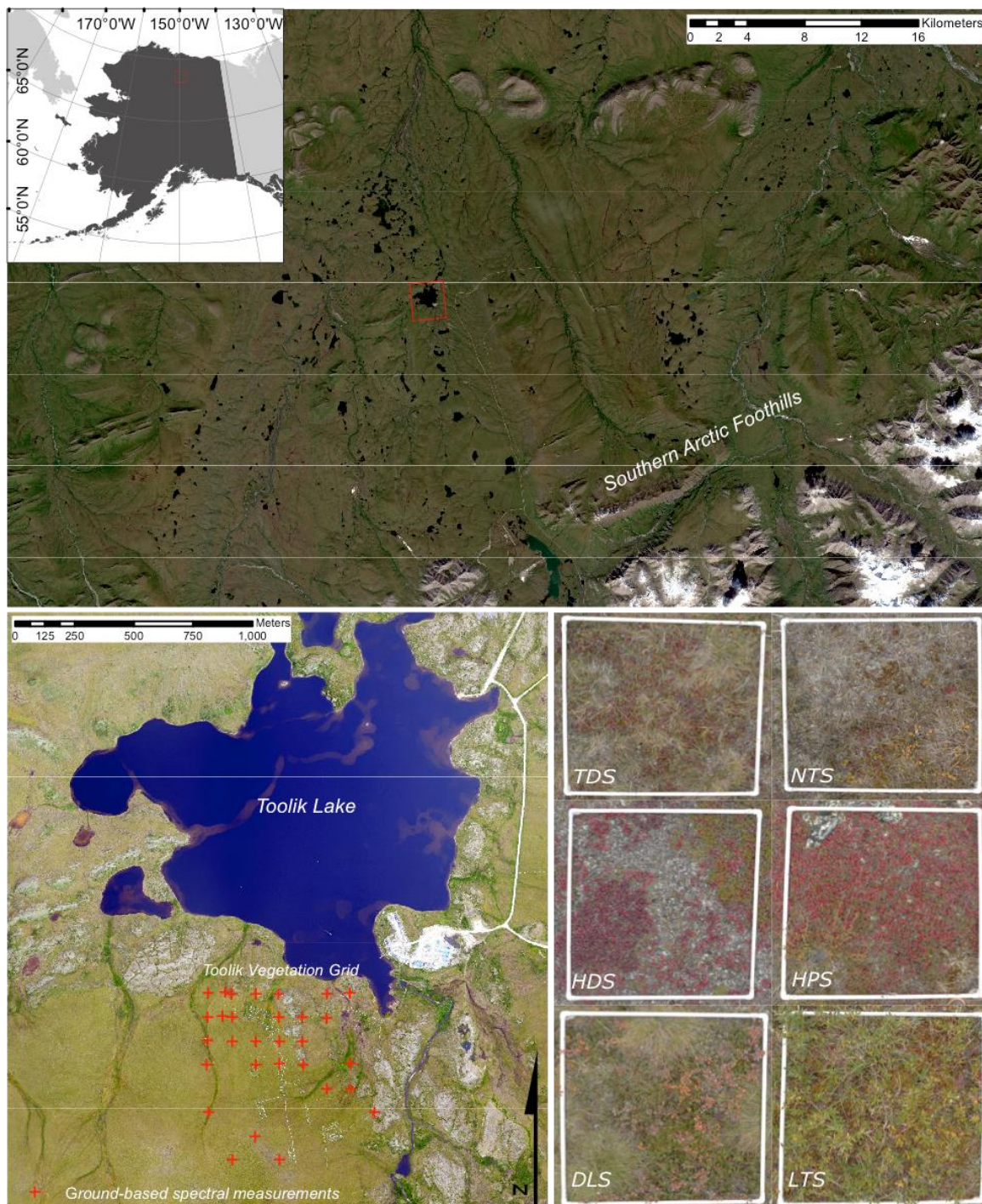
Figure 4-1 Toolik Lake Research Natural Area located in north central Alaska in the Southern Arctic Foothills on the North Slope of the Brooks Range. Lower left inset shows the Toolik Vegetation Grid where ground-based spectral measurements were collected. Lower right inset shows typical late season digital photographs of each of the six vegetation communities where ground-based spectra were collected. TDS: Tussock sedge, dwarf-shrub, moss tundra, NTS: Non-tussock sedge, dwarf-shrub, moss tundra, HDS: Hemi-prostrate and prostrate dwarf-shrub, forb, moss, fruticose-lichen tundra, HPS: Hemi-prostrate dwarf shrub fruticose-lichen tundra, DLS: Dwarf-shrub or low-shrub, sedge, moss, tundra, LTS: Low and tall shrublands.

Table 4-1 Toolik Lake Area Vegetation classification of the six sampled vegetation communities as defined by the Alaska Geobotany Center's hierarchal physiognomic classification.

Circum-polar Arctic	Toolik Lake Area	Description	Short form
Grami-noid tundra	Tussock sedge, dwarf-shrub, moss tundra	Moist acidic tussock tundra complexes dominated by graminoids. Dominant plant communities include: Eriophorum vaginatum-Sphagnum and Carex bigelowii-Sphagnum. Mesic to subhygric, acidic, shallow to moderate snow. Stable slopes. Some areas on steeper slopes with solifluction are dominated by Bigelow sedge (Carex bigelowii)	TDS
	Non-tussock sedge, dwarf-shrub, moss tundra	Moist nonacidic tundra complexes. Dominant plant communities include: Carex bigelowii-Dryas integrifolia and other subtypes of this unit (e.g., Salix glauca, Equisetum arvense and Cassiope tetragona). Includes some miscellaneous graminoid communities mostly on disturbed areas, such as Deschampsia caespitosa; Rumex arcticus-Carex saxatilis; Salix chamissonis-Carex aquatilis; Ranunculus pedatifidus-Poa glauca. Mesic to subhygric, circumneutral, shallow to moderate snow. Solifluction areas and somewhat unstable slopes, mainly on Itkillik II glacial surfaces. Some south-facing slopes have scattered glaucous willow (Salix glauca). Also includes some miscellaneous graminoid-dominated sites: deep-snow stream margins, landslides, some rocky drained lake basins and animal dens.	NTS
Pros-trate-shrub tundra	Hemi-prostrate and prostrate dwarf-shrub, forb, moss, fruticose-lichen tundra	Hemi-prostrate and prostrate dwarf-shrub, forb, moss, fruticose-lichen tundra. Snowbed communities dominated by either Cassiope tetragona or Salix rotundifolia. These communities are not differentiated at this scale, but include Cassiope tetragona-Carex microchaeta (acidic sites); Cassiope tetragona-Dryas integrifolia (nonacidic sites); Salix rotundifolia-Sanionia uncinata (deep snowbeds). Includes all snowbed types.	HDS
	Hemi-prostrate dwarf shrub fruticose-lichen tundra	Hemi-prostrate dwarf-shrub, fruticose-lichen tundra. Dry or moist shrublands with very low-growing or creeping dwarf-shrubs. Dominant plant communities include Betula nana-Hierochloe alpina; Salix pulchra-Hierochloe alpina; and those dominated by Ledum palustre ssp. decumbens, Empetrum nigrum or Vaccinium uliginosum. Subxeric to mesic, acidic, with shallow snow. Shallow depressions on dry glacial till or outwash.	HPS

Table 4-1 continued

Cir-cumpo-lar Arc-tic	Toolik Lake Area	Description	Short form
Erect-shrub tundra	Dwarf-shrub or low-shrub, sedge, moss, tun-dra	Moist acidic tundra complexes dominated by shrubs, includ-ing shrubby tussock tundra. Dominant plant communities in-clude Betula nana-Eriophorum vaginatum and Salix pulchra-Carex bigelowii. Also dwarf-shrub tundra dominated by dwarf birch or willows. Dominant plant communities in-clude Betula nana-Rubus chamaemorus and Salix pulchra-Sphagnum. Mesic to subhygric, moderate snow. Lower slopes and upland water-track margins, often with solifluc-tion. Or palsas and high-centered polygons.	DLS
	Low and tall shrub-lands	A wide variety of low to tall shrublands. Dominant plant communities include those growing in upland water tracks such as Salix pulchra-Eriophorum angustifolium and Erioph-orum angustifolium-Sphagnum squarrosum; those growing along streams such as Salix pulchra-Dasiphora fruticosa and other low and tall shrublands; upland shrublands dominated by Salix glauca and/or Alnus crispa or Populus balsamif-era and shrublands on river gravels dominated by feltleaf wil-low (S. alaxensis) or lanate willow (S. richardsonii). Low shrubs in upland water tracks, streamsides and south facing slopes, mesic to subhydric, often with deep snow.	LTS

4.4   Remote Sensing Data

4.4.1   Ground-based Image Spectroscopy Data

Ground-based spectral radiance measurements were acquired with a GER 1500 field spec-trometer (350–1050 nm; 512 bands, spectral resolution 3 nm, spectral sampling 1.5 nm, and 8° field of view, Spectra Vista Co., Poughkeepsie, USA). Data were collected on Au-gust 23rd 2016 (Day of Year (DOY) 236) under sunny conditions between 10:00 and 14:00 local time to ensure the highest solar zenith angle. Spectra were acquired at nadir approxi-mately 1 m off the ground resulting in a Ground Instantaneous Field of View (GIFOV) of approximately 15 cm in diameter. The average of nine point measurements of upwelling radiance (L_{up}) collected in 1×1 m plots was used to represent each of the six vegetation communities. Downwelling radiance (L_{down}) was measured as the reflectance from a white Spectralon© plate. Surface reflectance (R) was processed as $L_{up}/L_{down} \times 100$ (0–100%). Reflectance spectra were preprocessed with a Savitzky–Golay smoothing filter (n = 11) and subset to 400–900 nm to remove sensor noise at the edges of the radiometer detector and for comparison with airborne data.

4.4.2 Airborne AISA Hyperspectral Data

Hyperspectral imagery was acquired using an Airborne Imaging Spectrometer for Applications (AISA-Eagle sensor) mounted in a Basler BT-67 aircraft on August 27th 2016 (DOY 240) under clear conditions between 12:20 and 12:50 pm local time. The acquisition consisted of five flight lines flown south to north in an east to west pattern. The first three of the five flight lines flown were the focus of this study encompassing an area approximately 700 ha (Figure 4-2a). The AISA Eagle imager had 130 bands (404.9 – 1002.5 nm) with a bandwidth of 4 nm and a spatial resolution of 1.3 m at nadir (Figure 4-2b). The data were atmospherically and radiometrically corrected. The radiometric correction was performed using sensor specific instrument manufacturer's software. The direct geometric correction was performed also using manufacturers software by using the simultaneously measured IMU/GPS data stream. Subsequently, the geocorrected radiance data was atmospherically corrected based on ATCOR4. During this procedure a small spectral shift of the AISA sensor was detected and corrected (Richer and Schläpfer, 2018). The resulting surface reflectance flight lines were subset to the first 110 bands (404.9 – 907.6 nm).
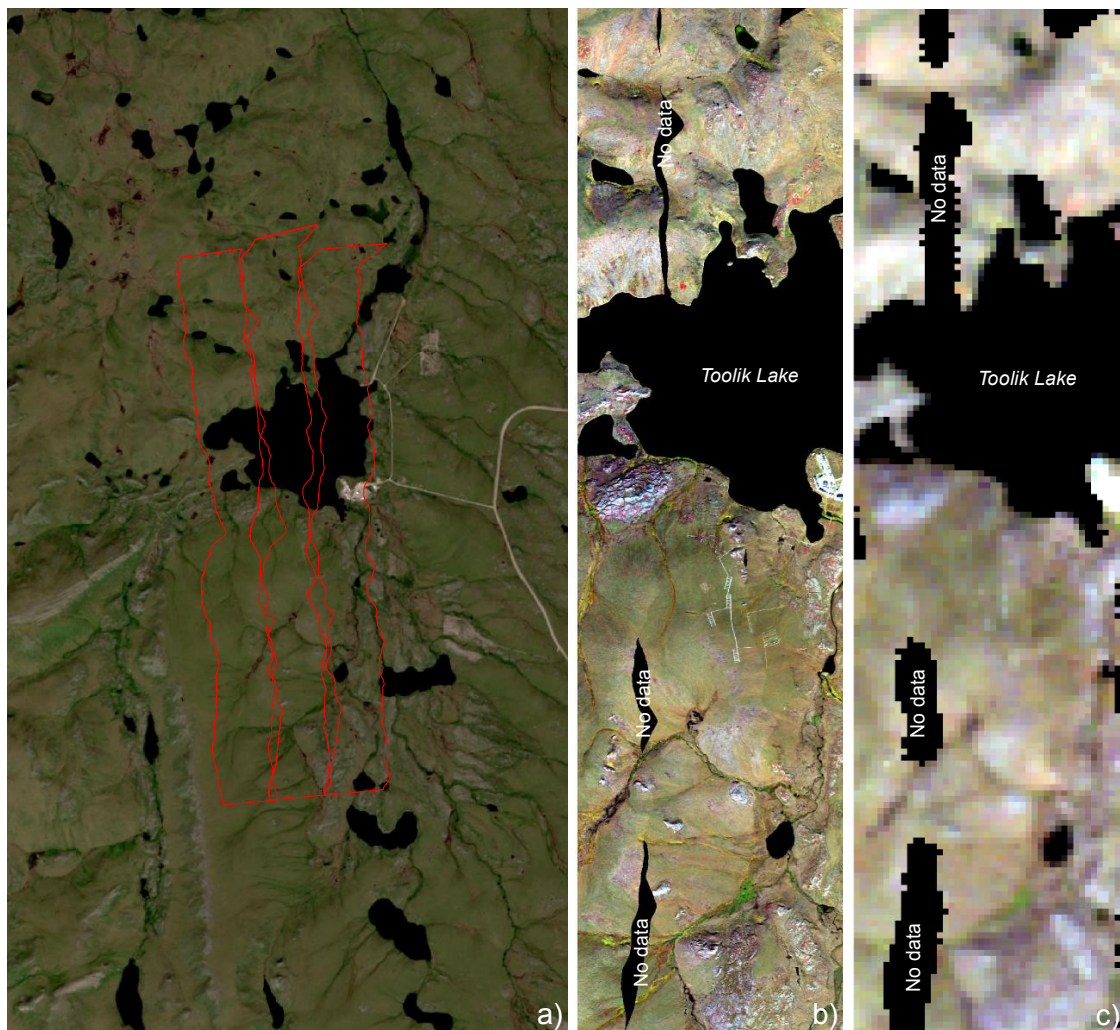
Figure 4-2 a) Footprint of the first two AISA flight lines flown south to north and west to east as shown on a peak season Sentinel 2 image. b) Orthomosaic of the AISA flight lines clipped to the general area where ground-based data were collected. c) Simulated EnMAP orthomosaic generated from the AISA data. Black areas marked with No data are the result of non-overlapping flight lines. Black areas not marked with No data are masked water bodies.

4.4.3   EnMAP Simulation

The upcoming hyperspectral EnMAP satellite will have 242 bands covering the visible to the short wave infrared (VSWIR; 420 – 2450 nm) with a bandwidth between 6.5 and 10 nm, and a ground sampling distance of approximately 30 m. As part of the scientific preparatory program, an EnMAP End-to-End Simulation tool (EeteS) was developed by the German Centre for Geosciences (GFZ) to provide a complete and accurate simulation of image generation, calibration, and the processing chain (Segl et al., 2012, 2010).

The individual AISA flight lines were used as input to the EeteS and Level 2A EnMAP-like flight lines of the study area were generated (Figure 4-2c). The simulation begins by transforming the AISA reflectance data to EnMAP reflectance data by modelling atmospheric conditions, and accounting for the differences in spatial, spectral, and radiometric specifications of the two sensors. An EnMAP image is then simulated through the processing chain from onboard calibration, to atmospheric correction to orthorectification. The resulting EnMAP image had 78 bands (423 – 903 nm).

4.4.4 Spectral Comparison by Wavelength

To first explore differences between the pure ground-based spectra, and AISA/EnMAP spectra in each vegetation community, the AISA and EnMAP spectra were normalized to the ground-based spectra. The ground-based data were first spectrally transformed to AISA and EnMAP resolution and then data were normalized and scaled by total reflectance using the following equation:

$$R_{norm} = \frac{(R_{i\lambda} - R_{j\lambda})}{R_{j\lambda}} \qquad (4.1)$$

Where R_i is the reflectance of AISA or EnMAP at wavelength λ and R_j is the percent reflectance of the spectrally transformed ground-based spectra at wavelength λ.

4.4.5 Linear Mixture Analysis

Spectral data from AISA and simulated EnMAP data were extracted based on the geolocation of ground-based spectral data (Figure 4-1). Table 4-2 shows the number of individual ground-based spectral measurements for each vegetation type and the corresponding number of AISA and EnMAP pixels. Nine point measurements were collected in each 1×1 m plot corresponding to one AISA/EnMAP pixel.

Table 4-2 The number of individual ground-based spectral measurements (n=9 per 1 × 1 m plot) and the corresponding number of AISA and simulated EnMAP pixels for each of the six vegetation communities.

Vegetation community	Ground-based	AISA/EnMAP
Tussock sedge, dwarf-shrub, moss tundra	81	9
Non-tussock sedge, dwarf-shrub, moss tundra	27	3
Hemi-prostrate and prostrate dwarf-shrub, forb, moss, fruticose-lichen tundra	27	3
Hemi-prostrate dwarf shrub fruticose-lichen tundra	36	5
Dwarf-shrub or low-shrub, sedge, moss, tundra	27	3
Low and tall shrublands	45	5
Litter	20	-
Moss	9	-
Water	-	11

Litter and moss spectral signatures were extracted from ground-based data collected with the GER concurrently with the other ground-based data and the water (dark) spectra were acquired from the AISA image (Figure 4-3). The litter spectra were extracted from a mesic sedge-dominated tussock community and a xeric prostrate-shrub dominated system. The moss spectra come from a mesic tussock tundra system in which all vascular plants were removed and the water spectra were extracted from Toolik Lake in the AISA image.
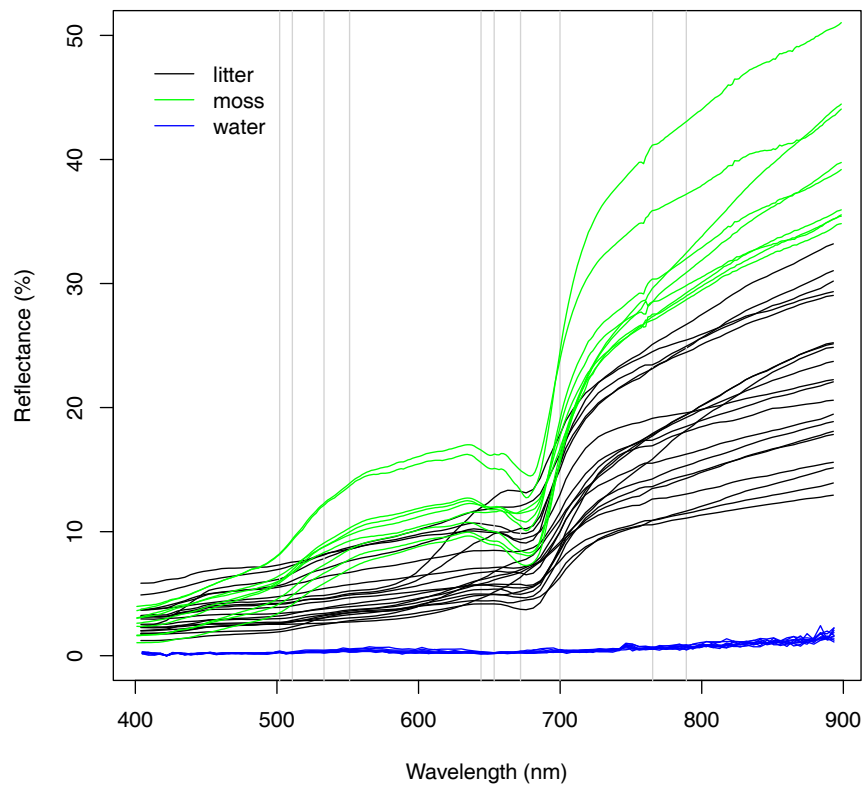
Figure 4-3 Litter, moss, and water spectra used in the linear mixing analysis. Vertical lines represent 10 biophysically important wavelengths from left to right chlorophyll/carotenoid absorption (502, 511, and 533 nm), green reflectance (551 nm), chlorophyll absorption (644, 653, and 672 nm), red-edge transition (699 nm), and the NIR plateau (765 and 789 nm).

To examine the influence of inherent ecosystem components on spatial aggregation, spectra of litter, water (dark), and moss spectra were mixed with ground-based spectra of each of the six vegetation communities and compared to corresponding AISA and EnMAP spectra. To do this, the litter, water, moss, and ground-based spectra in questions were spectrally transformed to ASIA and EnMAP resolution using the spectral response functions of each sensor. The spectrally transformed litter, water and moss spectra were then individually iteratively mixed 500 times with the spectrally transformed ground-based spectra of each of the six vegetation communities. We chose 500 iterations of each ecosystem component to obtain a wide range of artificial mixtures and conducted this at percentages from 1 to 79% of the total signal at increments of 5%. The various mixtures from each community were then compared to the corresponding AISA and EnMAP spectra using simple linear regression. Ten key wavelengths were chosen to explore the convergence results of the simple linear regression between mixed ground-based and AISA and EnMAP spectra (Fig-

ure 4-2). The wavelengths were chosen based on spectral regions used in narrowband pigment-driven VIs and are broadly categorized into chlorophyll/carotenoid absorption (502, 511, and 533 nm), green reflectance (551 nm), chlorophyll absorption (644, 653, and 672 nm), red-edge transition (699 nm), and NIR plateau (765 and 789 nm). We chose to perform the linear regression on ten key wavelengths as they represent wavelengths that are relevant to vegetation monitoring. A sensitivity analysis was conducted by examining the root mean square error (RMSE) through the 500 iterations of each percent mixture. The optimal mixture was chosen as the minimum RMSE value within 0.01% reflectance stabilized across a 5% increase in mixture percentage for AISA and 0.1% reflectance for EnMAP.

4.5 Results

4.5.1 Spatial Scaling of Spectral Signals

Ground-based, AISA, and simulated EnMAP spectra from the six sampled vegetation communities are presented in Figure 4-4. In all communities there is a clear shift in the position of the red-edge transition to shorter wavelengths from the ground-based to AISA and from AISA to EnMAP probably due to a mixture of several effects such as mixing in the sensor field-of-view, sensor characteristics and data processing. In general, the EnMAP spectra were flatter and had greater reflectance in the visible spectrum (400–700 nm) than the AISA data. Spectral variability in the NIR decreased from the ground to spaceborne scale in all but NTS, DLS and HDS. The AISA data showed strong water absorption components in the NIR around 750 and 810 nm that were not present in the ground-based or simulated EnMAP data due to smoothing from resampling.
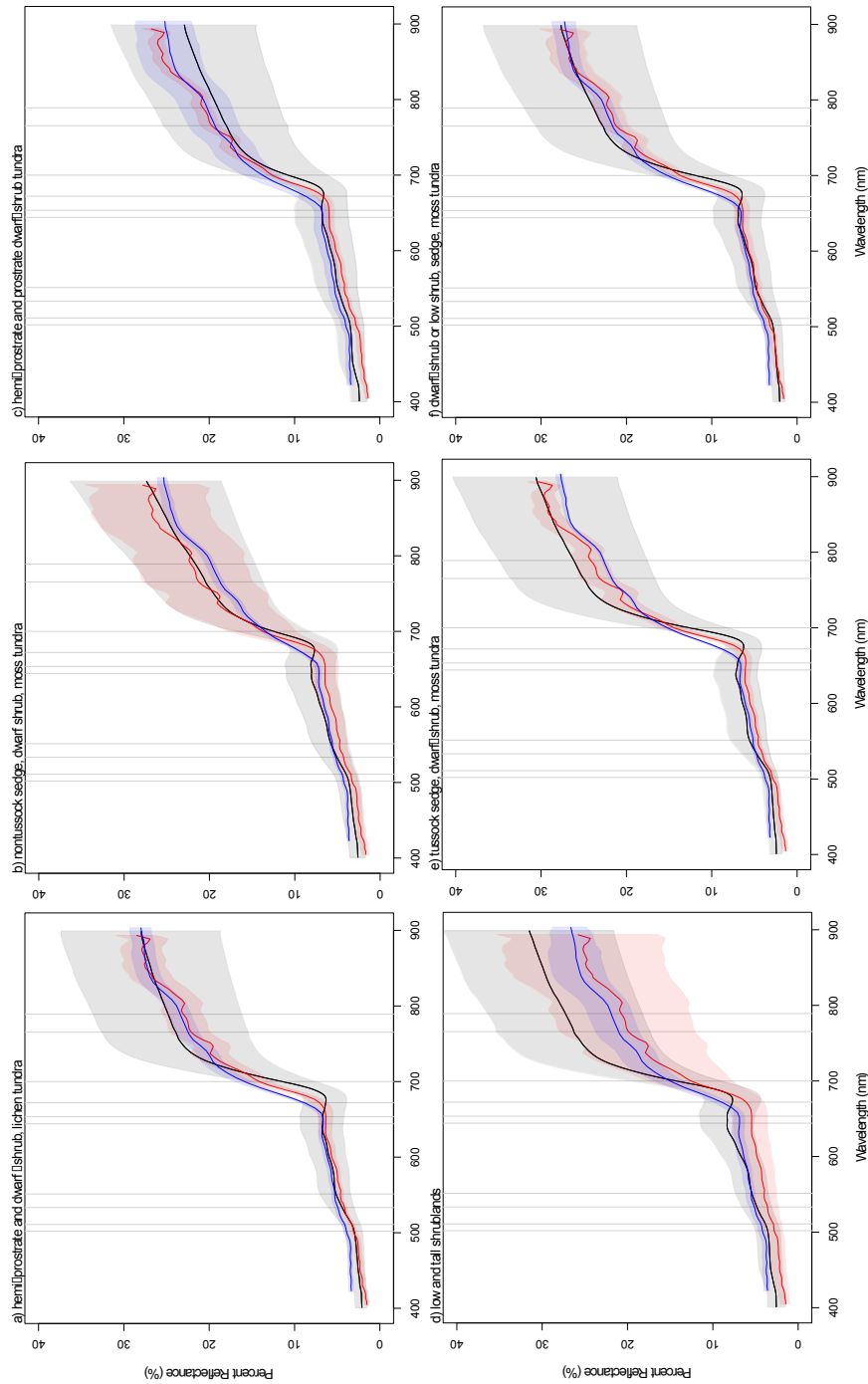
Figure 4-4 Spectral signatures from the six different vegetation communities as measured by the ground-based GER (black lines), aerial AISA (red lines), and simulated EnMAP satellite (blue lines). Vertical lines represent 10 biophysically important wavelengths from left to right chlorophyll/carotenoid absorption (502, 511, and 533 nm), green reflectance (551 nm), chlorophyll absorption (644, 653, and 672 nm), red-edge transition (699 nm), and the NIR plateau (765 and 789 nm).

Normalization plots confirm that AISA data from the mesic TDS and LTS had the greatest correspondence to the ground-based spectra while xeric HDS was the poorest (Figure 4-5). These plots also show that in general, the blue wavelengths (400–500 nm), followed by the red-edge transition have the greatest differences from the ground to the aerial and ground to the satellite scale. The NIR was relatively similar between the two scales with the exception of the xeric-mesic hemi-prostate communities of HDS and HPS. In all communities except TSD and LTS, reflectance around the chlorophyll/carotenoid wavelengths of 502 and 511 nm was greater in the ground-based data as demonstrated by the negative values. In all communities the reflectance was also greater in the ground-based data at the chlorophyll wavelengths of 644 and 653 nm, while for the chlorophyll absorption maximum at 672 nm, reflectance was relatively similar between the AISA and ground-based data. In TSD and LTS the differences were minimal at both the chlorophyll and chlorophyll/carotenoid absorption regions compared to the other vegetation communities.
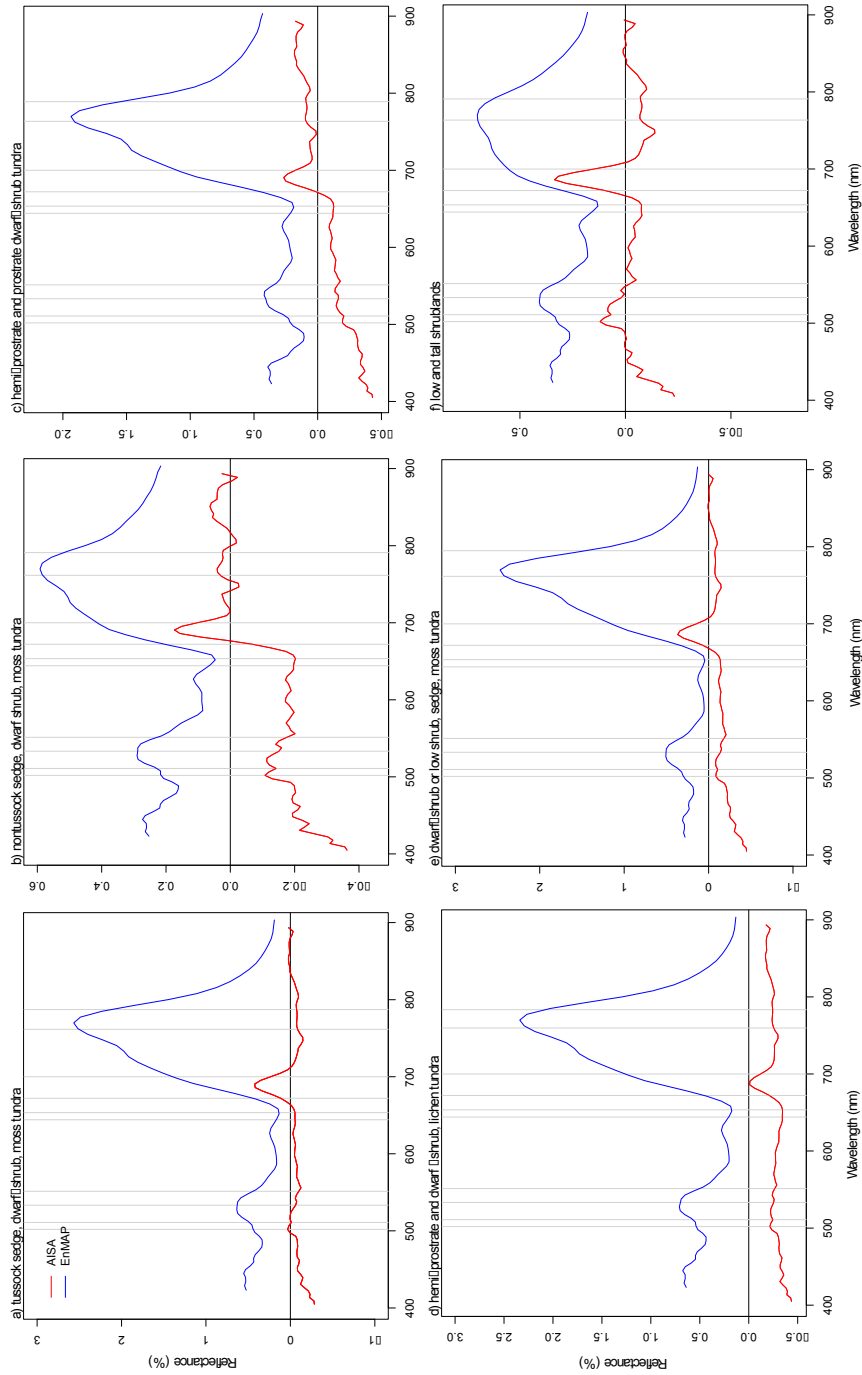
Figure 4-5 Normalized AISA (red lines) and simulated EnMAP (blue lines) spectra by vegetation community. Normalization was scaled by percent reflectace at each wavelength. Normalization was scaled by percent reflectace at each wavelength. Spectra from AISA and simulated EnMAP were normalized at each wavelength by the ground-based spectra data collected in the same location and community type. The red lines represent normalized AISA and the blue simulated ENMAP. Vertical lines represent 10 biophysically important wavelengths from left to right chlorophyll/carotenoid absorption (502, 511, and 533 nm), green reflectance (551 nm), chlorophyll absorption (644, 653, and 672 nm), red-edge transition (699 nm), and the NIR plateau (765 and 789 nm).

The results of the sensitivity analysis for both AISA and EnMAP are shown in Figure 4-6. Overall the RMSE at the EnMAP scale was greater than the AISA scale. The communities of TDS and DLS had the greatest RMSE between pure ground-based spectra and AISA/EnMAP spectra while HPS spectra had the lowest. The remaining communities showed similar patterns of RMSE at the AISA and EnMAP scale with the exception of NTS which had lower error at EnMAP scale.

Overall lichen mixtures resulted in the greatest minimization of error at both the AISA and EnMAP scale though the degree of minimization was community dependent. The greatest minimization of error was observed in TSD and DLS followed by LTS. At the AISA and EnMAP scale, the remaining communities of HPS, HDS, and NTS showed minimal improvements in error with increasing litter content.

Percent moss content had a variable effect on the RMSE with error minimization seen only in TDS, DLS and LTS at the AISA scale. TDS once again showed the greatest minimization with increasing moss content followed by DLS. In all other communities at the AISA scale and in all communities at the EnMAP scale, increasing moss content increased RMSE suggesting little moss contribution at the air and spaceborne scales. Water showed no error minimization effects at either the AISA or EnMAP scale.
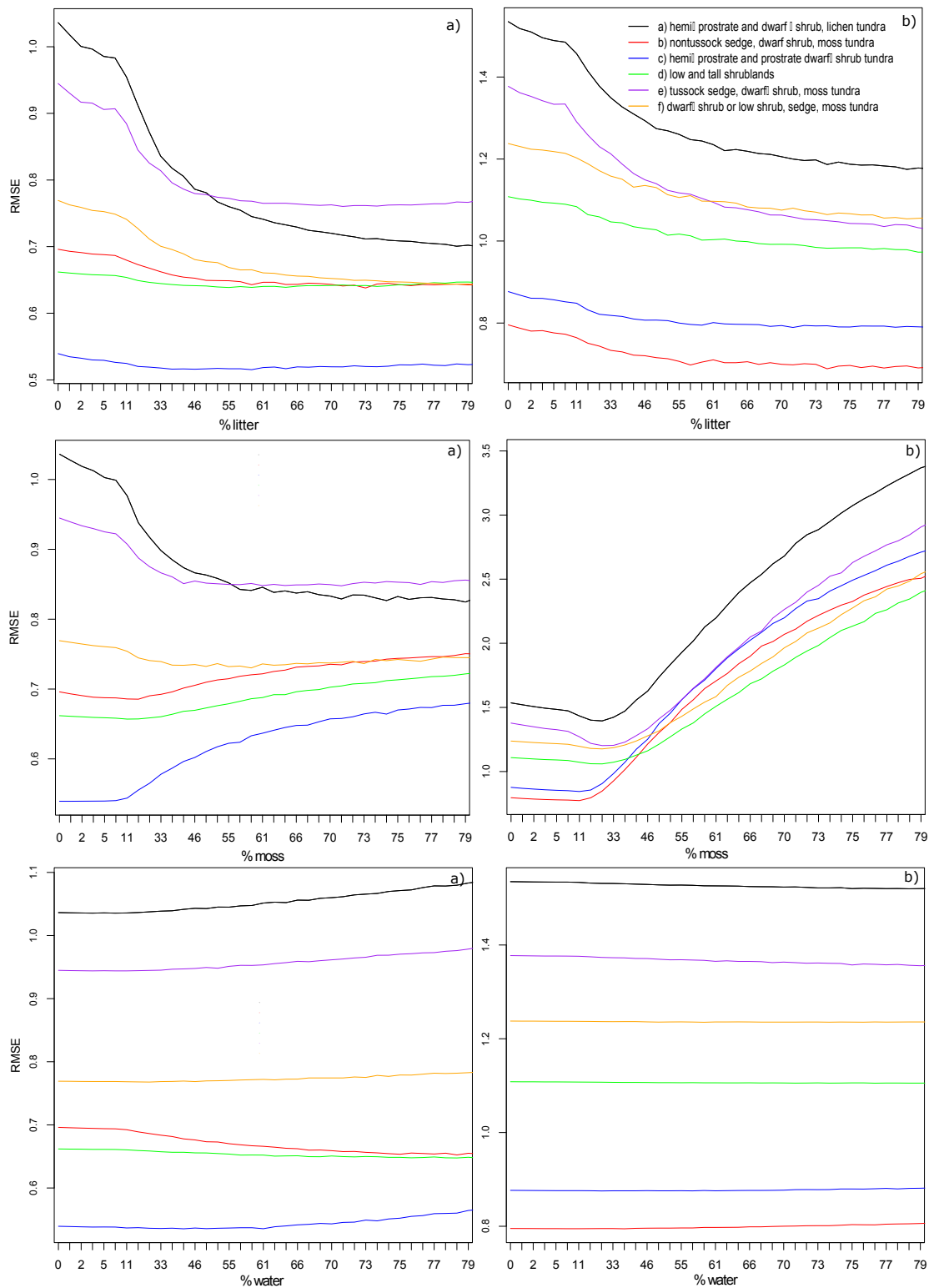
Figure 4-6 RMSEs (%) from the iterative linear mixing analysis. Lines represent the minimum RMSE from the 500 iterations of each percent mixture from linear regressions of ten key wavelengths between a) AISA and mixed ground-based and b) EnMAP and mixed ground-base.

The optimal mixtures of lichen and moss at the AISA scale, as well as lichen at the EnMAP scale are presented in Figure4-7, Figure4-8, Figure 4-9, and Table 4-3. The moss data at the EnMAP scale and water data at both scales were excluded, as there were no improvements in the error performance.

Table 4-3 Optimal mixtures from the linear mixture analysis of litter and moss. Data represent the mixture that minimized root mean square error (RMSE) or the linear regression between ten key wavelengths.

Vegetation	Litter				Moss	
	% mix	RMSE	% mix	RMSE	% mix	RMSE
	AISA		EnMAP		AISA	
Tussock sedge, dwarf-shrub moss tundra	70	0.72	75	1.18	55	0.87
Non-tussock sedge dwarf-shrub moss tundra	46	0.65	75	0.69	-	-
Hemi-prostrate and prostrate dwarf-shrub forb moss fruticose-lichen tundra	10	0.53	60	0.80	-	-
Hemi-prostrate dwarf shrub fruticose-lichen tundra	15	0.65	70	0.98	-	-
Dwarf-shrub - low-shrub sedge moss tundra	61	0.76	75	1.02	40	0.88
Low and tall shrublands	60	0.65	75	1.04	-	-

The percent litter in the optimal mixtures varied by vegetation community at both the AISA and EnMAP scale (Figure 4-7, Figure 4-8). The optimal litter mixtures at the EnMAP scale had greater percentages than at the AISA scale though in general the communities showed similar patterns between scales. At both scales, the tussock communities of TDS and DLS, and the erect shrub community of LTS had high percentage optimal mixtures while the dry communities of HDS and HPS had relatively low percentage optimal mixtures. However, at the AISA scale HDS and HPS had substantially lower percentage optimal mixtures relative to the other communities when compared to EnMAP. Only in TDS and DLS at the AISA scale did moss minimize error (Figure 4-9). TDS once again had a high percentage optimal mixture similar to the percentage optimal litter mixture.
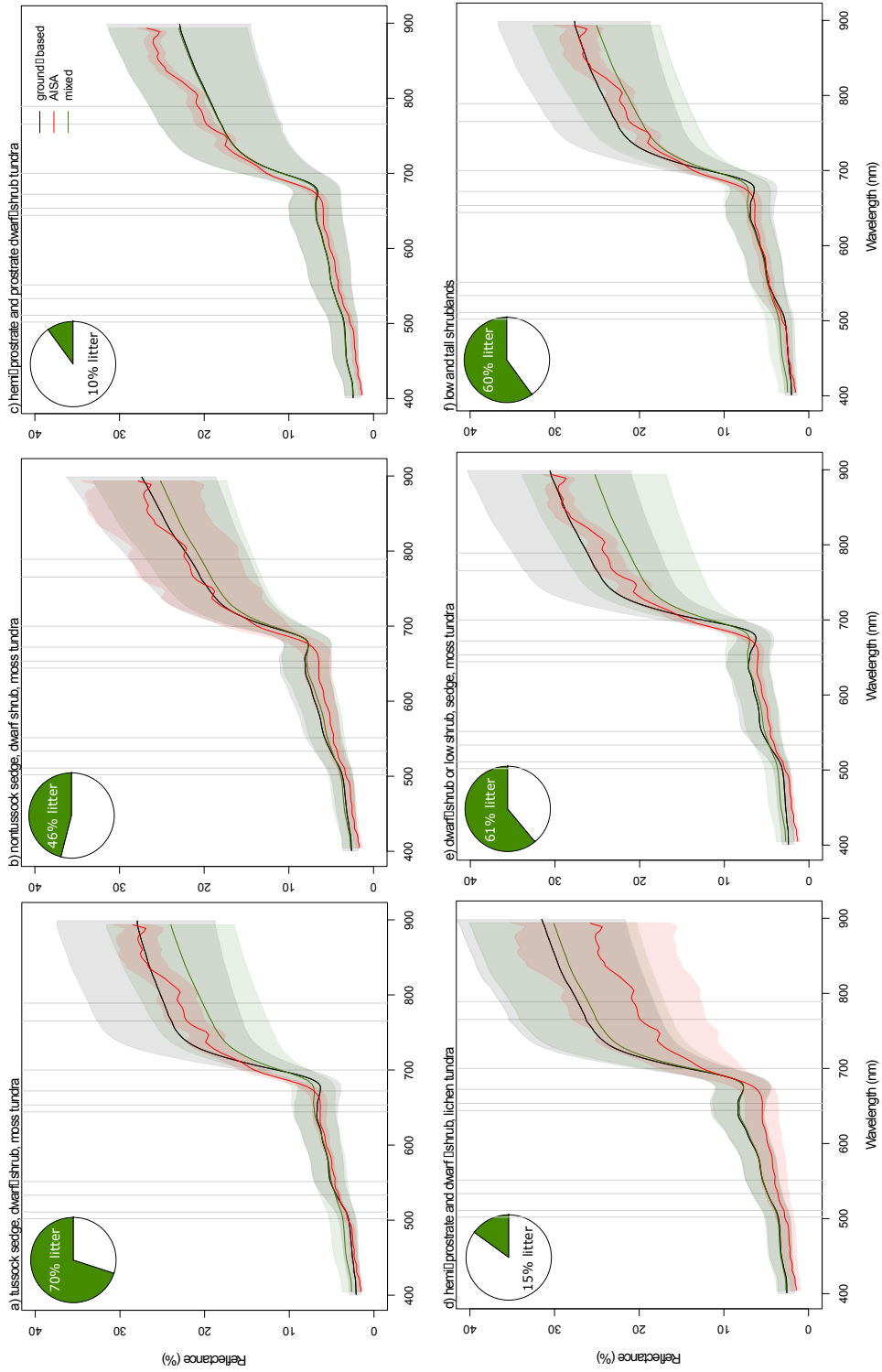
Figure 4-7 The litter mixtures with optimal model performance for the AISA data in the six vegetation communities (a–f). Inset pie charts define the percent litter (green) and the remaining vegetation community signal (white). The black line represents the pure ground-based spectra of each community type, the green is the optimal litter/vegetation signal and the red is the corresponding AISA spectra.
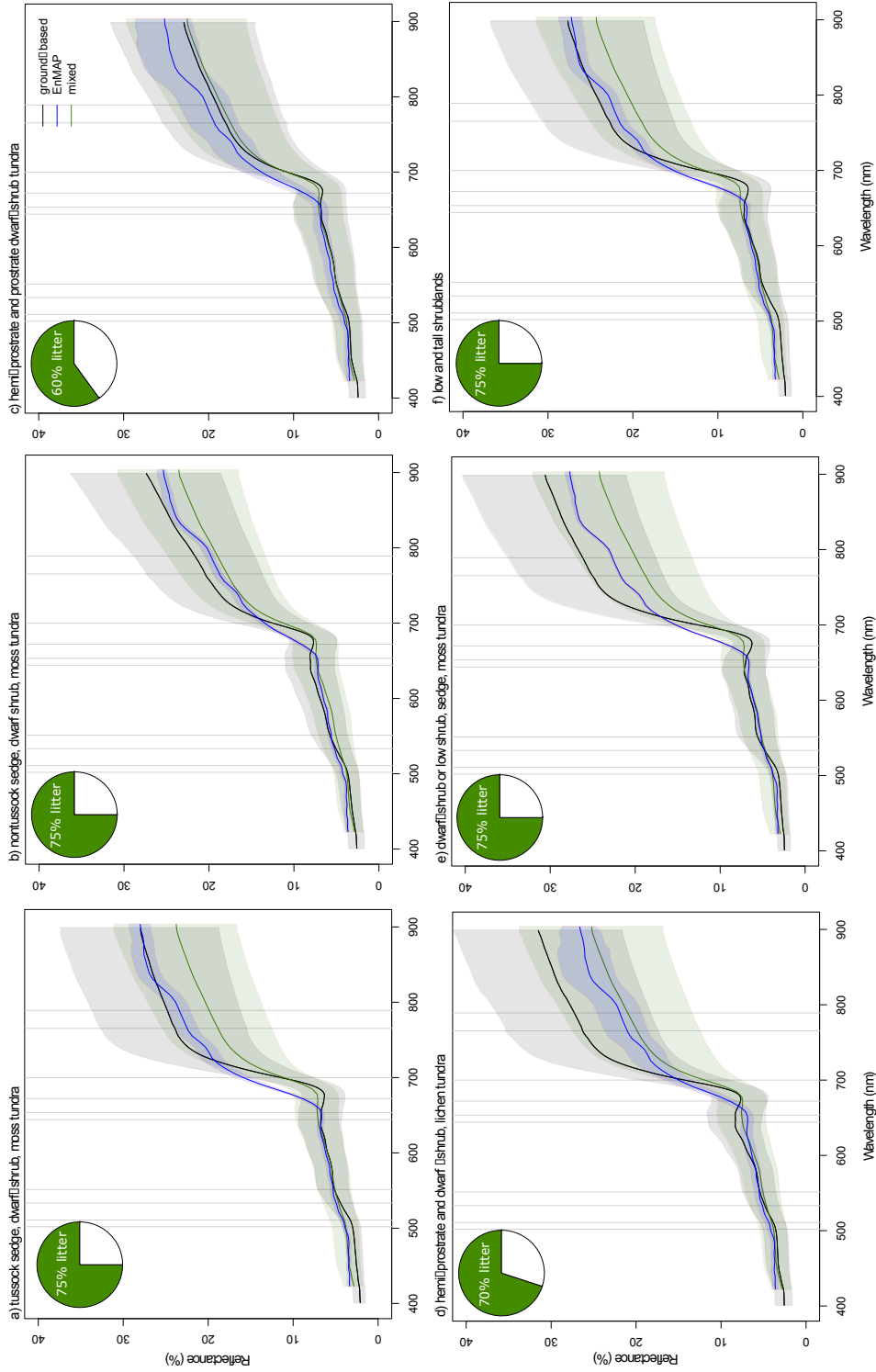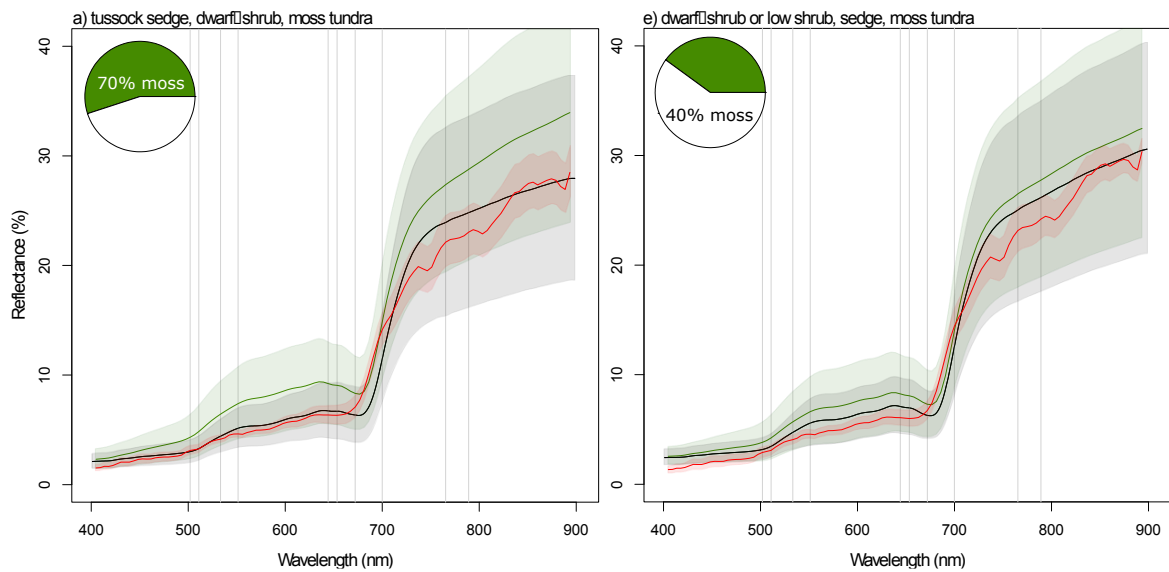
Figure 4-8 The litter mixtures with optimal model performance for the EnMAP data in the six vegetation communities (a–f). Inset pie charts define the percent litter (green) and the remaining vegetation community signal (white). The black line represents the raw ground-based spectra of each community type, the green is the optimal litter/vegetation signal and the blue is the corresponding EnMAP spectra.

Figure 4-9 The moss mixtures with optimal model performance for the AISA data in two vegetation communities (a, e). Inset pie charts define the percent litter (green) and the remaining vegetation community signal (white). The black line represents the raw ground-based spectra of each community type, the green is the optimal litter/vegetation signal and the red is the corresponding AISA spectra.

4.6 Discussion

This study illustrates the potential of hyperspectral satellite data like EnMAP to characterize low Arctic vegetation communities while also highlighting the important influence of non-photosynthetic (i.e. litter and water) and non-vascular (i.e. lichen and moss) ecosystems components when data are spatially aggregated from the ground (15 cm), to airborne (1.3 m), and to satellite (30 m) scales. The artificial linear mixture analysis suggests that the litter signal is the dominant non-vascular/non-photosynthetic ecosystem components influencing the spectral reflectance of ten biophysically important wavelengths when data are spatially aggregated and it increases with increasing spatial aggregation.

Standing litter is ubiquitous component of Arctic ecosystems but our results suggest this signal is more influential in tussock sedge-shrub vegetation communities. The greatest minimization of error for litter mixtures was seen in the Tussock sedge dwarf-shrub moss tundra community and the Dwarf-shrub to low-shrub sedge moss tundra, both of which are dominated by the tussock-forming sedge *Eriophorum vaginatum* (Walker et al., 1994). This important Arctic species and the tussock communities it creates are a dominant vegetation type across the western North American and Siberian Arctic. *E. vaginatum* tussocks have a high standing litter content due to the sequential growth and senescence of tillers within

101

one growing season and as a result of low decomposition rates of Arctic ecosystems (Shaver et al., 1986). van Leeuwen and Huete, (1996) previously demonstrated the significant influence of standing litter on the spectral reflectance of vegetation using artificial mixtures. They illustrated how without a priori knowledge of the vegetation/litter composition, the interpretation of biophysical signals from green vegetation could be inaccurate. In Arctic ecosystems it has been reported widely that narrowband VIs derived from hyperspectral data are superior for inferring biophysical parameters such as light-use efficiency and LAI from vegetation biomass and percent green cover (Buchhorn et al., 2013; Liu et al., 2017). Our linear regression results from ten biophysically important wavelengths, supported by the findings of van Leeuwen and Huete, (1996) suggest that when data are spatially aggregated the influence of litter on the overall vegetation signal will convolute the biophysical signal at the airborne and spaceborne scale.

Moss also appears to be influential in the two tussock communities at the airborne scale. The presence of moss is a common characteristic in larger tussocks, which are likely better represented at the airborne scale than smaller tussocks (Shaver et al., 1986). This could explain the observed RMSE minimization with the inclusion of moss spectra. The lack of importance of moss in the other communities could be explained by the fact that moss is often masked by vascular plants within the canopies of Arctic ecosystems (Liu et al., 2017). Although bryophytes often make up a large percentage of total biomass, they often occur under the canopy of vascular species and litter and therefore are likely not strongly represented at the airborne and satellite scale. Water showed a minimal influence in spatial aggregation of the spectral signals suggesting that at the time of acquisition, this ecosystem component was not dominant.

Direct comparison of spectral signatures showed particularly low correspondence between the ground-based, AISA and simulated EnMAP at the red-edge transition and the NIR plateau. A shift of up to 20 nm was observed in some communities even after the linear mixture analysis. It is clear there is an additional non-vascular component influencing reflectance in this area of the spectrum (Rock et al., 1988). This is of particular interest because some of the highest correspondence between the different scales was at the chlorophyll absorption region in the red part of the spectrum, which has implications for many VIs using ratios between red and NIR. This combination of lower NIR plateau and greater red reflectance

at the airborne and simulated satellite scale could lead to misinterpretation through under-estimation of the green vegetation signal at the airborne and satellite scales. The influence of ecosystem components like litter and moss within an actual 30 m EnMAP scene will of course depend on sub-pixel vegetation composition. Community composition, patch size, and patch location within a scene and pixel will be differently affected by spatial scaling. Through exercises like the one detailed in this study and further hyperspectral studies, improved characterization of litter and other non-vascular/non-photosynthetic components can improve spectral unmixing techniques and in turn the interpretation of the biophysical signals of living, green vegetation.

Extrinsic factors including bidirectional reflectance distribution function (BRDF), shadows, aerosols, and sensor distortions could also be effecting the spatial aggregation but are not considered in this study. Previous research has shown that in Alaskan Arctic tundra, BRDF effects increase with increasing spectral resolution and surface roughness, in turn effecting interpretation of VIs (Buchhorn et al., 2016). We can assume that the influence of solar zenith angle and shadow was consistent across spatial scales, and therefore minimized, given the ground-based and aerial data was acquired three days apart and within two hours of one another. The influence of aerosols is also likely minimal as wavelengths in the blue part of the spectrum were purposely avoided for this reason.

The results of this study have implications for the biophysical interpretation of satellite and airborne imagery in monitoring of Arctic tundra vegetation. The influence of the chosen ecosystem components is likely at a maximum during the senescent season when this study was conducted. An increase in the presence of litter and visibility of moss is assumed as the canopy senesces, however the spatio-temporal influence of these components as well as the aforementioned extrinsic factors must be considered for both phenological and long-term monitoring studies. The sensitivity of the ten chosen wavelengths has implications for other optical remote sensing platforms like Sentinel 2, which has wavelengths centred at 490, 560, 665, 705, 740, 783, 842, and 865 nm corresponding closely to the chosen wavelengths in this study. As the aforementioned increase in airborne and spaceborne hyperspectral missions continues, the potential for further spatiotemporal characterization of low Arctic ecosystems will also increase and in turn will help to inform the interpretation of broadband sensors.

Through this exercise we shed light on the effects of non-vascular/non-photosynthetic ecosystem components on spatial scaling, however, this study represents a temporal snap shot using mixtures with maximum variability and does not encompass all aspects of the spatio-temporal heterogeneity of Arctic tundra ecosystems. We provide here a preliminary insight into the role of non-vascular/non-photosynthetic ecosystem components in spatial aggregation of dominant low Arctic communities. Of particular importance are the findings from the dominant tussock sedge-shrub tundra types, which showed the greatest influence of litter and moss at airborne and spaceborne scales. This should be taken into consideration for current and future monitoring of low Arctic biophysical parameters at ecosystem and landscape scales.

4.7 Conclusions

This study represents a preliminary examination of the influence of non-vascular and non-photosynthetic components on the spatial aggregation of low Arctic vegetation spectral signatures. The artificial mixing analysis using litter, moss, and water spectra suggest that litter, followed by moss were the most influential ecosystem components that explain differences in spectral signals when data were spatially aggregated from the ground to the AISA airborne scale. Mixtures between 10 and 70% litter at the AISA scale, and 60 to 75% at the EnMAP scale resulted in the minimization of error between ground-based, airborne and simulated satellite spectral reflectance at ten biophysically important wavelengths. Moss at percentages of 40 and 70% also reduced error but only in the two tussock-sedge communities. Tussock sedge-shrub communities, which are dominant across the Arctic, showed the greatest sensitivity to the linear mixture analysis, which is important for monitoring Arctic tundra vegetation at the satellite scale. Though this study represents only a snap shot and does not explicitly consider extrinsic factors, it highlights the importance of considering the unique ecosystem components present in Arctic ecosystems when spatially scaling spectral data. As accessibility and coverage of high-resolution spectral data increases, spatio-temporal characterization of non-vascular/non-photosynthetic will improve furthering our understanding of Arctic heterogeneity and the environmental gradients driving it, which in turn will enable accurate monitoring of ecosystem change.

4.8   Acknowledgements

5   Synthesis and Discussion

The overall aim of this thesis was to improve the interpretation of optical remote sensing data related to vegetation by exploring relationships between multi-seasonal, multi-scale remote sensing data. In the thesis research chapters, data from dominant vegetation communities were acquired using remote sensing devices and laboratory analyses with an emphasis on bottom-up, in-situ data. The comprehensive database was assembled over two growing seasons and three major phenological phases in the low Arctic Toolik Lake Research Natural Area. The data collected support conclusions that hyperspectral remote sensing provides accurate spatial and temporal biophysical information from complex Arctic tundra ecosystems. Additionally, the outcomes provide a framework to improve interpretation of globally important vegetation parameters. This in turn will improve current and future understanding of the impact of climate change on terrestrial Arctic ecosystem functioning. The unique spectral database created can also be used as a reference for future studies of Arctic vegetation change.

The main thesis findings highlight the interplay between seasonal, spectral, and spatial complexity of low Arctic vegetation communities. Three overarching factors of phenological phase, vegetation colour, and intrinsic ecosystem components were identified as facilitating a more complete interpretation of hyperspectral remote sensing of low Arctic vegetation. These three factors are fundamentally connected, each influencing the characteristics of the others. However, each served independent functions in addressing different aspects of ecosystem complexity and linking data across seasonal, spectral, and spatial scales. The following synthesis discusses in detail the three major factors identified as they relate to the research questions outlined in Section 1.2.

5.1   Phenological Phase: does phenology influence the spectral variability of dominant low Arctic vegetation communities?

Globally, phenology has been identified as a sensitive indicator to climate change (Parmesan and Yohe, 2003). Vegetation phenology in Arctic ecosystems is predicted to be particularly sensitive as snowpack conditions and the timing of snowmelt are the primary drivers of the onset of phenology (Billings and Bliss, 1959; Bjorkman et al., 2015). The seasonal emergence, growth, and senescence of vegetation have been monitored for decades by field-based visitations to individual plants (Molau and Mølgaard, 1996) and by quantitative

remote sensing (Stow et al., 2004; Zeng et al., 2011). However, few remote sensing studies have explicitly examined the influence of phenological phase on the spectral variability of Arctic tundra vegetation communities. Fewer still have examined how this spectral variability is represented at different spatial and spectral resolutions. Most remote sensing studies of Arctic tundra, track long-term greening trends of peak season NDVI or monitor the timing of the onset and end of the growing season (Stow et al., 2004; Zeng et al., 2011).

Results from this thesis indicate that phenological phase does indeed influence the spectral variability of dominant vegetation communities and more importantly these phenological differences can be exploited to improve identification and characterization of vegetation. Methods associated with dimensionality reduction that calculate the ratio of between and within endmember variability provided a detailed picture of spectral variability by wavelength and also by phenological phase. Differentiation of several dominant and spectrally similar vegetation communities appears to be maximized at non-peak phenological phases (Chapter 1; Beamish et al., 2017). The result explains an overall reduction in spectral variability and comparable or greater differences in reflectance in the VNIR between communities. In non-peak seasons, vegetation is either emerging or senescing resulting in lower cellular and canopy scattering and lower reflectance in the NIR. This is also true of absorption by chlorophylls in the visible spectrum, which is minimized at emergence and senescence. The development and degradation of other photosynthetic pigments is less straight forward at non-peak times driving more diverse signals in narrow wavelength regions of the visible spectrum (Sims and Gamon, 2002).

The detailed reflectance signatures captured by ground-based and simulated hyperspectral satellite data, particularly in the late season, allows for the exploitation of differences in the visible spectrum not available to broadband sensors (Beamish et al., 2017). This provides a likely explanation of why the spectral variability of multispectral Sentinel-2 data was best differentiated at peak and early season when reflectance in the green spectrum is at a maximum. Spectral variability in red reflectance manifesting, as yellows, oranges, reds, and blues in the late season are lost in the averaging across blue and red wavelengths in broadband sensors. The vibrant colour differences observed in the late season could provide opportunities for differentiation of spectrally similar communities outside of the peak season with satellite scale hyperspectral data.

The explicit comparison of spectral variability between phenological phases and spectral

resolutions is a novel approach harnessing the information stored in different phenological phase as a tool to improve identification of Arctic vegetation communities. Accurate identification of vegetation communities provides crucial baseline data from which detailed changes to ecosystem functioning can be extracted. In the context of current and future Arctic climate change, inherent ecosystem heterogeneity is driven by (1) high spatial variability in snowpack conditions and snowmelt, (2) equally variable changes in winter precipitation (Weller et al., 2005), and (3) highly heterogeneous responses of vegetation to warming (Elmendorf et al., 2012). Hyperspectral remote sensing data collected in multiple phenological phases can provide detailed and spatially explicit biophysical data at resolutions not previously available to address this dynamic change.

5.2 Vegetation Colour: How does canopy-level vegetation colour relate to phenological changes in leaf-level photosynthetic pigment concentration?

Vegetation colour dictated by the development and degradation of the photosynthetic pigment groups of chlorophylls, carotenoids, and anthocyanins, is an indicator of vegetation status and as this thesis showed, a powerful monitoring tool. At fine spectral resolutions, pigment dynamics are tracked by distinct shifts in spectral reflectance in the visible part of the electromagnetic spectrum (350–700 nm) (Coops et al., 2003; Curran, 1989; Gitelson and Merzlyak, 1998; Gitelson et al., 2002). These shifts can be exploited to infer ecological parameters such as photosynthetic activity, leaf-level pigment concentration, and biomass (Asner and Martin, 2008; Mutanga and Skidmore, 2004; Mutanga et al., 2004; Ustin et al., 2009). Broader spectral bandwidths common to major satellites such as Landsat, Sentinel-2, and MODIS also track pigment dynamics by shifting reflectance in broad wavelength groups representing blue, green, red and infrared, rather than individual wavelengths. Proxies for biophysical parameters can also be extracted from the information stored in these wavelength groups (Laidler and Treitz, 2003; Park et al., 2016). In this thesis, data collected at even broader spectral resolutions of the red, green and blue (RGB) channels of a consumer-grade digital camera showed correlations with reputable biophysical indices and the photosynthetic pigment concentration driving them, suggesting that vegetation colour contributes strongly to the response of spectral reflectance (Beamish et al., 2018).

The utility of vegetation colour has exciting potential to support detailed remote sensing of vegetation at the ground and satellite scale and for linking vegetation signals from multiple

spatial and spectral scales. The strongest and most consistent relationships were found between green-based indices and chlorophyll content and red-based indices showed moderate correlations with the chlorophyll to carotenoid ratio. This represents one of the first direct comparisons of leaf-level pigment concentration to colour data stored in digital photographs and the results support the continued development and use of broadband pigment-driven biophysical indices like the ones currently available for Sentinel-2. The rise in availability of biophysical remote sensing products has been driven by a need for better parameterization of radiative transfer models, which are used to simulate leaf and canopy reflectance and transmittance for climate models (Blackburn, 2007; Gamon et al., 2016; Garbulsky et al., 2011). Of particular interest is the characterization of the xanthophyll cycle, driven by changes in carotenoid pigments, and ratios between the photosynthetic chlorophyll and carotenoid pigments. Even at low spectral resolutions, remote sensing of vegetation colour on the ground and from satellites can inform the dynamics of these important processes complementing detailed spectral characterization of these phenomena.

The results also support the use of digital cameras as a potential near field remote sensing link or proxy for ground-based spectroscopy to relate to satellite acquisitions. The simplicity of tracking vegetation status through changes in vegetation colour recorded by digital cameras in Arctic ecosystems has been previously documented in many ecosystems (Ahrends et al., 2009; Anderson et al., 2016; Beamish et al., 2016; Coops et al., 2010; Ide and Oguma, 2010; Migliavacca et al., 2011; Nijland et al., 2014; Westergaard-Nielsen et al., 2013). By adding pigment concentration and pigment-driven indices to the previous body of research the biological validity of this method is increased. With challenging acquisition conditions for high frequency optical remote sensing data, the findings also support the development of more extensive camera networks across the Arctic. A higher data volume will facilitate better baseline data to monitor vegetation and ecosystem change to inform northern communities as well as global policy on climate change mitigation and adaptation.

5.3 Intrinsic Ecosystem Components: How does spatial aggregation of high spectral resolution data influence low Arctic tundra vegetation signals?

Natural ecosystems are inherently heterogeneous and in Arctic ecosystems this heterogeneity has strong spatio-temporal patterns driven by environmental gradients. In the field of

quantitative optical remote sensing, how this heterogeneity is represented at different spatial scales is important for accurate interpretation of spectral signatures. By design, the measurement process of optical remote sensing is the acquisition of the average radiative signal from an area of interest (Townshend, 1981). When the signal is averaged, sub-pixel variations can be masked and this masking can be different at different spatial resolutions introducing bias with implications for ecological studies (Chen, 1999). Sub-pixel variations can be introduced by extrinsic components such as shadow, sensor viewing angle or sensor distortions, as well as from intrinsic components such as percent cover of bare soil, photosynthetic, non-photosynthetic, and non-vascular vegetation.

The snapshot of concurrently acquired senescent stage ground-based, aerial, and simulated satellite scale hyperspectral data presents a unique opportunity to examine how spatial aggregation influences vegetation signals of low Arctic tundra (Beamish et al. 2018, under review). Moving from the spatial resolution of ground-based, to airborne, to simulated satellite data, there was a clear shift in the position of the red-edge transition in all communities indicating a decline in photosynthetically active components (Sims and Gamon, 2002). However, all vegetation communities in the study site were 80–100% vegetated and with the exception of a few glacial erratics this is true at the landscape scale, suggesting an averaging bias introduced by spatial aggregation.

The dominant tussock tundra community has a high proportion of standing litter as well as the potential for bidirectional reflectance distribution function (BRDF) effects (briefly, the inhibition of direct interpretation of reflectance data due to shadowed and illuminated components of the canopy (Hapke, 1981, Hope et al., 1993). The results of an artificial mixture analysis showed that increasing the proportion of standing litter improved the coherence between spectral signatures at the three spatial scales. BRDF effects were not explicitly examined, but a dark water spectra which can be used as a proxy for shadows, had little impact on coherence suggesting BRDF effects were minimal.

The impact of spatial aggregation on spectral signatures was most pronounced in the NIR and least in the chlorophyll absorbing red spectrum. This shows that without proper characterization of the area of interest quantitative remote sensing data could be misinterpreted, particularly VIs using ratios between NIR and red at coarser spatial resolutions. Stow et al. (1993) previously showed community-specific relationships between vegetation quantity

and spectral reflectance. Laidler and Treitz (2003) succinctly summarize how these community-specific relationships must be explicitly characterized in relation to spatio-temporal ecosystem components such as phenological phase, terrain, climate conditions, illumination, viewing angle, sampling scheme and frequency of measurements to accurately relate in-situ and satellite scale observations.

As Arctic ecosystems continue to respond to climate change in a complex and heterogeneous manner, detailed characterization of the spatio-temporal contribution of intrinsic and extrinsic ecosystem components will be crucial for accurate quantitative remote sensing at the landscape-scale. Currently, the availability of hyperspectral remote sensing data is increasing through projects like NASA's ABoVE airborne campaigns and DLR's EnMAP satellite. These data, along with concurrent ground-based data will provide the opportunity to further understanding of spatial aggregation of complex Arctic tundra ecosystems.

5.4   Key Innovations

The research chapters of this thesis provide a framework with which to improve the interpretation of vegetation remote sensing data and to address some of the challenges associated with detailed remote sensing in Arctic ecosystems. The framework suggests the incorporation of more phenological phases, a greater focus on the power of vegetation colour to link multi-scale data, and finally detailed spectral characterization of non-photosynthetic ecosystem components. Below are the key innovations of the thesis:

- Data from multiple phenological phase can be used as tool for better identification of spectrally similar vegetation communities facilitating more accurate monitoring of vegetation change and ecosystem functioning
- Simple ratios of visible bands from broadband data can be used as proxies for reputable biophysical spectral indices increasing data volume and acquisition frequency
- Non-photosynthetic components of tundra ecosystems influence the spatial aggregation of hyperspectral remote sensing with implications for quantitative remote sensing of vegetation
- A highly detailed and unique spectral library that can be used as a reference for future studies

5.5 Limitations and Technical Considerations

With the above innovations also come limitations and technical considerations. The first is the emphasis on a phenological approach. Logistically and climatically, Arctic ecosystems are challenging even at peak season when the weather is most stable. Frequent cloud cover, forest fire smoke, low solar zenith angle, and snowfall are common throughout the rapidly advancing growing season, limiting the window for acquisition of data across multiple seasons. In addition, the remote location of most foci sites in the Arctic can make the collection of multi seasonal data prohibitively expensive. So while in practice multi-season remote sensing data would be ideal to improve vegetation characterizations, in reality this may be logistically challenging to achieve. Additionally, the results of Chapter 2 are based on data from a single digital camera and a single spectrometer. There was no comparison of different camera or spectrometer systems and how this might influence the relationships with biophysical spectral indices. A final limitation is the quality of the AISA and therefore simulated EnMAP imagery. Though a very valuable tool, the EetEs is still only a simulation of the EnMAP sensor and data quality issues in the AISA data are reflected in the simulated data. The NIR of the acquired AISA data was very noisy and there were illumination issues from the first to final flight line. Data quality issues of aerial remote sensing data are not unique to this research. As outlined, the challenges associated with acquisition of high quality optical remote sensing data in the Arctic are substantial.

5.6 Outlook: Opportunities for Future Research

Hyperspectral remote sensing at the landscape scale is in its infancy in Arctic ecosystems. With the increasing availability and application of hyperspectral remote sensing at both the aerial and satellite scales continued refinement of the interpretation of vegetation signals is needed for accurate landscape scale monitoring of Arctic tundra change. The following highlights opportunities for future research:

(1) Studies that collect or aggregate spectral reflectance data of Arctic tundra vegetation communities from a variety of circumpolar Arctic locations at multiple phenological phases are needed to support a more detailed and site-specific characterization of vegetation spectral variability. A latitudinal and longitudinal transect encompassing both sub- and high Arctic sites would be highly valuable to inform targeted acquisitions for maximized separability between vegetation communities and

parameters of interest.

(2) Refining the relationship between in-situ, true-colour digital photography, spectral reflectance and biophysical parameters could also be highly useful in supporting digital photography as a feasible gap-filling tool across the remote tundra biome. Inclusion of further parameters such as leaf-area-index, as well as leaf-level nutrient content to expand the use would also be interesting.

(3) More intermediate (i.e. aerial or tower) hyperspectral studies quantifying the relative input of intrinsic and extrinsic ecosystem components would be highly beneficial to upcoming hyperspectral satellite missions. As the spatio-temporal complexity of Arctic ecosystems drives the relative inputs of these two components, these studies would also benefit from a phenological or seasonal approach to acquisitions. Further on this, detailed spectral unmixing studies exploring the applicability of current algorithms to Arctic ecosystems to extract the spectral signatures of both intrinsic and extrinsic ecosystem components at sub-pixel quantities are necessary.

6 References

Ahrends, H., Etzold, S., Kutsch, W.L., Stöckli, R., Brügger, R., Jeanneret, F., Wanner, H., Buchmann, N., Eugster, W., 2009. Tree phenology and carbon dioxide fluxes: use of digital photography for process-based interpretation at the ecosystem scale. Clim Res 39, 261–274.

AMAP, 2017. AMAP Assessment 2016: Chemicals of Emerging Arctic Concern. Arctic Monitoring and Assessment Programme (AMAP), Oslo, Norway. pp. xvi+353

Anderson, H.B., Nilsen, L., Tømmervik, H., Karlsen, S., Nagai, S., Cooper, E.J., 2016. Using ordinary digital cameras in place of near-infrared sensors to derive vegetation indices for phenology studies of high Arctic vegetation. Remote Sens 8, 847.

Asner, G.P., 1998. Biophysical and biochemical sources of variability in canopy reflectance. Remote Sens Environ 64, 234–253.

Asner, G.P., Martin, R.E., 2008. Spectral and chemical analysis of tropical forests: Scaling from leaf to canopy levels. Remote Sens Environ 112, 3958–3970.

Bartley, G., Scolnik, P., 1995. Plant carotenoids: pigments for photoprotection, visual attraction, and human health. Plant Cell 7, 1027–1038.

Bayer, 1976. Color imaging array. U.S. Patent 3,971,065.

Beamish, A., Nijland, W., Edwards, M., Coops, N., Henry, G., 2016. Phenology and vegetation change measurements from true colour digital photography in high Arctic tundra. Arctic Sci 2, 33–49.

Beamish, A., Coops, N., Chabrillat, S., Heim, B., 2017. A Phenological Approach to Spectral Differentiation of Low Arctic Tundra Vegetation Communities, North Slope, Alaska. Remote Sens 9, 1200.

Beamish, A., Coops, N., Hermosilla, T., Chabrillat, S., Birgit, H., 2018. Monitoring pigment-driven vegetation changes in a low-Arctic tundra ecosystem using digital cameras. Ecosphere 9.

Bhatt, U., Walker, D., Raynolds, M., 2010. Circumpolar Arctic tundra vegetation change is linked to sea ice decline. Earth Interact 14, 1–20.

Bhatt, U.S., Walker, D.A., Raynolds, M.K., Bieniek, P.A., Epstein, H.E., Comiso, J.C., Pinzon, J.E., Tucker, C.J., Polyakov, I.V., 2013. Recent declines in warming and vegetation greening trends over pan-Arctic tundra. Remote Sens 5, 4229–4254.

Bjorkman, A.D., Elmendorf, S.C., Beamish, A.L., Vellend, M., Henry, G.H., 2015. Contrasting effects of warming and increased snowfall on Arctic tundra plant phenology over the past two decades. Glob Change Biol 21, 4651–4661.

Bjorkman, A.D., Vellend, M., Frei, E.R., Henry, G.H., 2017. Climate adaptation is not enough: warming does not facilitate success of southern tundra plant populations in the high Arctic. Glob Change Biol 23, 1540–1551.

Blackburn, 2007. Wavelet decomposition of hyperspectral data: a novel approach to quantifying pigment concentrations in vegetation. Int J Remote Sens 28, 2831–2855.

114

Blackburn, G., 1998. Spectral indices for estimating photosynthetic pigment concentrations: a test using senescent tree leaves. Int J Remote Sens 19, 657–675.

Blackburn, G., 1999. Relationships between Spectral Reflectance and Pigment Concentrations in Stacks of Deciduous Broadleaves. Remote Sens Environ 70, 224–237.

Bliss, L., Matveyeva, N., 1992. Circumpolar arctic vegetation, in: FS, RL, Reynolds, J., GR, Svoboda, J., Chu, E. (Eds.), Academia Press, Inc., San Diego, California, USA, pp. 59–89.

Bliss, L.C., Heal, O., Moore, J.J., Moore, J., 1981. Tundra ecosystems: a comparative analysis, in: Bliss, L., Heal, O. (Eds.), Cambridge University Press, Cambridge, UK.

Boelman, N., Stieglitz, M., Rueth, H., Sommerkorn, M., Griffin, K., Shaver, G., Gamon, J., 2003. Response of NDVI, biomass, and ecosystem gas exchange to long-term warming and fertilization in wet sedge tundra. Oecologia 135, 414–421.

Bratsch, S.N., Epstein, H.E., Buchhorn, M., Walker, D.A., 2016. Differentiating among four Arctic tundra plant communities at Ivotuk, Alaska using field spectroscopy. Remote Sens 8.

Buchhorn, M., Walker, D.A., Heim, B., Raynolds, M.K., Epstein, H.E., Schwieder, M., 2013. Ground-Based Hyperspectral Characterization of Alaska Tundra Vegetation along Environmental Gradients. Remote Sens 5, 3971–4005.

Callaghan, T.V., Jonasson, S., 1995. Arctic terrestrial ecosystems and environmental change. Philos T R Soc A 352, 259–276.

Chalker-Scott, L., 1999. Environmental Significance of Anthocyanins in Plant Stress Responses. Photochem Photobiol 70, 1–9.

Chance, C.M., Coops, N.C., Crosby, K., Aven, N., 2016. Spectral Wavelength Selection and Detection of Two Invasive Plant Species in an Urban Area. Can J Remote Sens 42, 27–40.

Chapin, Mcguire, Randerson, Pielke, Baldocchi, Hobbie, Roulet, Eugster, Kasischke, Rastetter, Zimov, Running, 2000. Arctic and boreal ecosystems of western North America as components of the climate system. Glob Change Biol 6, 211–223.

Chapin, Sturm, Serreze, McFadden, Key, Lloyd, McGuire, Rupp, Lynch, Schimel, Beringer, Chapman, Epstein, Euskirchen, Hinzman, Jia, Ping, C.-L., Tape, Thompson, Walker, Welker, 2005. Role of Land-Surface Changes in Arctic Summer Warming. Science 310, 657–660.

Chen, J., 1999. Spatial Scaling of a Remotely Sensed Surface Parameter by Contexture. Remote Sens Environ 69, 30–42.

Chuvieco, E., Martín, M., Palacios, A., 2002. Assessment of different spectral indices in the red-near-infrared spectral domain for burned land discrimination. Int J Remote Sens 23, 5103–5110.

Clark, King, T., 1987. Automatic continuum analysis of reflectance spectra. NASA, Pasadena, CA, USA.

Clark, R.N., Roush, T.L., 1984. Reflectance spectroscopy: Quantitative analysis techniques

for remote sensing applications. J Geophys Res: SE 89, 6329–6340.

Close, D., Beadle, C., 2003. The ecophysiology of foliar anthocyanin. Botanical Review 69, 149–161.

Cook, B., Wolkovich, E., 2012. Divergent responses to spring and winter warming drive community level flowering trends. PNAS 109, 9000–9005.

Coops, N., Hilker, T., Bater, C., Wulder, M., Nielsen, S., McDermid, G., Stenhouse, G., 2012. Linking ground-based to satellite-derived phenological metrics in support of habitat assessment. Remote Sens Lett 3, 191–200.

Coops, N., Hilker, T., Hall, F., Nichol, C., Drolet, G., 2010. Estimation of Light-use Efficiency of Terrestrial Ecosystems from Space: A Status Report. Bioscience 63, 788–797.

Coops, N., Stone, C., Culvenor, D., Chisholm, L., Merton, R., 2003. Chlorophyll content in eucalypt vegetation at the leaf and canopy scales as derived from high resolution spectral data. Tree Physiol 23, 23–31.

Curran, P.J., 1989. Remote sensing of foliar chemistry. Remote Sens Environ 30, 271–278.

Drusch, M., Bello, D.U., Carlier, S., Colin, O., Fernandez, V., Gascon, F., Hoersch, B., Isola, C., Laberinti, P., Martimort, P., Meygret, A., Spoto, F., Sy, O., Marchese, F., Bargellini, P., 2012. Sentinel-2: ESA's Optical High-Resolution Mission for GMES Operational Services. Remote Sens Environ 120, 25–36.

Elmendorf, S., Henry, G., Hollister, R., Björk, R., Bjorkman, A., Callaghan, T., Collier, L., Cooper, E., Cornelissen, J., Day, T., Fosaa, A., Gould, W., Grétarsdóttir, J., Harte, J., Hermanutz, L., Hik, D., Hofgaard, A., Jarrad, F., Jónsdóttir, I., Keuper, F., Klanderud, K., Klein, J., Koh, S., Kudo, G., Lang, S., Loewen, V., May, J., Mercado, J., Michelsen, A., Molau, U., Myers-Smith, I., Oberbauer, S., Pieper, S., Post, E., Rixen, C., Robinson, C., Schmidt, N., Shaver, G., Stenström, A., Tolvanen, A., Totland, Ø., Troxler, T., Wahren, C., Webber, P., Welker, J., Wookey, P., 2012a. Global assessment of experimental climate warming on tundra vegetation: heterogeneity over space and time. Ecol Lett 15, 164–175.

Elmendorf, S.C., Henry, G.H., Hollister, R.D., Björk, R.G., Boulanger-Lapointe, N., Cooper, E.J., Cornelissen, J.H., Day, T.A., Dorrepaal, E., Elumeeva, T.G., Gill, M., Gould, W.A., Harte, J., Hik, D.S., Hofgaard, A., Johnson, D.R., Johnstone, J.F., Jónsdóttir, I., Jorgenson, J.C., Klanderud, K., Klein, J.A., Koh, S., Kudo, G., Lara, M., Lévesque, E., Magnússon, B., May, J.L., Mercado-Diaz, J.A., Michelsen, A., Molau, U., Myers-Smith, I.H., Oberbauer, S.F., Onipchenko, V.G., Rixen, C., Schmidt, N., Shaver, G.R., Spasojevic, M.J., Þórhallsdóttir, Þ., Tolvanen, A., Troxler, T., Tweedie, C.E., Villareal, S., Wahren, C.-H., Walker, X., Webber, P.J., Welker, J.M., Wipf, S., 2012b. Plot-scale evidence of tundra vegetation change and links to recent summer warming. Nature Climate Change 2, 453–457.

Féret, J.-B., François, C., Gitelson, A., Asner, G., Barry, K., Panigada, C., Richardson, A., Jacquemoud, S., 2011. Optimizing spectral indices and chemometric analysis of leaf chemical properties using radiative transfer modeling. Remote Sens Environ 115, 2742–2750.

Filella, I., Penuelas, J., 1994. The red edge position and shape as indicators of plant chlorophyll content, biomass and hydric status. Int J Remote Sens 15, 1459–1470.

Gaalen, E., Flanagan, L., Peddle, D., 2007. Photosynthesis, chlorophyll fluorescence and

spectral reflectance in Sphagnum moss at varying water contents. Oecologia 153, 19–28.

Gamon, JA, Serrano, L, Surfus, JS, 1997. The photochemical reflectance index: an optical indicator of photosynthetic radiation use efficiency across species, functional types, and nutrient levels. Oecologia 112, 492 – 501.

Gamon, J., Peñuelas, J., Field, C., 1992. A narrow-waveband spectral index that tracks diurnal changes in photosynthetic efficiency. Remote Sens Environ 41, 35–44.

Gamon, J.A., Huemmrich, F.K., Wong, C.Y., Ensminger, I., Garrity, S., Hollinger, D.Y., Noormets, A., Peñuelas, J., 2016. A remotely sensed pigment index reveals photosynthetic phenology in evergreen conifers. PNAS 113, 13087–13092.

Garbulsky, M., Peñuelas, J., Gamon, J., Inoue, Y., Filella, I., 2011. The photochemical reflectance index (PRI) and the remote sensing of leaf, canopy and ecosystem radiation use efficiencies A review and meta-analysis. Remote Sens Environ 115, 281–297.

Gausman, H.W., 1974. Leaf reflectance of near-infrared. Photogram Eng 40, 183–191.

Gitelson, A., Merzlyak, M., 1997. Remote estimation of chlorophyll content in higher plant leaves. Int J Remote Sens 18, 2691–2697.

Gitelson, A., Merzlyak, M., 1998. Remote sensing of chlorophyll concentration in higher plant leaves. Adv Space Res 22, 689–692.

Gitelson, A., Merzlyak, M.N., Chivkunova, O.B., 2001. Optical properties and nondestructive estimation of anthocyanin content in plant leaves. Photochem Photobiol 74, 38–45.

Gitelson, A., Zur, Y., Chivkunova, O.B., Mark, 2002. Assessing Carotenoid Content in Plant Leaves with Reflectance Spectroscopy. Photochem Photobiol 75, 272–281.

Gitelson, A., Keydan, G.P., Merzlyak, M.N., 2006. Three-band model for noninvasive estimation of chlorophyll, carotenoids, and anthocyanin contents in higher plant leaves. Geophys Res Lett 33.

Gould, K., McKelvie, J., Markham, K., 2002. Do anthocyanins function as antioxidants in leaves? Imaging of H2O2 in red and green leaves after mechanical injury. Plant Cell Environ 25, 1261–1269.

Grosse, G., Harden, J., Turetsky, M., McGuire, D., Camill, P., Tarnocai, C., Frolking, S., Schuur, E., Jorgenson, T., Marchenko, S., Romanovsky, V., Wickland, K., French, N., Waldrop, M., Bourgeau-Chavez, L., Striegl, R., 2011. Vulnerability of high-latitude soil organic carbon in North America to disturbance. J Geophys Res Biogeosci 116.

Guanter, L., Kaufmann, H., Segl, K., Foerster, S., Rogass, C., Chabrillat, S., Kuester, T., Hollstein, A., Rossner, G., Chlebek, C., Straif, C., Fischer, S., Schrader, S., Storch, T., Heiden, U., Mueller, A., Bachmann, M., Mühle, H., Müller, R., Habermeyer, M., Ohndorf, A., Hill, J., Buddenbaum, H., Hostert, P., Linden, S. van der, Leitão, P.J., Rabe, A., Doerffer, R., Krasemann, H., Xi, H., Mauser, W., Hank, T., Locherer, M., Rast, M., Staenz, K., Sang, B., 2015. The EnMAP Spaceborne Imaging Spectroscopy Mission for Earth Observation. Remote Sens 7, 8830–8857.

Hamilton, T.D., 2003. Glacial geology of the Toolik Lake and upper Kuparuk River regions. Biological Papers of the University of Alaska, Fairbanks, Alaska, USA.

Hinzman, L., Bettez, N., Bolton, R., Chapin, S., Dyurgerov, M., Fastie, C., Griffith, B., Hollister, R., Hope, A., Huntington, H., Jensen, A., Jia, G., Jorgenson, T., Kane, D., Klein, D., Kofinas, G., Lynch, A., Lloyd, A., McGuire, D., Nelson, F., Oechel, W., Osterkamp, T., Racine, C., Romanovsky, V., Stone, R., Stow, D., Sturm, M., Tweedie, C., Vourlitis, G., Walker, M., Walker, D., Webber, P., Welker, J., Winker, K., Yoshikawa, K., 2005. Evidence and Implications of Recent Climate Change in Northern Alaska and Other Arctic Regions. Climatic Change 72, 251–298.

Hope, Kill, Stow, 1993. The relationship between tussock tundra spectral reflectance properties and biomass and vegetation composition. Int J Remote Sens 14, 1861–1874.

Høye, T.T., Post, E., Schmidt, N.M., Trøjelsgaard, K., Forchhammer, M.C., 2013. Shorter flowering seasons and declining abundance of flower visitors in a warmer Arctic. Nature Climate Change 3, 759–763.

Huemmrich, K., Gamon, J.A., Tweedie, C.E., Campbell, P.K., Landis, D.R., Middleton, 2013. Arctic Tundra Vegetation Functional Types Based on Photosynthetic Physiology and Optical Properties. IEEE J STARS 6, 265–275.

Hugelius, G., Strauss, J., Zubrzycki, S., Harden, J.W., Schuur, E., Ping, C.-L., Schirrmeister, L., Grosse, G., Michaelson, G.J., Koven, C.D., 2014. Estimated stocks of circumpolar permafrost carbon with quantified uncertainty ranges and identified data gaps. Biogeosci Discuss 11, 6573–6593.

Ide, R., Oguma, H., 2010. Use of digital cameras for phenological observations. Ecolog Inform 5, 339–347.

Ide, R., Oguma, H., 2013. A cost-effective monitoring method using digital time-lapse cameras for detecting temporal and spatial variations of snowmelt and vegetation phenology in alpine ecosystems. Ecolog Inform 16, 23–34.

Iler, A.M., Høye, T.T., Inouye, D.W., Schmidt, N.M., 2013. Nonlinear flowering responses to climate: are species approaching their limits of phenological change? Philos T R Soc B: Biol Sci 368, 20120489.

Inouye, D.W., McGuire, D.A., 1991. Effects of snowpack on timing and abundance of flowering in Delphinium nelsonii (Ranunculaceae): implications for climate change. Am J Botany 78, 997–1001.

IPCC, 2014: Climate Change 2014: Synthesis Report. Contribution of Working Groups I, II and III to the Fifth Assessment Report of the Intergovernmental Panel on Climate Change [Core Writing Team, R.K. Pachauri and L.A. Meyer (eds.)]. IPCC, Geneva, Switzerland, 151 pp.

Laidler, G., Treitz, P., Arctic, A.-D., 2008. Remote sensing of arctic vegetation: relations between the NDVI, spatial resolution and vegetation cover on Boothia Peninsula, Nunavut. Arctic 16, 1–13 .

Laidler, G.J., Treitz, P., 2003. Biophysical remote sensing of arctic environments. Prog Phys Geog 27, 44–68.

Leeuwen, W.J. van, Huete, A., 1996. Effects of standing litter on the biophysical interpretation of plant canopies with spectral indices. Remote Sens Environ 55, 123–138.

Lehnert, Meyer, Bendix, 2016. Hsdar: Manage, Analyse and Simulate Hyperspectral Data

in R. R Package Version 0.4 1.

Leitão, P.J., Schwieder, M., Suess, S., Okujeni, A., Galvão, L., Linden, S. van der, Hostert, P., 2015. Monitoring Natural Ecosystem and Ecological Gradients: Perspectives with EnMAP. Remote Sens 7, 13098–13119.

Liu, N., Budkewitsch, P., Treitz, P., 2017. Examining spectral reflectance features related to Arctic percent vegetation cover: Implications for hyperspectral remote sensing of Arctic tundra. Remote Sens Environ 192, 58–72.

Matveyeva, N., Chernov, Y., 2000. Biodiversity of terrestrial ecosystems, in: Nuttall, M., Terry V (Eds.), Harwood Academic Publisher, Amsterdam, NL.

Mayo, J., Despain, D., Jr., E. van, 1973. CO2 assimilation by Dryas integrifolia on Devon Island, Northwest Territories. Can J Botany 51, 581–588.

Merzlyak, M., Gitelson, A., Chivkunova, O., Rakitin, V., 1999. Non-destructive optical detection of pigment changes during leaf senescence and fruit ripening. Physiol Plantarum 106, 135–141.

Migliavacca, M., Galvagno, M., Cremonese, E., Rossini, M., Meroni, M., Sonnentag, O., Cogliati, S., Manca, G., Diotri, F., Busetto, L., 2011. Using digital repeat photography and eddy covariance data to model grassland phenology and photosynthetic CO 2 uptake. Agr Forest Meteorol 151, 1325–1337.

Mølgaard, P., 1982. Temperature observations in high arctic plants in relation to microclimate in the vegetation of Peary Land, North Greenland. Arctic Alpine Res 14, 105–115.

Muller, S., Racoviteanu, A., Walker, D., 1999. Landsat MSS-derived land-cover map of northern Alaska: Extrapolation methods and a comparison with photo-interpreted and AVHRR-derived maps. Int J Remote Sens 20, 2921–2946.

Mutanga, O., Skidmore, A.K., 2004. Hyperspectral band depth analysis for a better estimation of grass biomass (Cenchrus ciliaris) measured under controlled laboratory conditions. Int J App Earth Obs and Geoinform 5, 87–96.

Mutanga, Skidmore, A.., Prins, H.H.., 2004. Predicting in situ pasture quality in the Kruger National Park, South Africa, using continuum-removed absorption features. Remote Sens Environ 89, 393–408.

Nijland, W., Jong, D.R., Jong, D., Wulder, M., 2014. Monitoring plant condition and phenology using infrared sensitive consumer grade digital cameras. Agr Forest Meteorol 184, 98–106.

Oberbauer, S.F., Dawson, T.E., Svoboda, J., Chu, E.W., 1992. Water relations of arctic vascular plants, in: Chapin III, F.S., Jefferies, R.L., Reynolds, J.F., Shaver, G.R. (Eds.), Academia Press, Inc. , San Diego, California, USA, pp. 259–279.

Oechel, W.C., Vourlitis, G.L., 1994. The effects of climate charge on land—atmosphere feedbacks in arctic tundra regions. Trends Ecol Evol 9, 324–329.

Olthof, I., Latifovic, R., 2007. Short-term response of arctic vegetation NDVI to temperature anomalies. Int J Remote Sens 28, 4823–4840.

Park, T., Ganguly, S., Tømmervik, H., Euskirchen, E.S., Høgda, K.-A., Karlsen, S., Brovkin, V., Nemani, R.R., Myneni, R.B., 2016. Changes in growing season duration and productivity of northern vegetation inferred from long-term remote sensing data. Environ Res Lett 11, 084001.

Parmentier, F.-J., Christensen, T., 2013. Arctic: Speed of methane release. Nature 500, 529.

Parmesan, C., Yohe, G., 2003. A globally coherent fingerprint of climate change impacts across natural systems. Nature 421, 37–42.

Peterson, S.H., Roberts, D.A., Beland, M., Kokaly, R.F., Ustin, S.L., 2015. Oil detection in the coastal marshes of Louisiana using MESMA applied to band subsets of AVIRIS data. Remote Sens Environ 159, 222–231.

Porra, R., Thompson, W., Kriedemann, P., 1989. Determination of accurate extinction coefficients and simultaneous equations for assaying chlorophylls a and b extracted with four different solvents: verification of the concentration of chlorophyll standards by atomic absorption spectroscopy. BBA-Bioenerg 975, 384–394.

Prevéy, J., Vellend, M., Rüger, N., Hollister, R., Bjorkman, A., Myers-Smith, I., Elmendorf, S., Clark, K., Cooper, E., Elberling, B., Fosaa, A., Henry, G., Høye, T., Jónsdóttir, I., Klanderud, K., Lévesque, E., Mauritz, M., Molau, U., Natali, S., Oberbauer, S., Panchen, Z., Post, E., Rumpf, S., Schmidt, N., Schuur, E., Semenchuk, P., Troxler, T., Welker, J., Rixen, C., 2017. Greater temperature sensitivity of plant phenology at colder sites: implications for convergence across northern latitudes. Glob Change Biol 23, 2660–2671.

Raynolds, M., Walker, D., Epstein, H., Pinzon, J., Tucker, C., 2011. A new estimate of tundra-biome phytomass from trans-Arctic field data and AVHRR NDVI. Remote Sens Lett 3, 403–411.

Raynolds, M.K., Walker, D.A., Maier, H.A., 2006. NDVI patterns and phytomass distribution in the circumpolar Arctic. Remote Sens Environ 102, 271–281.

Richardson, A., Jenkins, J., Braswell, B., Hollinger, D., Ollinger, S., Smith, M.-L., 2007. Use of digital webcam images to track spring green-up in a deciduous broadleaf forest. Oecologia 152, 323–334.

Riedel, Epstein, H., Walker, D., 2005. Biotic controls over spectral reflectance of arctic tundra vegetation. Int J Remote Sens 26, 2391–2405.

Roberts, D.A., Roth, K.L., Perroy, R.L., A, H., 2011. Hyperspectral Vegetation Indices, in: P, T.S., J, L.G. (Eds.), CRC Press/Taylor and Francis Group, Boca Raton, FL, USA/London, UK/NewYork, NY, USA, pp. 309–328.

Rock, B., Hoshizaki, T., Miller, J., 1988. Comparison of in situ and airborne spectral measurements of the blue shift associated with forest decline. Remote Sens Environ 24, 109–127.

Rogge, D., Rivard, B., Segl, K., Grant, B., Feng, J., 2014. Mapping of NiCu–PGE ore hosting ultramafic rocks using airborne and simulated EnMAP hyperspectral imagery, Nunavik, Canada. Remote Sens Environ 152, 302–317.

Schaepman, M.E., Ustin, S.L., Plaza, A.J., Painter, T.H., Verrelst, J., Liang, S., 2009. Earth system science related imaging spectroscopy—An assessment. Remote Sens Environ 113, S123–S137.

Schaaf, C., Li, X., Strahler, A.H., 1994. Topographic effects on bidirectional and hemi-spherical reflectances calculated with a geometric-optical canopy model. IEEE Trans Geosci Remote Sens 32.

Schuur, McGuire, Schädel, Grosse, Harden, Hayes, Hugelius, Koven, Kuhry, Lawrence, Natali, Olefeldt, Romanovsky, Schaefer, Turetsky, Treat, Vonk, 2015. Climate change and the permafrost carbon feedback. Nature 520, 171–179.

Schwieder, M., Leitão, P.J., Suess, S., Senf, C., Hostert, P., 2014. Estimating fractional shrub cover using simulated EnMAP data: A comparison of three machine learning regression techniques. Remote Sens 6, 3427–3445.

Segl, K., Guanter, L., Kaufmann, H., Schubert, J., Kaiser, S., Sang, B., Hofer, S., 2010. Simulation of Spatial Sensor Characteristics in the Context of the EnMAP Hyperspectral Mission. IEEE Trans Geosci Remote Sens 48, 3046–3054.

Segl, K., Guanter, L., Rogass, C., Kuester, T., Roessner, S., Kaufmann, H., Sang, B., Mogulsky, V., Hofer, S., 2012. EeteS—The EnMAP End-to-End Simulation Tool. IEEE J STARS 5, 522–530.

Serreze, M., Walsh, J., III, C.F., Osterkamp, T., Dyurgerov, M., Romanovsky, V., Oechel, W., Morison, J., Zhang, T., Barry, R., 2000. Observational evidence of recent change in the northern high-latitude environment. Climatic Change 46, 159–207.

Shaver, G.R., Chapin III, F.S., Gartner, B.L., 1986. Factors limiting seasonal growth and peak biomass accumulation in Eriophorum vaginatum in Alaskan tussock tundra. J Ecology 45, 472–8.

Sims, D.A., Gamon, J.A., 2002. Relationships between leaf pigment concentration and spectral reflectance across a wide range of species, leaf structures and developmental stages. Remote Sens Environ 81, 337–354.

Somers, B., Asner, G., Tits, L., Coppin, P., 2011. Endmember variability in spectral mixture analysis: A review. Remote Sens Environ 115, 1603–1616.

Somers, B., Asner, G.P., 2013. Invasive Species Mapping in Hawaiian Rainforests Using Multi-Temporal Hyperion Spaceborne Imaging Spectroscopy. IEEE J STARS 6, 351–359.

Somers, B., Cools, K., Delalieux, S., Stuckens, J., 2009. Nonlinear hyperspectral mixture analysis for tree cover estimates in orchards. Remote Sens of Environ 113, 1183–1193.

Somers, B., Delalieux, S., Verstraeten, W., Aardt, J. van, Albrigo, G., Coppin, P., 2010. An automated waveband selection technique for optimized hyperspectral mixture analysis. Int J Remote Sens 31, 5549–5568.

Steyn, Wand, Holcroft, Jacobs, 2002. Anthocyanins in vegetative tissues: a proposed unified function in photoprotection. New Phytol 155, 349–361.

Stow, D., Hope, A., McGuire, D., Verbyla, D., J, Huemmrich, F., Houston, S., Racine, C., Sturm, M., Tape, K., Hinzman, L., Yoshikawa, K., Tweedie, C., Noyle, B., Silapaswan, C., Douglas, D., Griffith, B., Jia, G., Petersen, A., Zhou, L., Myneni, R., 2004. Remote sensing of vegetation and land-cover change in Arctic Tundra Ecosystems. Remote Sens Environ 89, 281–308.

Sturm, M., Schimel, J., Michaelson, G., Welker, J., 2005. Winter biological processes could

help convert arctic tundra to shrubland. Bioscience 55, 17–26.

Stylinski, Gamon, Oechel, 2002. Seasonal patterns of reflectance indices, carotenoid pigments and photosynthesis of evergreen chaparral species. Oecologia 131, 366–374.

Tarnocai, C., Canadell, J., Schuur, E., Kuhry, P., Mazhitova, G., Zimov, S., 2009. Soil organic carbon pools in the northern circumpolar permafrost region. Glob Biogeochem Cycl 23.

Tenhunen, J., Lange, O., Hahn, S., Siegwolf, R., Oberbauer, S., 1992. The ecosystem role of poikilohydric tundra plants, in: Chapin III, F., Jefferies, R., Reynolds, J., Shaver, G. (Eds.), Academia Press, Inc., San Diego, CA, USA, pp. 213–239.

Thenkabail, P.S., Smith, R.B., Pauw, E., 2000. Hyperspectral Vegetation Indices and Their Relationships with Agricultural Crop Characteristics. Remote Sens Environ 71.

Tieszen, L.L., 1972. The seasonal course of aboveground production and chlorophyll distribution in a wet arctic tundra at Barrow, Alaska. Arctic Alpine Res 4, 307–324.

Townshend, J.R., 1981. The spatial resolving power of earth resources satellites. Prog Phys Geog 5, 32–55.

Tucker, C., 1979. Red and photographic infrared linear combinations for monitoring vegetation. Remote Sens Environ 8, 127–150.

Ustin, S.L., Curtiss, B., 1990. Spectral characteristics of ozone-treated conifers. Environ Experim Botany 30, 293–308.

Ustin, S., Gitelson, A., Jacquemoud, S., 2009. Retrieval of foliar information about plant pigment systems from high resolution spectroscopy. Remote Sens Environ 113, S67–S77.

Walker, D.A., Auerbach, N.A., Shippert, M.M., 1995. NDVI, biomass, and landscape evolution of glaciated terrain in northern Alaska. Polar Record 31, 169–178.

Walker D.A., Gould W., Maier H., Raynolds M.K., 2002. The Circumpolar Arctic Vegetation Map: AVHRR-derived base maps, environmental controls, and integrated mapping procedures. Int J Remote Sens 23, 4551–4570.

Walker, D.A., Raynolds, M.K., Daniëls, F., Einarsson, E., Elvebakk, A., Gould, W.A., Katenin, A.E., Kholod, S.S., Markon, C.J., Melnikov, E.S., Moskalenko, N.G., Talbot, S.S., Yurtsev, B., and other members of the CAVM team, 2005. The Circumpolar Arctic vegetation map. J Veg Sci 16, 267–282.

Walker, M., Walker, D., Everett, K., Segelquist, C., 1989. Wetland soils and vegetation, Arctic Foothills, Alaska. U.S. Fish and Wildlife Service Biological Report 89.

Walker, M.D., Walker, D., Auerbach, N., 1994. Plant communities of a tussock tundra landscape in the Brooks Range Foothills, Alaska. J Veg Sci 5, 843–866.

Walker, M.D., Wahren, H.C., Hollister, R.D., Henry, G.H., Ahlquist, L.E., Alatalo, J.M., Bret-Harte, S.M., Calef, M.P., Callaghan, T.V., Carroll, A.B., Epstein, H.E., Jónsdóttir, I.S., Klein, J.A., Magnússon, B., Molau, U., Oberbauer, S.F., Rewa, S.P., Robinson, C.H., Shaver, G.R., Suding, K.N., Thompson, C.C., Tolvanen, A., Totland, Ø., Turner, L.P., Tweedie, C.E., Webber, P.J., Wookey, P.A., 2006. Plant community responses to experimental warming across the tundra biome. PNAS 103, 1342–1346.

Walker, M.D., Wahren, H.C., Hollister, R.D., Henry, G.H., Ahlquist, L.E., Alatalo, J.M., Bret-Harte, S.M., Calef, M.P., Callaghan, T.V., Carroll, A.B., Epstein, H.E., Jónsdóttir, I.S., Klein, J.A., Magnússon, B., Molau, U., Oberbauer, S.F., Rewa, S.P., Robinson, C.H., Shaver, G.R., Suding, K.N., Thompson, C.C., Tolvanen, A., Totland, Ø., Turner, L.P., Tweedie, C.E., Webber, P.J., Wookey, P.A., 2006. Plant community responses to experimental warming across the tundra biome. PNAS 103, 1342–1346.

Walker, M., Walker, D., Everett, K., Segelquist, C., 1989. Wetland soils and vegetation, Arctic Foothills, Alaska. U.S. Fish and Wildlife Service Biological Report 89.

Wheeler, H., Høye, T., Schmidt, N., Svenning, J.-C., Forchhammer, M., 2015. Phenological mismatch with abiotic conditions—implications for flowering in Arctic plants. Ecology 96, 775–787.

Westergaard-Nielsen, A., Lund, M., Hansen, B., Tamstorf, M., 2013. Camera derived vegetation greenness index as proxy for gross primary production in a low Arctic wetland area. ISPRS J Photogram Remote Sens 86, 89–99.

Wrona, F.J., Johansson, M., Culp, J.M., Jenkins, A., Mård, J., Myers-Smith, I.H., Prowse, T.D., Vincent, W.F., Wookey, P.A., 2016. Transitions in Arctic ecosystems: Ecological implications of a changing hydrological regime. J Geophys Res: Biogeosci 121, 650–674.

Young, A., Britton, G., 1990. Carotenoids and stress, in: Alscher, R., Cummings, J. (Eds.), Wiley, New York, NY, USA, pp. 87–112.

Yu, H., Luedeling, E., Xu, J., 2010. Winter and spring warming result in delayed spring phenology on the Tibetan Plateau. PNAS 107, 22151–22156.

Zhang, X., Tarpley, D., Sullivan, J.T., 2007. Diverse responses of vegetation phenology to a warming climate. Geophys Res Lett 34.

Zeng, H., Jia, G., Epstein, H., 2011. Recent changes in phenology over the northern high latitudes detected from multi-satellite data. Environ Res Lett 6, 045508

Acknowledgements

I owe gratitude to many people for the completion of this thesis. First and foremost I would like to thank my supervisor **Dr. Birgit Heim** without whom this project would not exist. Thank-you for taking a chance on me and for your encouragement, generosity, and support both academically and personally. From picking me up at the airport on my first day ever in Germany to enjoying hard-earned refreshments after long field days at Toolik, your enthusiasm has been a constant throughout the last three years and for that, I am very grateful.

To my defacto secondary supervisor **Prof. Dr. Nicholas Coops**, I cannot thank you enough for all you have given me in the last five years. I credit much of my desire to pursue this degree to my experiences working with you and the IRSS Lab. Your unwavering support and generosity over the last three years has been integral to my success and the completion of this degree. Thank you, truly.

I would like to extend warm thanks to **Dr. Sabine Chabrillat**. Your inclusion in this thesis was so valuable both personally and professionally for me, thank you for being generous with your time and your encouragement throughout. I would also like to thank **Dr. Skip Walker** for sharing his unparalleled knowledge of the Alaskan North Slope and Toolik area. The development of my project and personal knowledge was deeply informed by my exchanges with you. To **Dr. Marcel Buchhorn**, thank you for providing your technical expertise and guidance during the early stages of the project. Many thanks to **Dr. Torsten Sachs** and the AIRMETH team for the successful AISA acquisition. I would also like to thank **Dr. Karl Segl** for the many EnMAP simulations and **Dr. Maximilian Brell**, for his technical assistance and expertise. To **Prof. Dr. Guido Grosse** thank you for your input and steady support throughout the last three years. To **Prof. Dr. Hugues Lantuit** and members of the COPER lab **Samuel Stettner**, **Dr. George Tanski**, **Dr. Anna Irrgang**, **Justine Ramage**, **Caroline Coch**, and **Dr. Jule Wolter** thank you for adopting me as an honorary member and providing your guidance and support throughout the last three years. To my officemates **Ingma Nitze** and **Sebastian Laboor** thanks for being patient with my German and the lunchtime chats. I also owe great thanks to **Prof. Dr. Rob Guy** and **Dr. Mina**

Momayyezi for their generosity with laboratory space, time, and equipment. Without you those analyses would have been near impossible. To the incredible Toolik Field Station staff, thank-you for providing an unparalleled field station experience. And also to all the amazing, smart, and supportive people I met at Toolik Field Station and in Fairbanks, thank you for all the unforgettable experiences. Alaska will forever hold a very special place in my heart. To my dear friends **Txomin Hermosilla**, **Wiebe Nijland**, **Doug Bolton**, and **Piotr Tompalski**, thank you for being such important people in my life in so many ways.

I am especially grateful to **Samuel Stettner** and **George Tanski** for becoming my German family, Berlin is home for me now because of you. Thank you for the scientific exchange, conferences, bike rides, lake swims, Feierabends, breakfast club, German class, and more fun than there is space in these acknowledgements.

None of this would have been possible without my loving parents **Jim** and **Gail** and siblings **Laura**, **Jennifer**, and **David**. Mom and dad, I am in awe of you both on a regular basis as I move through the world and words cannot express the gratitude I have for you and the life you have given us.

Eidesstattliche Erklärung

Hiermit versichere ich, dass ich die vorliegende Arbeit selbstständig verfasst und keine anderen als die angegebenen Quellen und Hilfsmittel verwendet habe.

Ich habe diese kumulative Dissertation am Alfred-Wegener-Institut Helmholtz Zent- rum für Polar und Meeresforschung in Potsdam erarbeitet und in englischer Sprache angefertigt. Diese Dissertation wird erstmalig und ausschließlich an der Universität Potsdam einge- reicht.

Die dem Promotionsverfahren zugrundeliegende Promotionsordnung vom 01.04.2015 ist mir bekannt.

Potsdam, den 30.04.2018,   Alison Beamish